Journal of Engineering

ISSN 1726-4073

A Scientific Refereed Journal Published by College of Engineering University of Baghdad

September 2014

Number 9

Volume 20

مجلة الهندسة

ISSN 1726-4073

مجلة علمية محكمة تصدرها
كلية الهندسة ـ جامعة بغداد

أيلول

٢٠١4

العدد ٩

المجلد ٢٠

ENGINEERING

List of Contents

Evaluation of Pedestrians Walking Speeds in Baghdad City

Saad Issa Sarsam
Professor
College of engineering- University of Baghdad
E-mail: saadisasarsam@coeng.uobaghdad.edu.iq

Marwa Wahab Abdulameer
MSc. student
College of engineering- University of Baghdad
E-mail: marwawahab87@gmail.com

ABSTRACT

This research examines the factors which influence pedestrian's walking speed in Baghdad. the variations in walking speed of pedestrians are related to pedestrian characteristics such as gender, age group, and clothing traditions. Using the established methodology, the counts of pedestrians were performed using manual and video counting. The case study was performed in two streets located in a highly crowded commercial zone at the city center of Baghdad: Al-Karada Dakhel and Al- Sina'a Street. Data were subjected to statistical analysis using IBM SPSS Statistics 19 software. It has been found that Iraqi pedestrians walk slower than other pedestrians in the developed countries or in the region with minimum walking speed of 29.85 m/min. Age, gender, and clothing traditions were found to significantly contribute to pedestrian speed. Pedestrians in the age range from 18-50 years old were the fastest group of pedestrians and pedestrians over 50 years old were the slowest. Male pedestrians had significantly faster walking speeds than female pedestrians did. Pedestrians wearing western style were found to be faster than those wearing Arabic style.

Key words: walking speed; pedestrian characteristics; age; gender; clothing traditions.

تقييم سرعة مسير المشاة في مدينة بغداد

سعد عيسى سرسم
أستاذ
جامعة بغداد – كلية الهندسة – قسم الهندسة المدنية

مروة وهاب عبد الأمير
طالبة ماجستير
جامعة بغداد – كلية الهندسة – قسم الهندسة المدنية

الخلاصة

يتناول هذا البحث دراسة سرعة سير المشاة في مدينة بغداد والعوامل التي تؤثر على هذه السرع ومن هذه العوامل الجنس والفئة العمرية ونمط الملابس. باستخدام المنهجية المتبعة اجريت عمليات العد للمارة باستخدام طريقة العد اليدوي وتقنية التصوير بالفيديو وقد تم اجراء الدراسة في شارعين يقعان في مناطق تجارية مزدحمة وسط مدينة بغداد ، هما شارع الكرادة داخل وشارع الصناعة. خضعت البيانات الى تحليل احصائي باستخدام البرنامج الاحصائي IBM SPSS 19 , وجد من خلال الدراسة والتحليل ان سرعة المشاة في العراق هي اقل من سرع المشاة في البلدان المجاورة والمتقدمة ، حيث وجد ان الحد الادنى لسرعة السير في بغداد هي 29.85 م/الدقيقه . وتم التوصل الى ان الجنس والفئة العمرية واسلوب الملابس من العوامل المؤثرة بشكل كبير على سرعة المشي والعبور للسابلة وان المارة الذين ينتمون للفئة العمرية بين 18-50 سنة هم الاسرع اما المشاة الاكبر من 50 عاما فهم الابطأ, وان سرعة المشي للذكور هي اعلى منها للإناث. كما وجد ان المشاة الذين يرتدون نمط الملابس الغربية (البنطلون) هم الاسرع من حيث العبور والمشي الاعتيادي من الاشخاص اللذين يرتدون الزي العربي .

1. INTRODUCTION

Environment is being contaminated by the increment of vehicles, particularly in Central Business Districts (CBDs) where most of the government offices and trading centres of a city are located. To reduce environmental pollution, pedestrianization has become an integral part of sustainable modern urban design. Thus, the design, arrangement and development of support infrastructures should be in favour of pedestrian movements to popularize walking. To achieve so, pedestrian facilities should be planned and based on the concrete information on user characteristics, **Finnis and Walton, 2006.**

2. BACK GROUND

A 'pedestrian' is any person on foot or who is using a means of conveyance propelled by human power, other than a bicycle. Similarly, the term 'walking' refers to the act of self-propelling along a route, whether this is on foot or on small wheels, or assisted by additional aids, **Roads and Traffic Authority, 2007**. Pedestrians Free flow speed indicates the average movement speed of pedestrians when they are not hindered by other pedestrians in an obstacle-free environment under normal condition. Its value, however, requires extensive data collection for calibration as the walking speed is subject to many factors. **Daamen, 2004,** found that the walking speeds of individual appear to follow a normal distribution, with an estimated mean of 1.34m/s and standard deviation of 0.37. Besides, **Finns and Walton, 2006,** conducted survey on mean walking speed of different countries/cities. the results show that the mean walking speed of different countries can range from 0.7m/s (Itea, Greece) to 1.8m/s (Prague, Czech Republic). The literature review suggests men and women have different walking speeds, flows and density relationships. **White, 1994,** showed that pedestrians might vary their walking speeds over a wide range, when unimpeded by crowd density or other frictions.

a controlled study by **Murray, 1986,** of walking speeds for men, ranging in age from 20 to 87, revealed that normal walking speed declined with age, He concluded that this would indicate that a healthy person in their 40's in a hurry could exceed the normal relaxed walking speed of a 20-year-old. Normal walking speeds declined from 84 m/min for the 20-to-25 age group, to 65 m/min for the 81 -to-87 groups, with most of the speed decline occurring after the age of 65.

3. SCOPE OF THE STUDY

This study is mainly concerned with the effect of variables such as age, gender, and clothing style, on walking speed. To investigate how urban characteristics affect pedestrian mobility, field investigation was carried out in Baghdad at different land use locations, and data was collected regarding pedestrian characteristics and behaviour.

4. METHODOLOGY

4.1 Site Description

The case study was performed in the city of Baghdad. To conduct the speed studies in the concentrated CBD areas, several sidewalks along the main streets were selected as the observation sites. The pedestrian volume and speed data were collected at two selected locations in Baghdad

CBD area. The first site is located in a recreational and shopping zone (AL- karada Dakhil); the second site is a commercial and educational zone holding colleges, (Al- Sina'a Street). The studied segment of sidewalks has dimensions shown in **Table1**; where the arcades widths are measured as the available space for pedestrian to walk.

4.2 Sampling

The collection of the field data was made for sample lengths of 1 hour and during good weather conditions. The hours in which the counts were performed, were the ones where the peak hour was expected to take place. These hours were selected considering the background information of the place. Specifically, the ranges selected were 13:00-14:00 and 17:00-18:00 for Baghdad.

The workdays were used as the main sample days for this study. In this respect, random days among this group were chosen of April 2013.

4.3 Counts Method

The technique adopted in the field work is by marking a longitudinal section of known length and width on the pedestrian facility and continuously recording the movement of pedestrians within this section. Pedestrians were manually timed over a measured test length, volume and speeds were then calculated. Random pedestrian about to enter the section was selected and tracked through the study area. The time taken by a pedestrian to traverse the test length was measured using a digital stop watch, the entry and exit times in and out of the test area were recorded. Walking speed is then derived by dividing the known length of the section by the walking time. Data were subjected to statistical analysis using IBM SPSS Statistics 19 software. The speed was calculated using the mathematical models below, **Pignataro, 1973; Khisty and Lall, 1998.** From this data, regression models have been constructed and the predictive performances of these models were assessed.

$$S_N = L / T_N \tag{1}$$

$$S_S = L / T_S \tag{2}$$

Where:

T_N; T_S represents travel time in each direction (min)

S_N; S_S represents the space mean speed (meter / minutes) in each direction

L = the test section length (meters)

5. RESULTS AND DISCUSSION

5.1 Variation of Walking Speed with Gender

Table 2, shows pedestrian mean and 15th percentile speeds in relation to pedestrian gender for Baghdad. The 15th percentile speed is the one normally used in design and it means that 85% of pedestrians walk faster than this speed. As indicated in **Table 2**, male pedestrian walks faster than female for all of the tested sites. The walking speed detected for both gender at Baghdad site two, which is an educational zone (mean walking speed) is 35.84 m/min - 33.783 m/min. for male and female respectively, **Fig. 1,** show the minimum, maximum, and mean walking speed for males and females for Baghdad.

This may be attributed to the fact that most of the pedestrians at the educational zone are young. The present study findings are comparable to walking speeds reported by **koushki, 1988** for Saudi Arabia (mean walking speed 65 m/min).

5.2 Effect of Age Groups on Walking Speed

As indicated in **Table 3**, adult pedestrians (18-50 years) were the fastest compared to other age groups with an average speed of 43.092 m/min and 39.458 m/min for males and females respectively at Baghdad site 2. Pedestrians 50 years or older (elderly) were the slowest among others, with an average walking speed of nearly 20 m/min.

These findings are in agreement with those reported by **Fruin, 1971, koushki, 1988, Sarsam, 2002, and Sarsam, 2013.**

Fig. 2 shows the variation of walking speed with gender and age groups for Baghdad. On the other hand, **Fig.3** shows the variation of walking speed with gender and clothing tradition.

5.3 Effect of Clothing Tradition on Walking Speed

Table 4 shows pedestrian mean speed in relation to pedestrian clothing tradition for Baghdad and it detected two clothing styles: Arabic style, and western style (trousers) for both male and female. It was found that males who wearing trousers are faster than males with Arabic style for both sites by about 3.9 m/min. This may be attributed to the limitations practiced in the step length which is restricted due to clothing when using the Arabic clothing tradition. When female pedestrian are considered, females who wearing trousers are faster than whom wearing Arabic style by about 0.65 m/min and such variation was not significant for female pedestrians. This could be attributed to the slower average speed of female as compared to male. It found to be in agreement with results found by **kuishki, 1988** in Saudi Arabia, and **Sarsam, 2013** in Baghdad.

6. CONCLUSIONS

Within the limitations of field investigation procedure and assumptions, the following conclusions may be drawn:

1. Male pedestrian have significantly faster walking speeds than female pedestrians by about 5% with mean walking speed of 35.9m/min for Baghdad.
2. Pedestrians of 18–50 years old are the fastest group of pedestrians with an average speed of 43.092 m/min at Baghdad, Pedestrians over 50 years old were found to be the slowest group with an average walking speed of nearly 20 m/min.
3. Male wearing western style is walking faster than males with Arabic style by an average of 3.9 m/min and such variation was not significant for female pedestrians.

REFERENCES

- Abdulameer M. W, 2014. *Modeling Pedestrians Speeds n Baghdad and Erbil cities*, MSc. Thesis, Department of Civil Engineering, College of Engineering, University of Baghdad, Iraq.

- Daamen, W. and Hoogendoorn, S. P. , 2003. *Experimental Research on Pedestrian Walking Behavior*". 82nd Annual Meeting at the Transportation Research Board, USA.

- Fruin, J. , 1971.*Pedestrian Planning and Design*, Metropolitan Association of Urban Designer and Environmental Planners, Inc., New York.

- Finnis, K. K. and Walton, D. , 2006. *Field Observations of Factors Influencing Walking Speeds*. Ergonomics, 2006.

- Koushki, P. A. , 1988. *Walking Characteristics in Central Riyadh, Saudi Arabia*, J. Transp. Eng., ASCE, 114(6), 735-744.

- Murray, K ,1986.*the Characteristics of Walking and Age*, Transportation Research Record, USA.

- Pignataro L. 1973. *Traffic Engineering Theory and Practice*" Prentice-Hall.

- Sarsam S. , 2013. *Assessing Pedestrian flow characteristics at Baghdad CBD area*, 2nd Scientific Engineering Conference, University of Mosul, 19-21 November, Mosul, Iraq.

- Sarsam S. , 2002. *Modeling Pedestrian Crossing and Walking Behavior at Mosul CBD.* Proceedings, Safety on roads: 2nd international conference 21- 23 October-2002 Bahrain SORIC` 02.

- Transportation Research Board , 1994. *Highway Capacity Manual*, Special Report 209, National Research Council, Washington, USA

- White, J , 1994. *A Walk on the (not so) Wild Side - Promoting the Pedestrian in York* , PTRC Proceedings, Vol. P3 8 1, pp 1- 13, London, UK

Table 1. Dimension of sidewalk for each street.

City	Site	Street	Section length (m)	Section width (m)
Baghdad	1	Al-Karada Dakhil	10	2.5
	2	Al-Sina'a	10	3

Table 2. Pedestrian speed in relation to gender for Baghdad city.

Pedestrian walking speed (m/min)			
Site	Gender	Mean	15^{th} percentile
Site 1	Male	30.76	19.12
	Female	29.85	23.48
Site 2	Male	35.84	23.99
	Female	33.78	26.56

Table 3. Variation of walking speed with gender and age groups for baghdad.

Pedestrian walking speed (m/min)						
Site 1	Male age group			Female age group		
	Young	**Adult**	**Elder**	**Young**	**Adult**	**Elder**
Site 2	35.13	37.16	20.11	31.59	34.30	19.57
	39.59	43.09	24.98	35.17	39.46	26.83

Table 4. Variation of Walking Speed with Gender and Clothing Tradition for Baghdad.

Pedestrian walking speed (m/min)				
Site	Male clothing tradition		Female clothing tradition	
	Arabic style	Western style	Arabic style	Western style
Site 1	28.84	32.73	29.54	30.17
Site 2	33.92	37.81	33.46	34.11

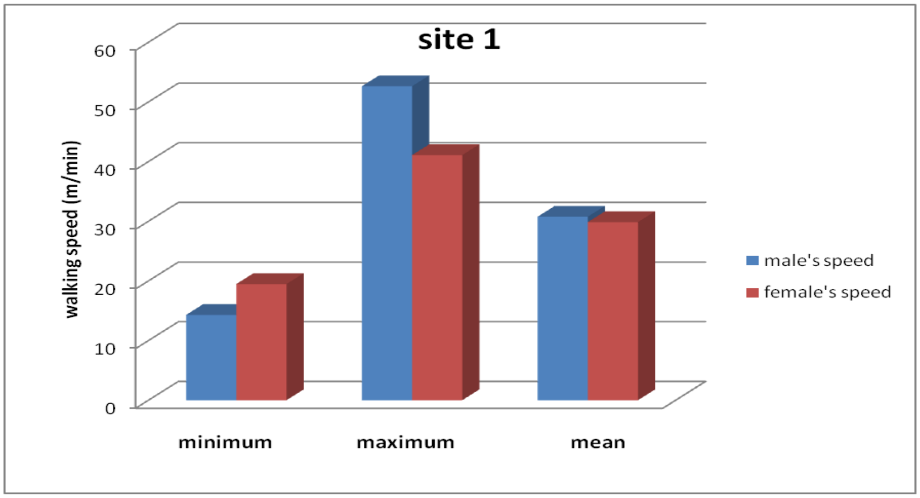

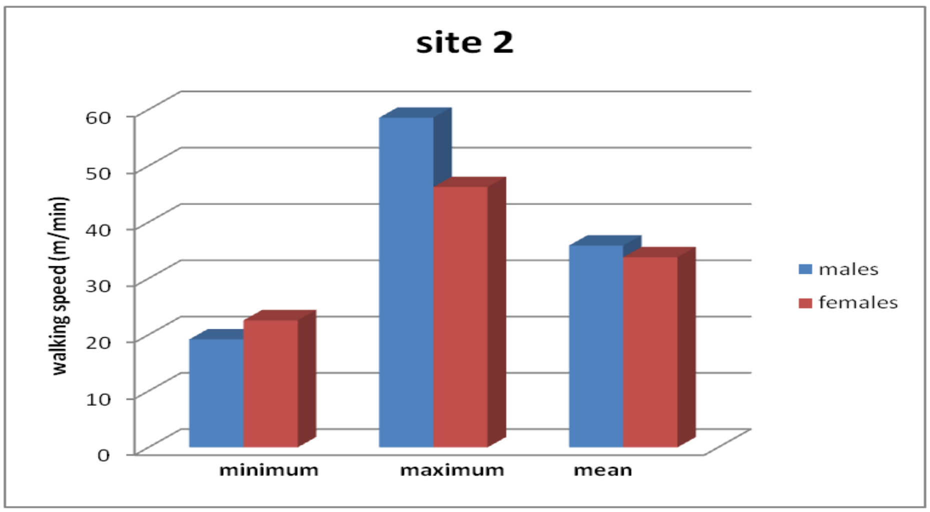

Figure 1. Variation of walking speed with gender for Baghdad city.

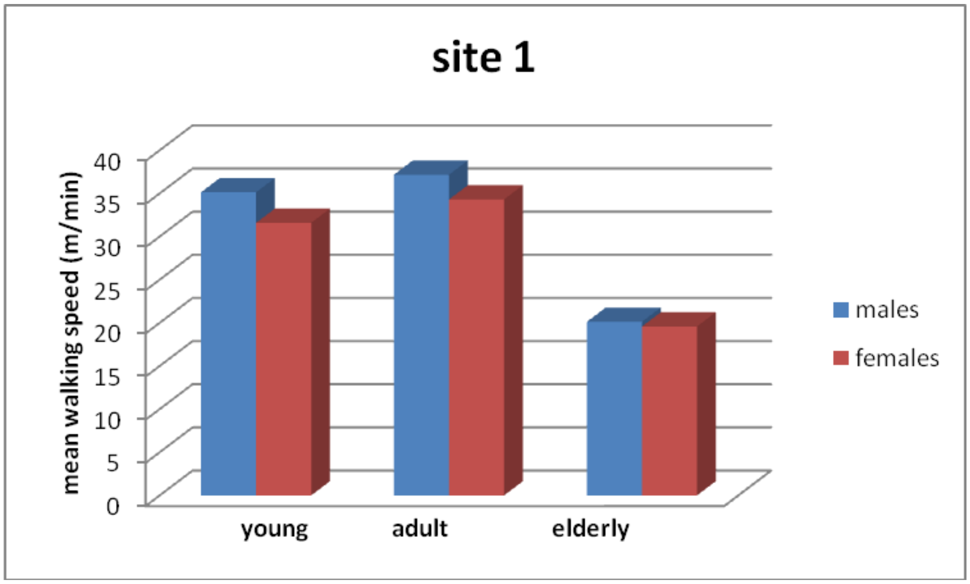

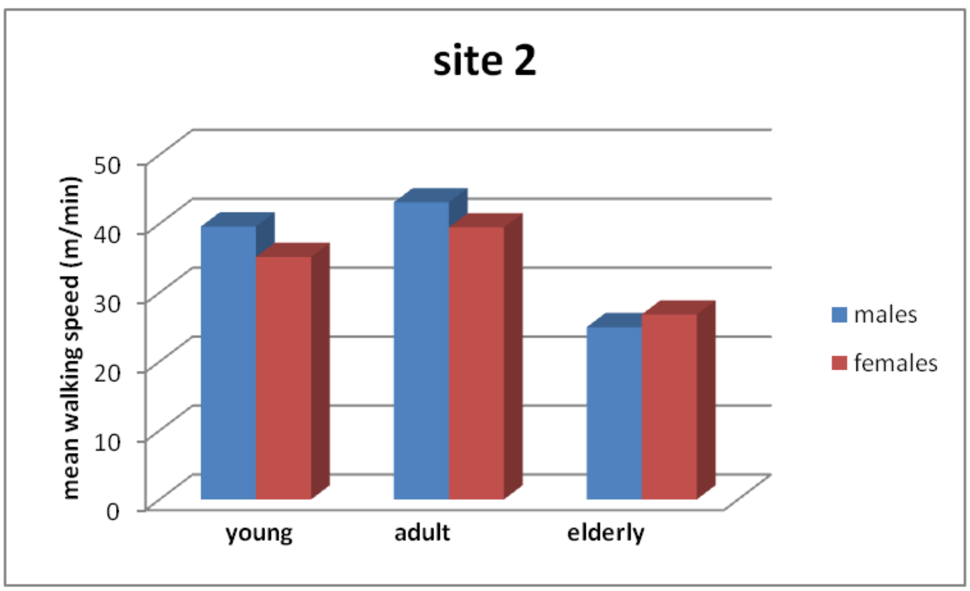

Figure 2. Variation of walking speed with gender and age groups for Baghdad.

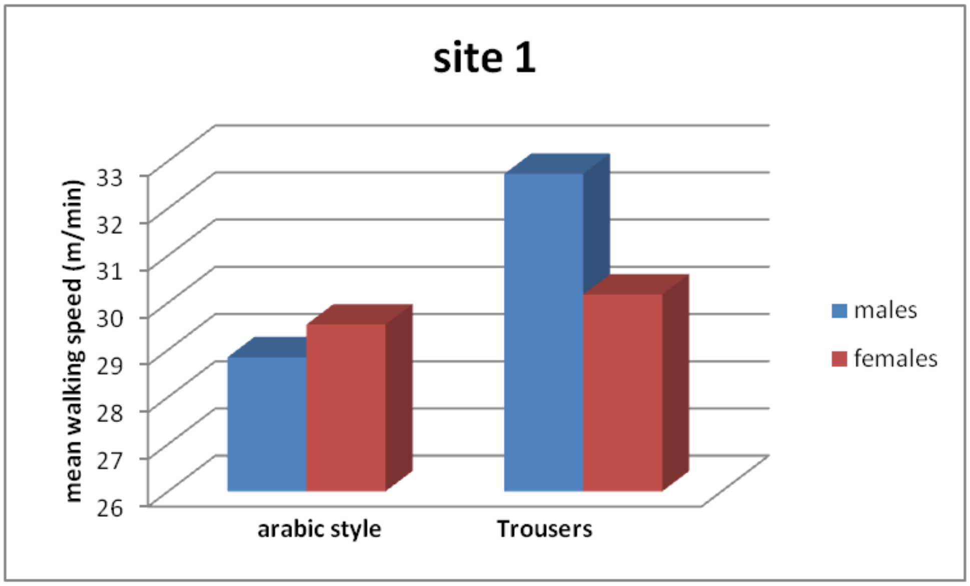

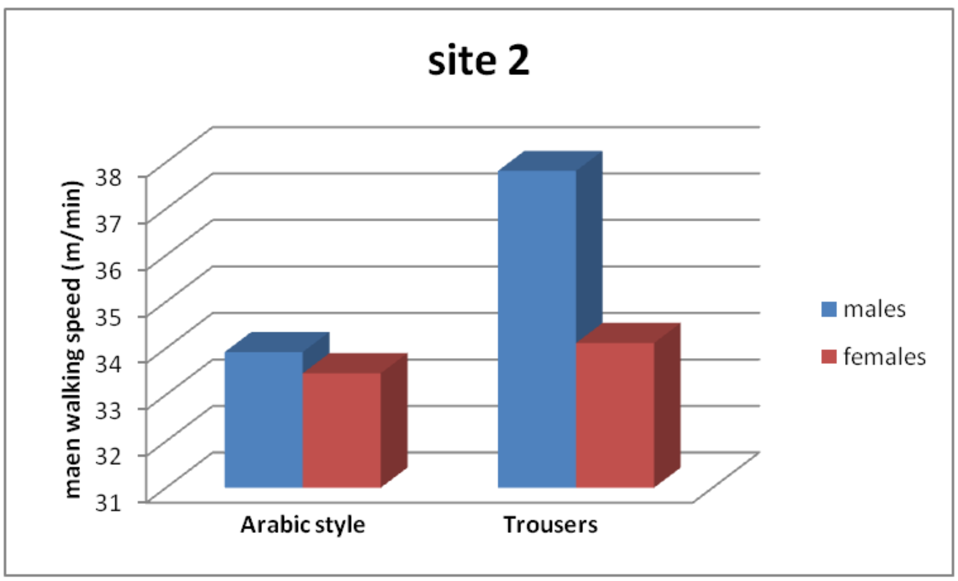

Figure 3. Variation of walking speed with gender and clothing traditions.

Solving Time-Cost Tradeoff Problem with Resource Constraint Using Fuzzy Mathematical Model

Sosan M. Rashed
Assistant Professor
College of Engineering - University of Baghdad
Email:Sawsan_2@yahoo.com

Ahmed M. R. Mahjoob
Instructor
College of Engineering- University of Baghdad
email:mrahmed.civil@yahoo.com

ABSTRACT

Scheduling considered being one of the most fundamental and essential bases of the project management. Several methods are used for project scheduling such as CPM, PERT and GERT. Since too many uncertainties are involved in methods for estimating the duration and cost of activities, these methods lack the capability of modeling practical projects. Although schedules can be developed for construction projects at early stage, there is always a possibility for unexpected material or technical shortages during construction stage.

The objective of this research is to build a fuzzy mathematical model including time cost tradeoff and resource constraints analysis to be applied concurrently. The proposed model has been formulated using fuzzy theory combining CPM computations, time-cost trade off analysis and resource constraint. MATLAB software has been adopted to perform ranking process, for each case, that facilitates obtaining the optimum solution. This research infers that it is possible to perform time-cost trade off analysis with resource restriction simultaneously, which ensures achieving scheduling optimum solution reducing the effort and the time when performing these techniques in succession using traditional methods.

Key words: fuzzy mathematical model, CPM, resource constraint, MATLAB, linear programming.

حل توافق الزمن- الكلفة مع محددات المصادر باستخدام نموذج التعرج الرياضي

سوسن محمد رشيد
كلية الهندسة- جامعة بغداد

أحمد محمد رؤوف محجوب
كلية الهندسة- جامعة بغداد

الخلاصة

تعتبر الجدولة واحدة من اهم المباديء والقاعدة الاساسية في اداراة المشاريع. توجد عدة طرق لجدولة المشاريع مثل (CPM, PERT, GERT). ومع وجود الكثير من عدم التيقن المتضمنة في طرق تخمين مدد الفعاليات وكلف الفعاليات, فأن هذه الطرق تفتقد القدرة لنمذجة المشاريع العملية (الواقعية). بالرغم من أن الجداول ممكن ان تعد للمشاريع الانشائية في مراحل مبكرة من المشروع، توجد أحتمالية ظهورعجزتقني او نقص في الموارد غير متوقع أثناء مرحلة الانشاء.

أن الهدف من هذا البحث هو بناء أنموذج التعرج الرياضي متضمناً تطبيق توافق الكلفة مع الزمن و محددات المصادربالتوازي. لقد صيغ الأنموذج المقترح باستخدام نظرية التعرج مدموجاً مع تطبيق طريقة المسار الحرج، توافق الوقت مع الكلفة ومحددات الموارد. تم تبني برنامج (MATLAB) لانجاز عملية الترتيب لكل حالة والتي تسهل أيجاد الحل الامثل. استنتج البحث الى امكانية اجراء تحليل توافق الوقت مع الكلفة ومحددات الموارد في آن واحد مما يضمن الوصول الى الحل الامثل للتخطيط وبشكل يقلل من الجهد والوقت عند اجراء هذه العمليات بالتعاقب وبالطرق التقليدية المعمول بها والتي من المطلوب فيها غالباً تكراراعادة الجدولة للوصول الى الحل الأمثل.

1-INTRODUCTION

Decisions in construction management are made based on schedules that are developed during the early planning stage of projects, while many possible scenarios need to be considered during actual construction stage which may cause many changes in schedule. Many restrictions appear during construction stage, therefore, taking these restrictions into account helps project managers to evaluate situations and make better decisions. In order to adopt more integrated construction project plans including the requirements for implementing the project plans in possible least costly manner, time-cost trade off analysis with resource constraints techniques were developed to apply in succession. In real projects, the trade-off between the project cost and the completion time, and the uncertainty are both considerable aspects for managers. Resources are the main factor that affect implementing project schedule, providing the accurate resources at the right time means that the schedule will probably run smoothly. But when there are insufficient resources available for activities (especially concurrent activities), which use the same type of resource, some of these activities are delayed to relieve the resource constraints. Usually, the solutions for the optimum time cost trade off may not be suitable for resource allocation. Although optimization programming processes the capability of producing accurate solutions, it requires elaborate formulation and extensive computation.

Fuzzy Logic has emerged as a nontraditional tool in construction management applications and as such has been employed in resource scheduling and time cost trade off analysis individually. To obtain optimum solution for time schedule, it is necessary to make time cost trade off, resource allocation applied simultaneously within fuzzy environment to produce optimum time schedule considering cost and resource constraints.

Many researcher performed studies about using fuzzy theory in project scheduling. **Zhang et al, 2005** Incorporate fuzzy set theory and a fuzzy ranking measure with discrete-event simulation in order to model uncertain activity duration in simulating a real-world system, especially when insufficient or no sample data are available. **LIANG, 2006** presents an interactive Fuzzy Linear Programming (FLP) approach for solving project management (PM) decision problems in a fuzzy environment. **Soltani** and **Haji, 2007** have developed a new method based on fuzzy theory to solve the project scheduling problem under fuzzy environment. Assuming that the duration of activities are trapezoidal fuzzy numbers (TFN), in this method they compute several project characteristics such as earliest times, latest times, and, slack times in term of TFN.

Lin, 2008 introduces a fuzzy time-cost tradeoff problem based on statistical confidence-interval estimates and a distance ranking for fuzzy numbers to derive the level $(1 - \alpha)$ of fuzzy numbers from $(1 - \alpha) \times 100\%$ statistical data confidence-interval estimates. **Shankar, et al. 2010** presents a method for finding critical path in the fuzzy project network. Trapezoidal fuzzy numbers are used to represent activity times in the project network. **Liang, et al. 2011** presents a fuzzy mathematical programming approach to solve imprecise project management decision problems with fuzzy goal and fuzzy cost coefficients.

The research has many difficulties when applying such models due to unavailability of the required information or emphasizing it on the logic part of fuzzy theory rather than presents a new method to solve scheduling problem. Thus this research will focus on making integration between fuzzy logic and the management theories to provide an improved method used in project scheduling.

2- FUZZY SETS

Fuzzy sets can be considered as an extension of classical or 'crisp' set theory. In classical set theory, an element x is either a member or non-member of set A. Thus, the membership μA (x) of x into A is given by:

$$\mu A\,(x) = \begin{cases} 1, \text{ if } x \in A \\ \\ 0, \text{ if } x \notin A \end{cases}$$

In contrast to classical set theory, the fuzzy set methodology introduces the concept of degree to the notion of membership. More formally, a fuzzy set A of a universe of discourse X (the range over which the variable spans) is characterized by a membership function μA(x): X → [0, 1] which associates with each element x of X a number μA(x) in the interval [0, 1], with μA(x) representing the grade of membership of x in A. So, Membership Function (MF) is a curve that defines how each point in the input space is mapped to a membership value (or degree of membership) between 0 and 1. **Sivanandam et al, 2007.**

Various membership functions can be established depending on how we can represent the context of the practical problem, the most familiar membership function presented in **Fig. 1 Lorterapong and Moselhi, 1996.** The mathematical representation of the membership function presented in **Fig. 1** is as follows:

2-1 Triangular Membership Function **Fig. 1 a,** The membership function for this type is

$$\mu\,(x) = \begin{cases} 1-(|x-b|/a-b) & \text{if } a < x < c \\ \\ 0, & \text{otherwise} \end{cases}$$

2-2 Trapezoidal Membership Function **Fig.1 a,** The membership function for this type is

$$\mu\,(x) = \begin{cases} 0 & \text{if } x \le a \\ x-a\,/b-a & \text{if } a < x \le b \\ 1 & \text{if } b < x \le c \\ x-d\,/c-d & \text{if } c < x \le d \\ 0 & \text{if } x > d \end{cases}$$

2-3 Open Right Membership Function **Fig. 1 c,** The membership function for this type is

$$\mu\,(x) = \begin{cases} 1 & \text{if } x \ge b \\ x-a\,/b-a & \text{if } a < x < b \\ 0 & \text{if } x < a \end{cases}$$

2-4 Open Left Membership Function **Fig. 1 d,** The membership function for this type is

$$\mu\,(x) = \begin{cases} 1 & \text{if } x \le a \\ b-x\,/b-a & \text{if } a < x < b \\ 0 & \text{if } x > b \end{cases}$$

3- FUZZY NUMBERS ARTHIMATIC

Let A and B be two trapezoidal fuzzy numbers parameterized by the quadruple A= $[a_1, b_1, c_1, d_1]$ and B= $[a_2, b_2, c_2, d_2]$ respectively. The simplified fuzzy number arithmetic operations between the trapezoidal fuzzy numbers A and B are as follows **Shankar et al (2010)**.

Addition $\oplus$

$A\oplus B= [a_1+ a_2, b_1 +b_2, c_1+c_2 ,d_1+d_2]$

Subtraction $\ominus$

$A\ominus B= [a_1- d_2, b_1- c_2, c_1- b_2 , d_1- a_2]$

Multiplication $\otimes$

$A\otimes B= [a_1 a_2, b_1b_2, c_1c_2 , d_1d_2]$

Division $\oslash$

$A\oslash B= [a_1/ d_2, b_1/ c_2, c_1/ b_2, d_1/ a_2]$

4-FUZZIFICATION AND DEFUZZIFICATION

According to **Ross, 2004**, Fuzzification is the process of making a crisp quantity fuzzy. This is done by simply recognizing that many of the quantities that are considered to be crisp and deterministic are actually not deterministic at all: They carry considerable uncertainty.

While defuzzification is a mathematical process used to extract crisp output from fuzzy output set(s). This process is necessary because all fuzzy sets inferred by fuzzy inference in the fuzzy rules must be aggregated to produce one single number as the output of the fuzzy model, **Asmuni, 2008.**

Many methods that have been proposed in the literature in recent years, seven are described here for defuzzifying fuzzy output functions (membership functions), **Ross, 2004,** Max membership principle, Centroid method, Weighted average method, Mean max membership, Center of sums, Center of largest area and First (or last) of maxima.

5- TIME- COST TRADEOFF ANALYSIS

Time-Cost Trade off (TCT) analysis represents the process of optimally reducing the project duration in a least costly manner. The objective of TCT analysis is to search for the optimum set of activities methods of construction that minimizes the total project cost (direct and indirect) while not increasing project completion time. The TCT analysis involve estimating, if possible, the cost of crashing normal time for the project activities so as total project completion time will be decreased.

6- RESOURCE RESTRICTION

Two problems arise in developing a resource constrained project schedule. **Hendrickson and Au (2003)** First, it is not necessarily the case that a critical path schedule is feasible. Because one or more resources might be needed by numerous activities, it can easily be the case that the shortest project duration identified by the critical path scheduling calculation is impossible. The difficulty arises because critical path scheduling assumes that no resource availability problems or bottlenecks will arise. As a second problem, it is also desirable to determine schedules which have low costs or, ideally, the lowest cost. To overcome these problems, all the possible scenarios of resource allocation with associated time schedule get developed, considering restricted availability of recourses, and the schedule that satisfies both the time and cost criteria is identified. This will be done by changing different activities start time, depending on the availability of the resources, and the most optimum schedule is selected.

7- FUZZY MATHEMATICAL MODEL

The time and cost of the project activities, as well as the project itself, may be expressed using a range of values rather than exact numbers. This fact makes the theory of Fuzzy logic applicable in such cases to represent the uncertainty in time and cost of construction project. Since the time and cost of the activities are considered fuzzy numbers, the project total time and cost will be expressed by fuzzy numbers. To prepare a mathematical model for project scheduling using Fuzzy theory the following proposed algorithm will be applied

1- Define the project activities by answering the question " what must be done"
2- Define the logical relationship between activities
3- Estimate the activities cost and time
4- Specify, if possible, the crash time and cost for crashing the activity
5- Convert the activity time to fuzzy time for the project activities; this is done by finding the max number of crash time in all activities considering it as the fuzzy membership function. For example if the max number of crash time in all project activities is 3 days and the normal time for this activity is 8 days, then we will use four point fuzzy membership function (trapezoidal Function) and fuzzy numbers will be (5, 6, 7 and 8).
6- For the activities having no or less crash time, consider the following: -
A- The activities with less than max crash time, repeat one of the numbers. For example if an activity have 2 days crash time and 3 days normal time then fuzzy time may be written as minimum (1, 1, 2 and 3) , middle (1, 2, 2 and 3) and maximum fuzzy time (1, 2, 3 and 3).
B- For the activities with no crash time, repeat the same activity time. For example if an activity has 2 days of time then the fuzzy time will be (2, 2, 2 and 2).
7- For the activities with crashing cost per unit of time greater than indirect cost set the fuzzy time equal to normal time.
8- Specify: -
A- The required resources for each activity.
B- The available resources and the time of availability.
9- Examine the possible scenarios for the project scheduling (consider availability of the resources and the time of availability).
10- For each scenario, develop a number of networks by considering different fuzzy time.
11- Develop a mathematical model for each scenario and solve it by using fuzzy logic toolbox presented in the commercial program (MATLAB).

8- CASE STUDY

For applying the proposed algorithm a case study project from **Mohammed, 2004** will be adopted, normal, crash time and cost presented in **Table 1.** While the **Fig. 2** presents the AOA network for this project.

While the first four steps in the proposed algorithm are satisfied in the case study, other steps will be implemented as follows: -

1- Converting the activity duration to fuzzy duration, according to step 5 & 6 in the proposed algorithm, the conversion process was done depending on the maximum amount of crashed time available in the project activities, while fuzzy cost depending on crashing rate for each activity, that's mean increasing in unit of time will be associated with decreasing in cost using crashing rate, **Table 2** present the fuzzy duration and cost for each activity, the above conversion actually determines the linguistic variables. As mentioned in paragraph four "Fuzzification is the process of

making a crisp quantity fuzzy” that means the activity time, and cost, are converted from crisp (single value) value to fuzzy value (membership value) by using linguistic variables .
2- For step number 8, the required resources for each activity are presented in **Table 1.** While the available resources and the time of availability are stated by only 12 units of material (m) available and the rest are going to be delivered after days 12.
3- Considering step number 9 in the proposed algorithm, in addition to the case of normal resources availability, there are two possible scenarios for the project scheduling consider availability of the resources and the time of availability.
4- In step number 10, each scenario developed in step number 9 will be tested with the possible combination of activity fuzzy time (min, middle and max fuzzy time) using the scenario network, the result represents project total fuzzy times (the project membership functions). This step will be done by using the planned case (Normal resource availability) and resource restriction cases as follows

A- Normal resources availability
Three networks are developed considering normal availability of the resources. For each network the project completion time represents project membership function, that means three trapezoidal membership functions are developed, **Fig. 3** presents the networks of normal recourse availability scenario with min fuzzy time. It is clear that crashing some activity in the above network will not reduce the project total time while increasing the total cost (activity D, F and H) because the following activities have greater start time than their finish time, so set the activity time equal to normal time as in **Fig. 4**. The same procedure will be implemented in the other network (middle and maximum fuzzy time) presented in **Fig. 5** and **Fig. 6**.

B- Resource restriction first scenario
In this scenario, the activities (A, B, C, D and E) will be performed during the first 12 days and the rest of activities will be implemented after that. This action requires inserting dummy activity (40-45) with early start time equal to 13 days. **Fig. 7** shows the network developed for this scenario and the resulting project completion time. The network in **Fig. 7** shows that crashing some activities will not reduce the project total time while increasing the total cost because the following activities have greater start time than their finish time, so the backward adjustment involves activities (A, D, E and G) by setting activity time equal to normal time as in Figure **Fig. 8**. The same procedure will be implemented in the other network (middle and maximum fuzzy time) presented in **Fig. 9** and **Fig. 10**.

C- Resource restriction second scenario
The second scenario shows that the activities (A, B, C, E and F) will be performed during the first 12 day and the rest of activities will be implemented after that. To perform this action, the dummy activity (30-35) will be inserted in the project network with early starting time of 13 days. **Fig. 11** illustrates the network developed for this scenario with the project fuzzy completion time. The same procedure of backward adjustment is implemented in this scenario involving activities (E, F, G and H) by setting the normal activity time as a fuzzy time. **Fig. 12, Fig. 13** and **Fig. 14** show the network for second scenario.

The associated cost for each time will be calculated using the following equation

$$TC= \sum C+[IC * Xn] \qquad (1)$$

Where:
TC= total Cost
C= activity direct cost for specified time (**Table 2**).
Xn= project completion time
IC= indirect cost / unit of time (1500$/day)
Table 3 summarizes the project fuzzy time for each scenario with the associated fuzzy total cost. The information in this table is the basis for creating membership functions for using in fuzzy mathematical models.

9- THE MATHEMATICAL MODEL

Developing the mathematical model for each scenario as follows
A- For normal resource availability, the proposed model will be developed using the information resulting from planned case (**Table 3**). The cost model can be expressed as: -

$$\mu (t) = \begin{cases} 1 & \text{if } t \leq 21 \\ (27-t) / 5 & \text{if } 22<t\leq 27 \\ 0 & \text{otherwise} \end{cases}$$

Where the variable (t) represents completion time for the project, 22 is the preferred completion time and 27 is the normal completion time. The graphical representation for this model is shown in **Fig. 15**. While the following model represents the cost model with graphical illustration in **Fig. 16**.

$$\mu(c) = \begin{cases} 1 & \text{if } c\leq 68200 \\ (70000-c)/1800 & \text{if} 68200<c\leq 70000 \\ 0 & \text{otherwise} \end{cases}$$

Where the variable (c) is the completion time for the project, (68200) represents the preferred completion cost and (70000) is the normal completion cost.

B- For resource restriction first scenario the following model represents time and cost model using the information in **Table 3** with same procedure used in developing planned case models. The models graphical illustration is presented in **Fig. 17** and **Fig. 18**.

$$\mu (t) = \begin{cases} 1 & \text{if } t\leq 27 \\ (29-t) / 2 & \text{if } 27<t\leq 29 \\ 0 & \text{otherwise} \end{cases}$$

$$\mu (c) = \begin{cases} 1 & \text{if } c\leq 72100 \\ (73000-c) / 900 & \text{if } 72100<c\leq 73000 \\ 0 & \text{otherwise} \end{cases}$$

C- The models for case two is developed using information in **Table 3** (case two) as shown below with graphical representation in **Fig. 19** and **Fig. 20**.

$$\mu\ (t) = \begin{cases} 1 & \text{if } t \le 25 \\ (27-t)\ /\ 2 & \text{if } 25 < t \le 27 \\ 0 & \text{otherwise} \end{cases}$$

$$\mu\ (c) = \begin{cases} 1 & \text{if } c \le 70000 \\ (72000-c)\ /\ 2000 & \text{if } 70000 < c \le 72000 \\ 0 & \text{otherwise} \end{cases}$$

10- SOLVING THE MATHEMATICAL MODEL USING MATLAB PROGRAM

Now the proposed mathematical model developed for each case will be solved by using MATLAB fuzzy logic toolbox (Graphical User Interface GUI) as follows

1- Construct two inputs (time and cost) one output (rank) system using FIS Editor. While the inputs represent the fuzzy time and cost for each case, which are defined in the mathematical model, the output will represent the scale to measure optimum time and cost as shown in Figure **Fig. 21**.

2- Define the membership function for system. One trapezoidal membership functions will be used for each input and one triangular membership function for the output, while the defuzzification method will be smallest of maximum (som). State the range for the time input (0-30), while the cost input will be entered in thousands and the range will be (0-80). The output range will be (0-1) which represents the rank for each time and associated cost.

3- Write down the rules using Rule Editor. The rule will be added as presented in Figure **Fig. 22**.

4- Finally the time value can be fed with associated cost by using rule viewer to get their rank. The value of each input variable can be classified by sliding the lines in the input column and generating the output value or by writing those in the input field as shown in figure **Fig. 23**. The output of each input is presented in **Table 4** which summarizes the final rank for each case.

11- DEVELOPING GENERAL MODEL

Now if it is required to choose between the times generated from the restriction cases, case one and two, a general model will be developed which represents the min and max time and cost of the restriction cases, the resulting model is as follows

$$\mu\ (t) = \begin{cases} 1 & \text{if } t \le 25 \\ (29-t)\ /\ 4 & \text{if } 25 < t \le 29 \\ 0 & \text{otherwise} \end{cases}$$

$$\mu\ (c) = \begin{cases} 1 & \text{if } c \le 70000 \\ (73000-c)\ /\ 3000 & \text{if } 70000 < c \le 73000 \\ 0 & \text{otherwise} \end{cases}$$

The graphical representation is shown in Figures **Fig. 24** and **Fig. 25**.

The final rank for each time and associated cost is obtained using MATLAB (GUI) and the final result is summarized in **Table 5.**

12- MODEL VERIFICATION

The verification processes involve converting normal and resource restriction cases to Linear optimization models and solving them using commercial computer program called (WinQSB). The results generated from solving these models summarized in **Table 6.**

13- RESULTS DISSCUSION

The results generated from solving fuzzy mathematical models reflect the required purposes of the models developed for each case individually which can be summarized in finding the optimum reduction time and the associated cost. For the planned case, the result shows that the optimum time is 22 days with associated cost of $68200, which has the highest rank, and this result matches the result of the optimization model which satisfy the model verification requirement, but another time and cost has the same rank which is 21 days with cost of $68500, and that have reflect the enhancement of this method which gives the decision maker flexibility to choose what he favorite, min time or min cost. For case one the results shows that the optimum time is 27 days with associated cost of $72100 which is exactly the same result of the optimization model. For the case two, the result shows that the optimum time is 26 days with cost of $71000 and this result differs from the result of the optimization model, but again this result gives the decision maker option to choose between minimum time and cost.

The general model result shows that the optimum time is 26 days with cost of $71000, but still the decision maker has the option to choose what he favors min time or min cost according to project situation. The above models provide decision makers with a range of time that is between the normal time and the maximum crash time.

14- CONCLUSIONS

1- Fuzzy mathematical model has the capability to determine the optimum solution for time-cost trade off analysis with inclusion of resource restriction simultaneously. The presented solution is identical to manual solution in which time-cost trade off analysis and resource allocation are performed in succession, and requires no effort of network rescheduling as it is performed manually.

2- Fuzzy mathematical model provides accurate results and that the optimization model is performed correctly. In addition optimization model finds the minimum completion time for projects while fuzzy model provides a range of time that is between the normal time and the maximum crash time.

3- The model allows the decision maker to examine different scenarios for project execution, and their impact on total time and cost, done by changing the order of performing activities which causes automatic change in project duration and cost.

4- This model could be used for examining the possibility of material or technical shortages. The analysis could be done by comparing other alternatives such as using a more costly material that could be delivered at the right time.

5- This model can be used for the project in Iraqi construction sector which have the right required information for project scheduling such as normal and crash time and cost, the expected resource shortage and the cost of the available alternatives.

REFRENCES

- Asmuni, H. , 2008. *Fuzzy Methodologies for Automated University Timetabling Solution Construction and Evaluation*, Thesis submitted to the University of Nottingham for the degree of Doctor of Philosophy, p 59.

- Haji, R. and Soltani, A. , 2007. *A Project Scheduling Method Based on Fuzzy Theory*, Journal of Industrial and Systems Engineering, Vol. 1, No. 1, pp 70-80.

- Liang, Tien-Fu, Huang, Tien-Shou and Yang, Ming-Feng, , 2011. *Application of fuzzy mathematical programming to imprecise project management decisions*. DOI 10.1007/s11135-011-9460-y, Springer Science& Business Media B.V. 2011.

- LIANG, T. F., 2006. *Project management decisions using fuzzy linear programming*. International Journal of Systems Science Vol. 37, No. 15, 1141–1152.

- Lin, Feng-Tse , 2008. *Time-Cost Trade-off Problem Based on Confidence-Interval Estimates and Level (1 − α) Fuzzy Numbers*. International Journal of Innovative Computing, Information and Control, Volume 4, Number 10, pp. 2551—2564.

- Lorterapong, P. and Moselhi, O. , 1996. *Project-Network Analysis using Fuzzy Sets Theory*. Journal of Construction Engineering and Management, Vol. 122, No.4, December, ASCE.

- Ross, T. J., 2004. *Fuzzy logic with Engineering Application*. John Wiley & Sons Ltd, 2nd Edition, p 96.

- Shankar N. R., Sireesha V. and Rao P. P. B. , 2010. *Critical Path Analysis in the Fuzzy Project Network*. Advances in Fuzzy Mathematics, Volume 5, number 3, pp. 285–294.

- Sivanandam, S.N, Deepa, S. N, and Sumathi, S, 2007. *Introduction to Fuzzy Logic using MATLAB* " Springer -Verlag Berlin Heidelberg.

- Soltani, A. and Haji, R. , 2007. *A Project Scheduling Method Based on Fuzzy Theory*, Journal of Industrial and Systems Engineering, Vol. 1, No. 1, pp 70-80.

- Zhang, H., Tam, C.M. and Li H., 2005.*Modeling uncertain activity duration by fuzzy number and discrete-event simulation*. European Journal of Operational Research 164 , 715–729, Elsevier.

- Hendrickson, Chris and Au, Tung, 2003. *Project Management for Construction*. Version 2.1 prepared summer, 2003. Chris Hendrickson, Department of Civil and Environmental Engineering, Carnegie Mellon University, Pittsburgh, PA l52l3 Copyright C. Hendrickson

- Mohammed Rashed, Sawsan , 2004.*Solving Critical path Problems with linear Programming*. Journal of Engineering, Vol. 10, No. 4

Table 1. Case study project information.

Activity	Followed by	Time (Days)		Cost ($)		The required no. of resources
		Normal	Crash	Normal	Crash	
A	B C	3	1	1000	3000	1
B	D E	4	3	4000	6000	3
C	E F	2	2	2000	2000	2
D	I	6	4	3000	6000	3
E	G H	5	4	2500	3800	3
F	H	3	2	1500	3000	2
G	I	7	4	4500	8100	4
H	I	5	4	3000	3600	3
I		8	5	8000	12800	5

Table 2. Fuzzy duration and cost for case study project activities.

Activity	Activity fuzzy duration				Activity fuzzy cost			
A	1	1	2	3	3000	3000	2000	1000
	1	2	2	3	3000	2000	2000	1000
	1	2	3	3	3000	2000	1000	1000
B	3	3	3	4	6000	6000	6000	4000
	3	3	4	4	6000	6000	4000	4000
	3	4	4	4	6000	4000	4000	4000
C	2	2	2	2	2000	2000	2000	2000
D	4	4	5	6	6000	6000	4500	3000
	4	5	5	6	6000	4500	4500	3000
	4	5	6	6	6000	4500	3000	3000
E	4	4	4	5	3800	3800	3800	2500
	4	4	5	5	3800	3800	2500	2500
	4	5	5	5	3800	2500	2500	2500
F	2	2	2	3	3000	3000	3000	1500
	2	2	3	3	3000	3000	1500	1500
	2	3	3	3	3000	1500	1500	1500
G	4	5	6	7	8100	6900	5700	4500
H	4	4	4	5	3600	3600	3600	3000
	4	4	5	5	3600	3600	3000	3000
	4	5	5	5	3600	3000	3000	3000
I	5	6	7	8	12800	11200	9600	8000

Table 3. Case study project fuzzy total time and total cost.

Case		Fuzzy total time				Fuzzy total cost			
Planned case(Normal resource availability)		21	22	24	27	68500	68200	69000	70000
		21	23	25	27	68500	68700	69200	70000
		21	24	26	27	68500	68900	69700	70000
Resource restriction	Case one	27	27	27	29	72100	72100	72100	73000
		27	27	29	29	72100	72100	73000	73000
		27	29	29	29	72100	73000	73000	73000
	Case two	25	25	26	27	72000	72000	71000	70000
		25	26	26	27	72000	71000	71000	70000
		25	26	27	27	72000	71000	70000	70000

Table 4. Final rank for the three cases.

Planned case	Time	21	22	23	24	24	25	26	27
	Cost	68500	68200	68700	68900	69000	69200	69700	70000
	Rank	0.42	0.42	0.33	0.25	0.24	0.17	0.09	0.01
Case one	Time	27	29						
	Cost	72100	73000						
	Rank	0.5	0.02						
Case two	Time	25	26	27					
	Cost	72000	71000	70000					
	Rank	0.02	0.26	0.02					

Table 5. Final rank of the general case.

Two cases	Time	25	26	27	27	29
	Cost	72000	71000	70000	72100	73000
	Rank	0.18	0.34	0.26	0.16	0.01

Table 6. Model verification results.

Case		Total time	Total cost
Planned case (Normal resource availability)		22	68200
Resource restrictions	Case one	27	72100
	Case two	27	70000

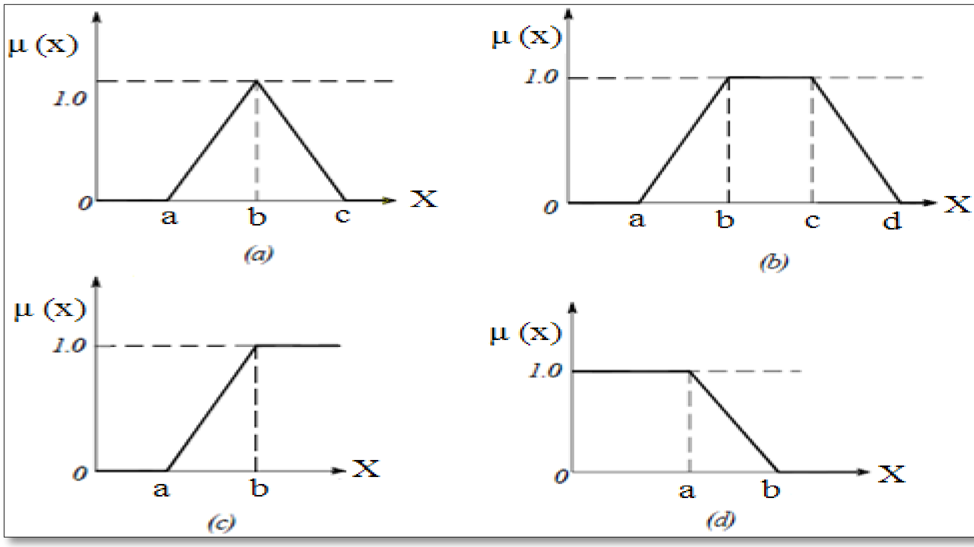

Figure 1. Common fuzzy membership functions.

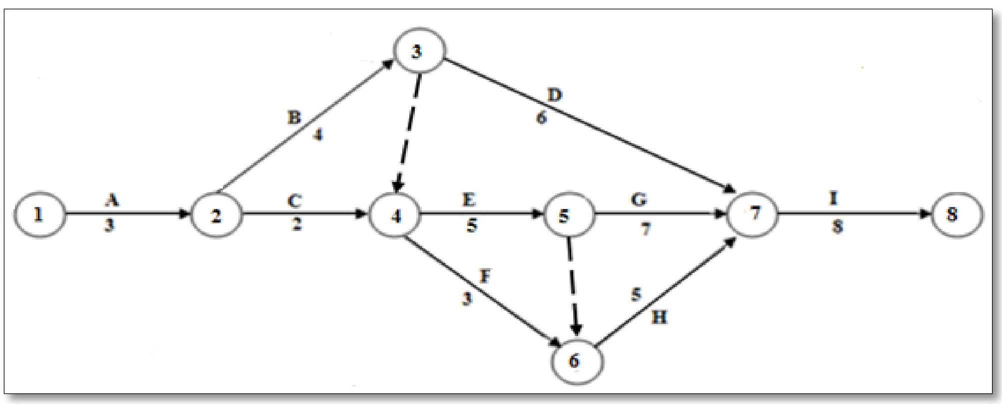

Figure 2. AOA network for case study project.

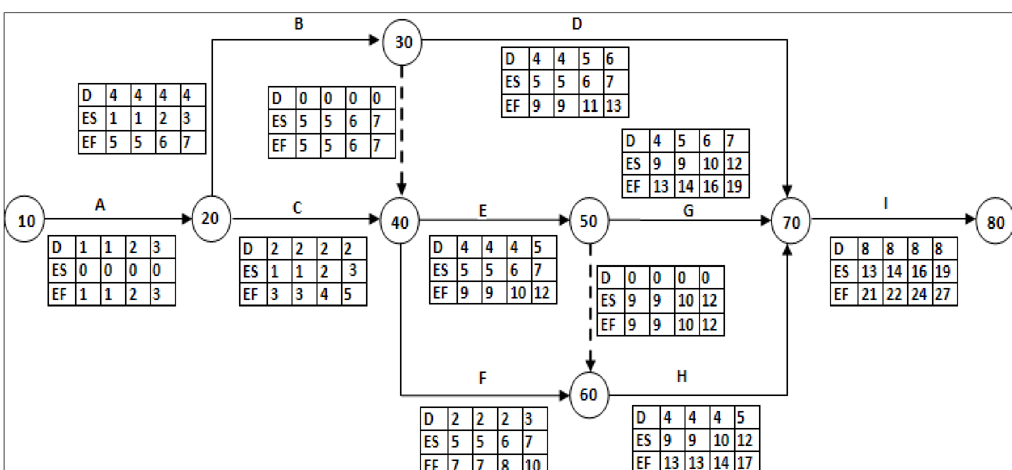

Figure 3. AOA network for normal recourse availability with min fuzzy time.

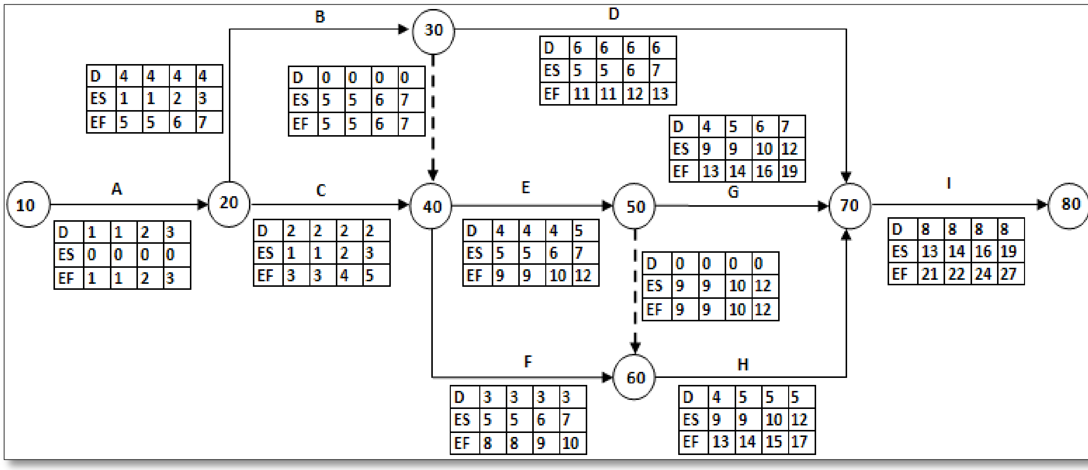

Figure 4. Adjusted AOA network for normal recourse availability with min fuzzy time.

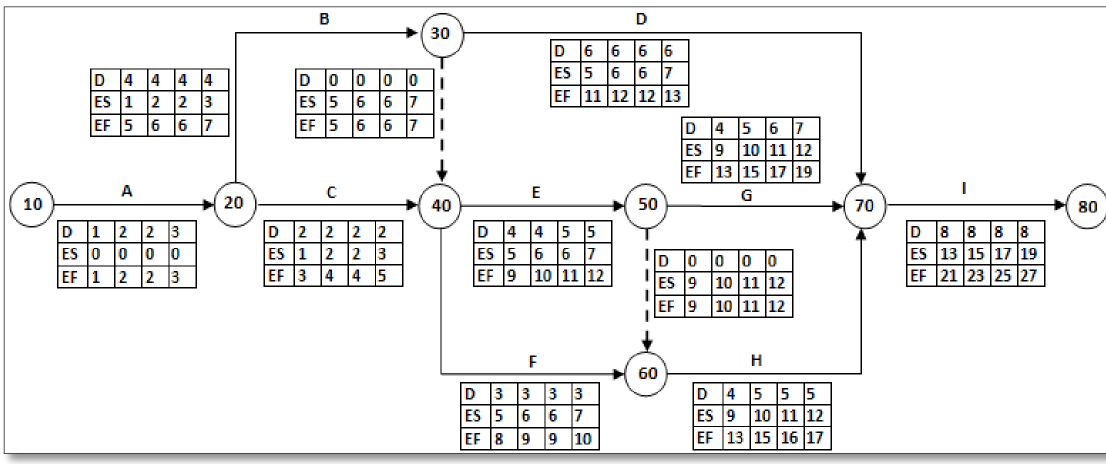

Figure 5. Adjusted AOA network for normal recourse availability with middle fuzzy time.

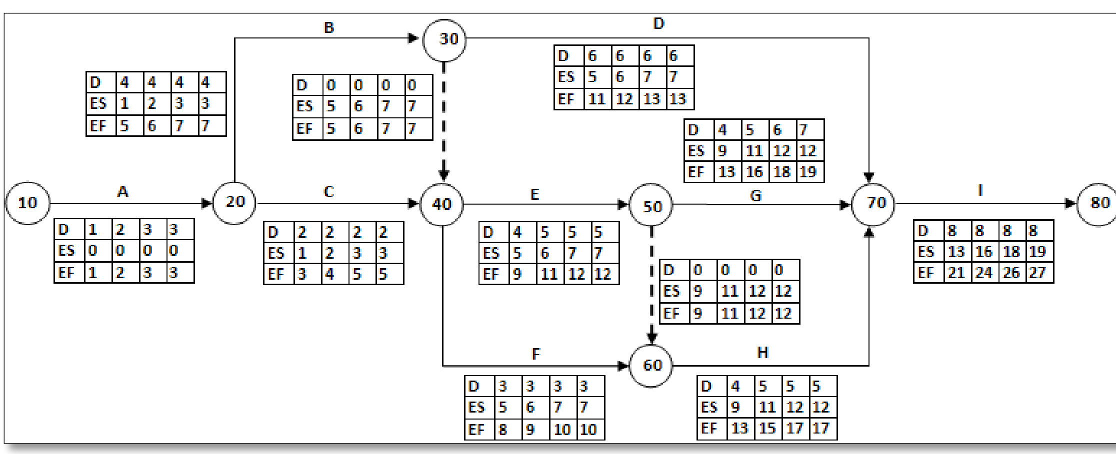

Figure 6. Adjusted AOA network for normal recourse availability with max fuzzy time.

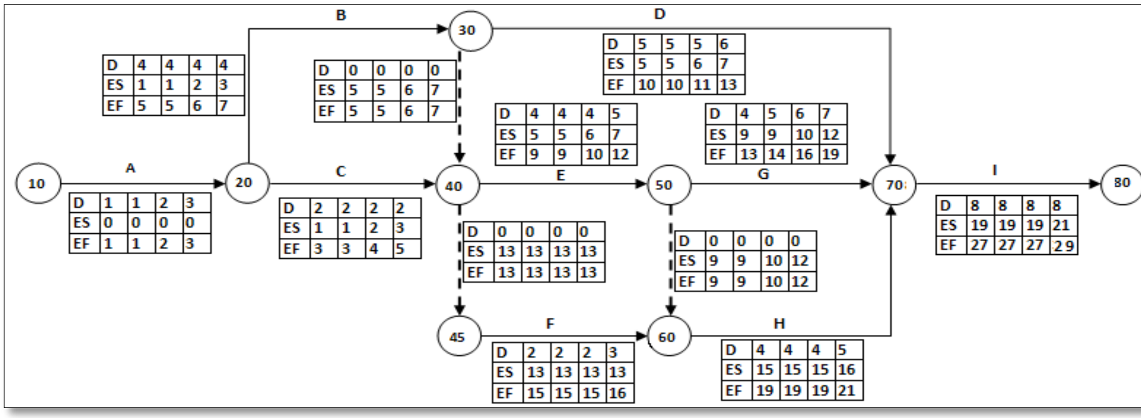

Figure 7. AOA network for the first scenario with min fuzzy time.

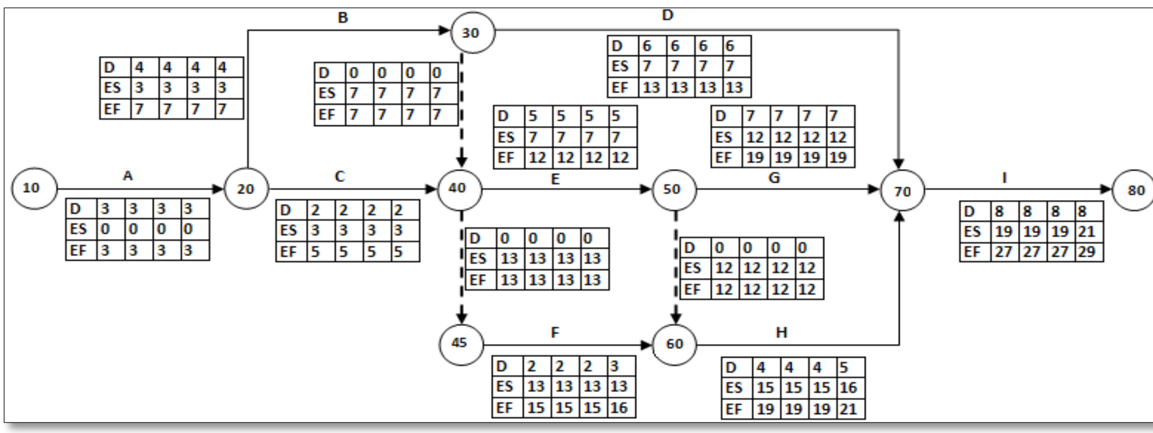

Figure 8. Adjusted AOA network for the first scenario with min fuzzy time.

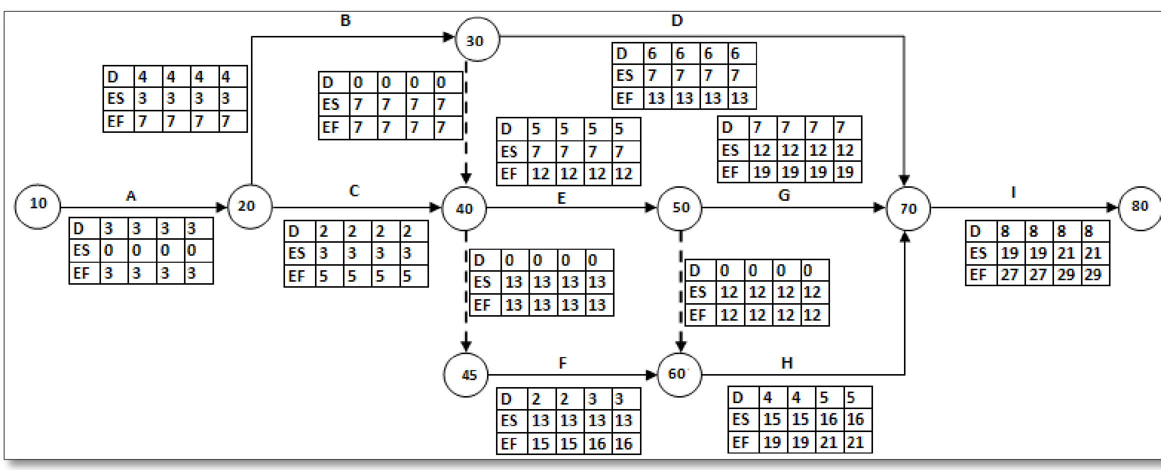

Figure 9. Adjusted AOA network for the first scenario with middle fuzzy time.

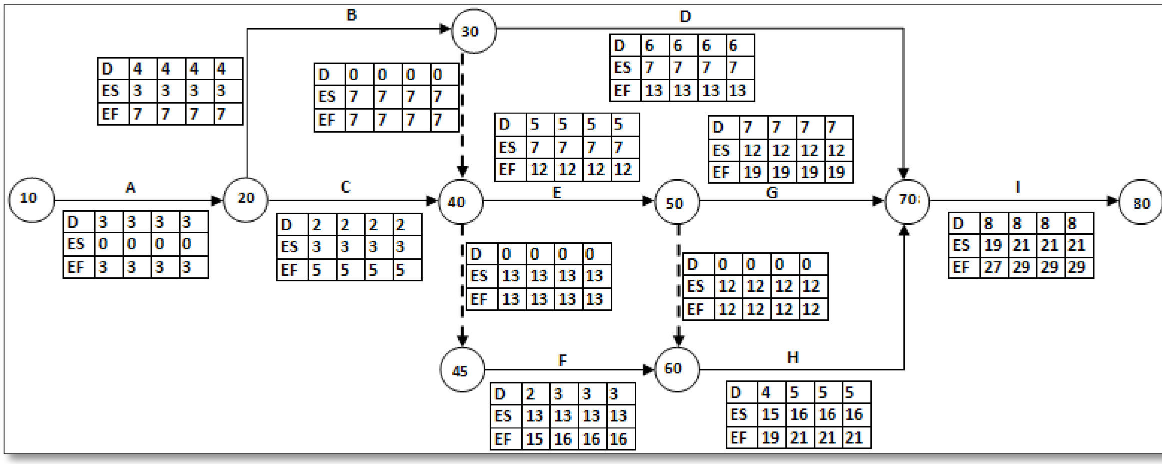

Figure 10. Adjusted AOA network for the first scenario with max fuzzy time.

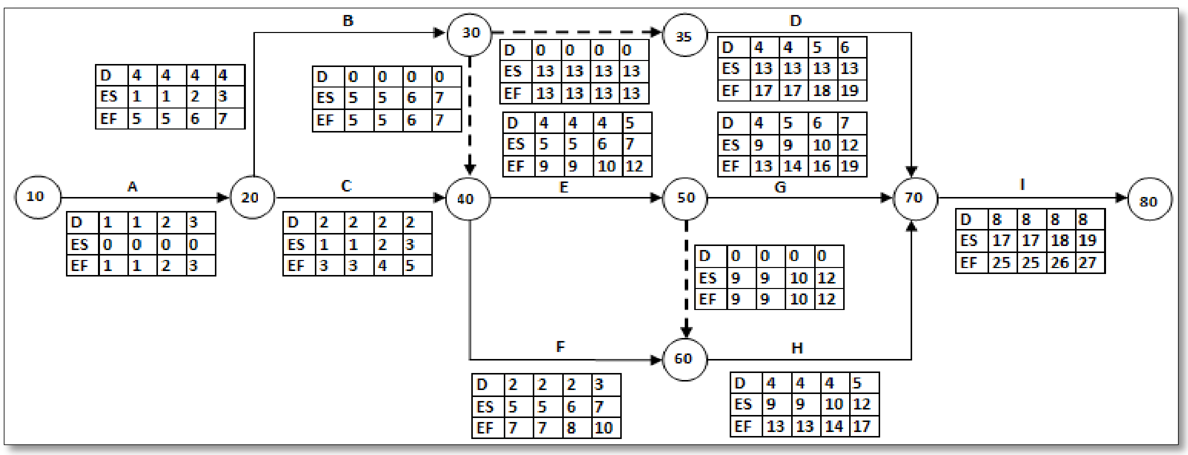

Figure 11. AOA network for the second scenario with min fuzzy time.

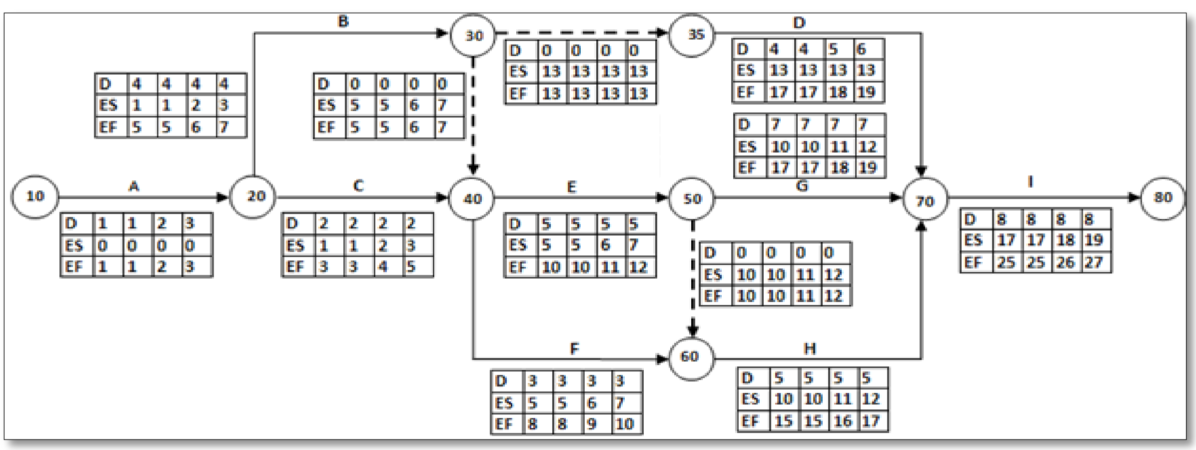

Figure 12. Adjusted AOA network for the second scenario with min fuzzy time.

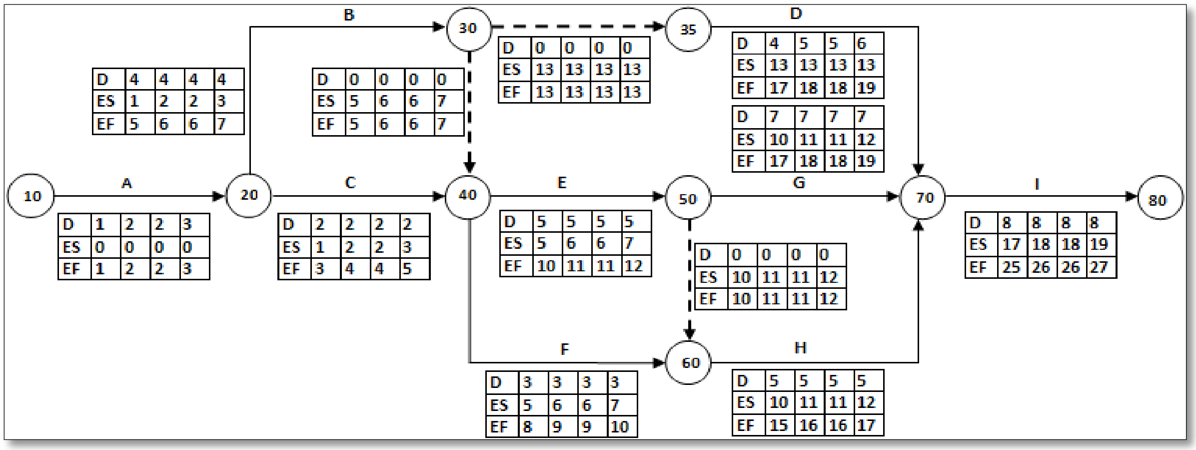

Figure 13. Adjusted AOA network for the second scenario with middle fuzzy time.

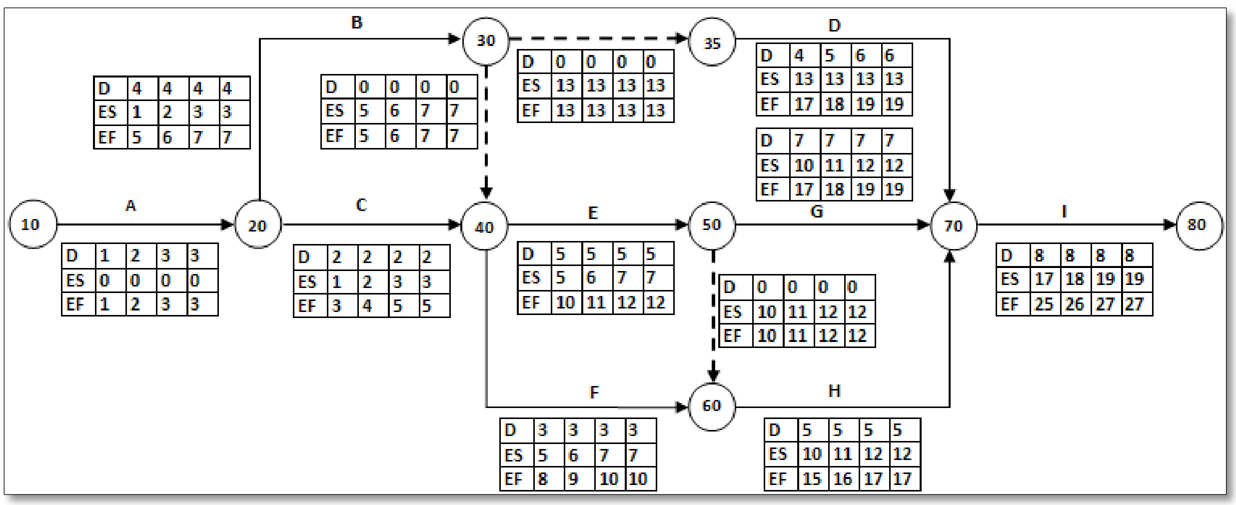

Figure 14. Adjusted AOA network for the second scenario with max fuzzy time.

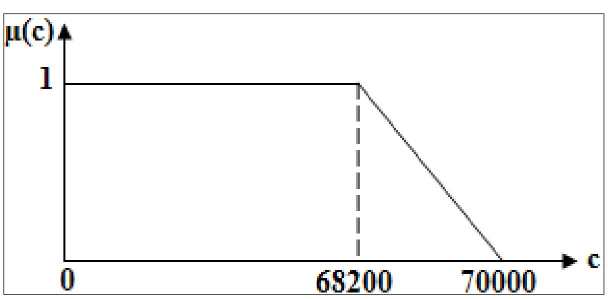

Figure 15. Graphical representation of cost model (planned case).

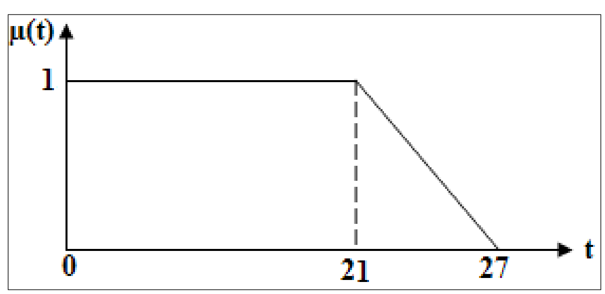

Figure 16. Graphical representation for time model (planned case).

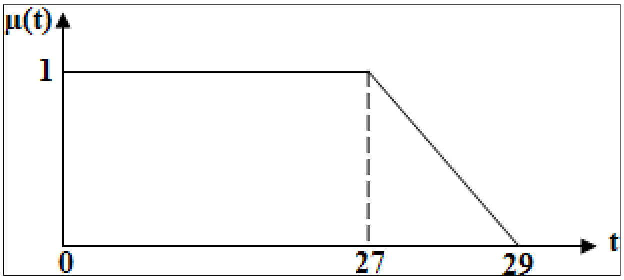

Figure 17. Graphical representation of time model (first scenario).

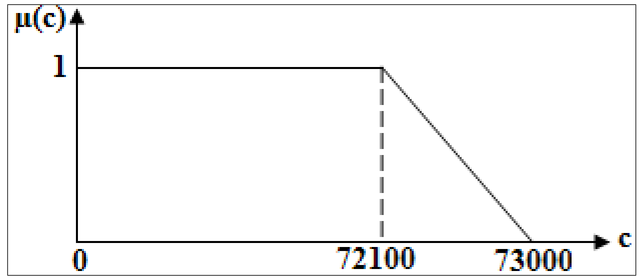

Figure 18. Graphical representation for cost model (first scenario).

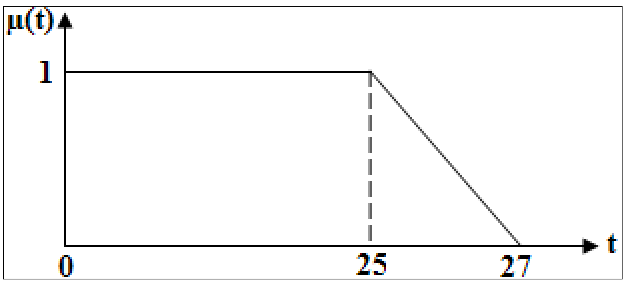

Figure 19 . Graphical representation of time model (second scenario).

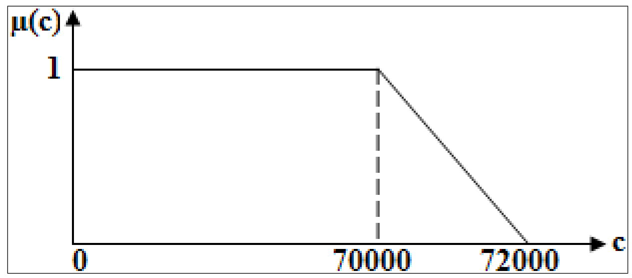

Figure 20. Graphical representation for cost model (second scenario).

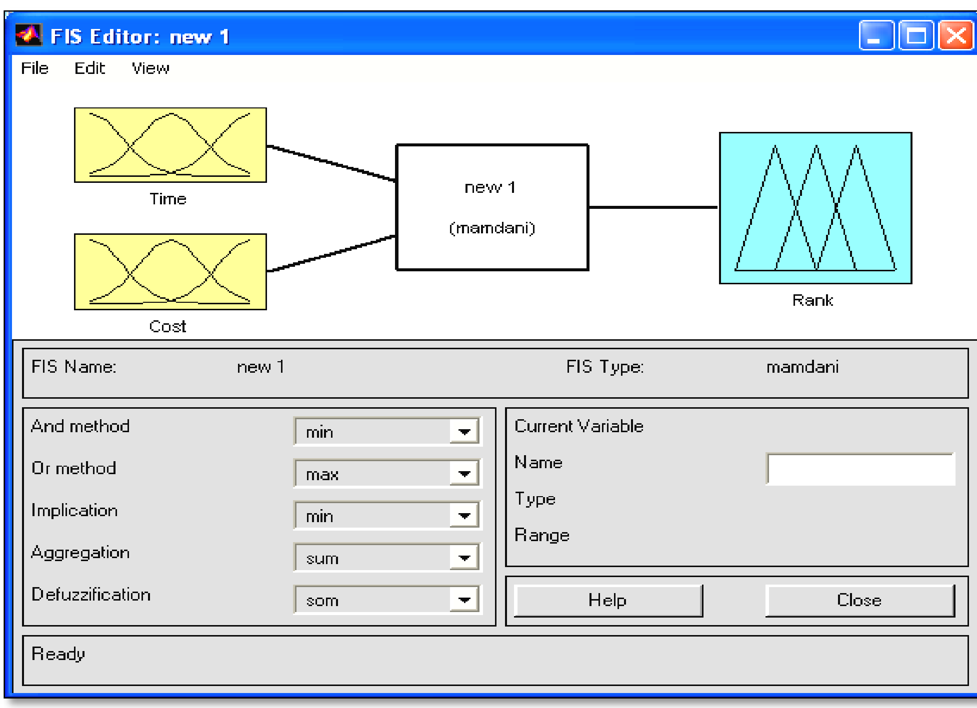

Figure 21. Fuzzy inference system for the mathematical model.

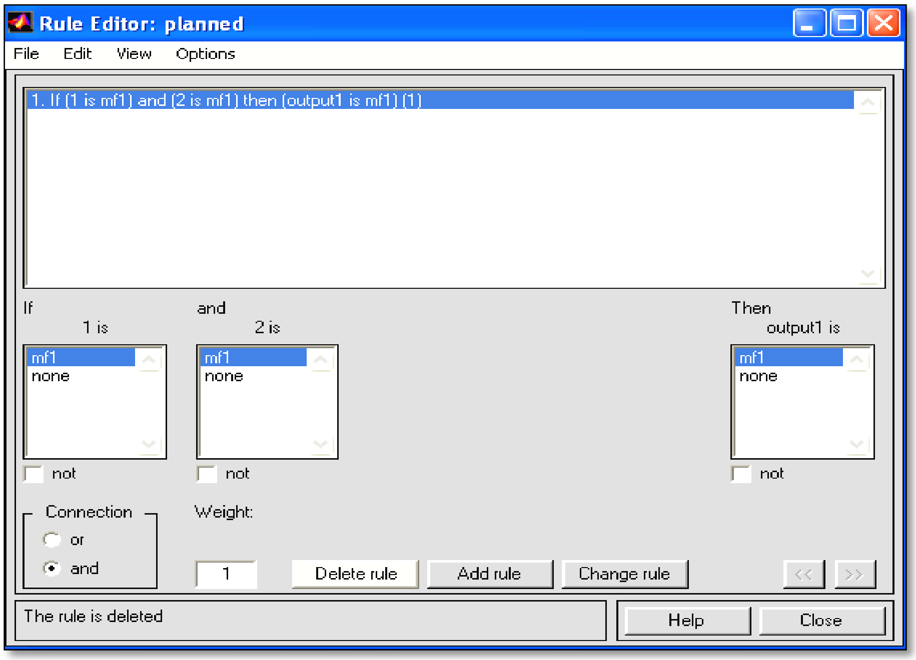

Figure 22. Rule editor for the mathematical model.

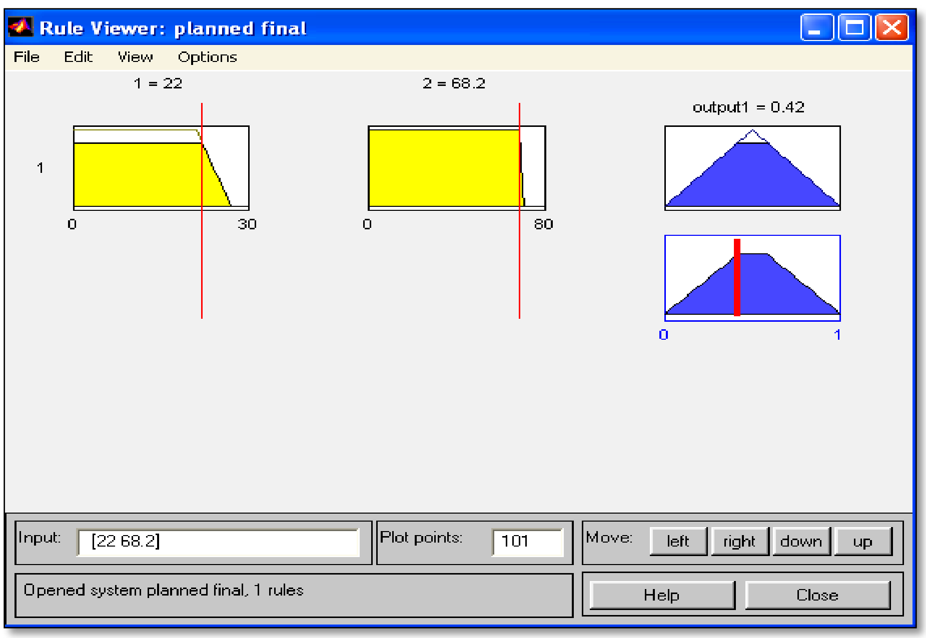

Figure 23. Rule viewer for the mathematical model.

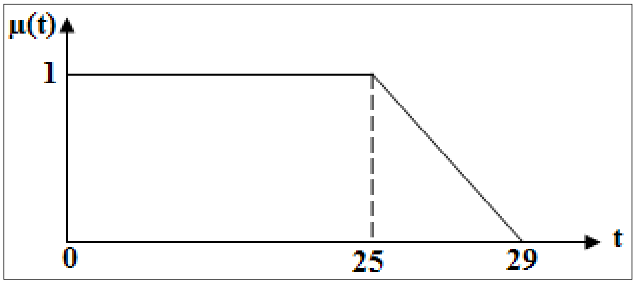

Figure 24. Graphical representation of time model (General case).

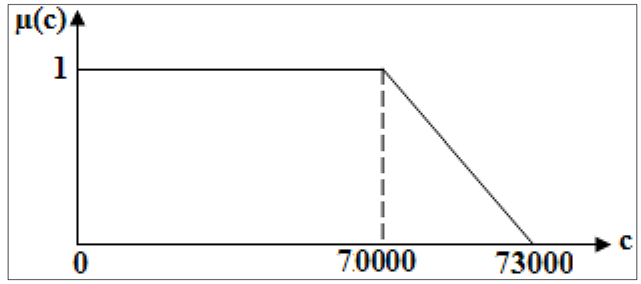

Figure 25. Graphical representation for cost model (General case).

Comparative Study for Risk Criteria of Al-Qudus Plant between the Present and Planning of MOE

Yesar Noori Lafta
Assistant Instructor
AL Khawarizmi College of Engineering, University of Baghdad
E-mail: yasarnoori@yahoo.com

ABSTRACT

The main function of a power system is to supply the customer load demands as economically as possible.
Risk criterion is the probability of not meeting the load. This paper presents a methodology to assess probabilistic risk criteria of Al-Qudus plant before and after expansion; as this plant consists of ten generating units presently and the Ministry Of Electricity (MOE) is intending to compact four units to it in order to improve the performance of Iraqi power system especially at Baghdad region. The assessment is calculated by a program using Matlab programming language; version 7.6.
Results show that the planned risk is (0.003095) that is (35 times) less than that in the present plant risk; (0.1091); which represents respectable improvement.
This probabilistic method can also be used to find the planned risk level of every plant to be compact in the Iraqi electrical network on the future; or any other power systems; and compare it with the present criterion which is very useful to determine the necessary generation capacity expansion.

Keywords: unit outage, risk level, forced outage rate, n generators, planned risk assessment.

دراسة مقارنة لمعامل الخطورة لمحطة القدس
بين الحاضر ومخطط وزارة الكهرباء

يسار نوري لفتة
مدرس مساعد
كلية هندسة الخوارزمي, جامعة بغداد

الخلاصة

إن الغرض الرئيس من نظام القدرة هو تجهيز المستهلك بالحمل المطلوب وبشكل إقتصادي.
معامل الخطورة هو إحتمالية عدم تجهيز الحمل. إن هذا البحث يعرض طريقة تثمين عامل الخطورة, بطريقة الإحتمالية, لمحطة القدس قبل التوسعة وبعدها ؛ فهذه المحطة تتضمن عشر وحدات توليدية حالياً وستقوم وزارة الكهرباء بحسب خطتها التطويرية باضافة اربع وحدات توليدية في المستقبل لتحسين أداء منظومة القدرة الكهربائية وبالخصوص في منطقة بغداد. إن حساب عامل الخطورة تم باستعمال برنامج بلغة ماتلاب 7.6.
النتائج توضح أن معامل الخطورة المخطط هو(0,003095) وهذا اقل (35) مرة من معامل الخطورة الحالي؛(0,1091) ؛ والتي تمثل نسبة تطوير جيدة .
يمكن استعمال هذه الطريقة لايجاد عامل الخطورة المخطط له لأي محطة توليد تحتويها الشبكة الكهربائية العراقية في المستقبل او أي منظومة قدرة أخرى ومقارنته مع عامل الخطورة الحالي وهو مفيد لتحديد التوسع الضروري في سعة المحطة.

1. INTRODUCTION

Electrical energy supply should be sufficient to meet demand at all times. However, since supplies and demands are uncertain, there is always a small probability of loss i.e. the supply will be insufficient to meet demand.

Generation adequacy of a power system is an assessment of the ability of the generation on the power system to match the consumption on the same power system. This general definition implies that such an “ability” of the power system should be ensured at all times. However, capacity values are typically defined to correspond to an extended period such as a year, where the relevant probability distributions vary from day to day, or hour to hour, within that extended period, **Cailliau et al., 2011 and Zachary,** and **Dent, 2012**.

Adequacy is associated with static conditions, which do not include system disturbances. The adequacy studies of power supply system are conducted individually in three functional zones: generation, transmission, and distribution. The functional zones can be combined to give the hierarchical levels.

A model of bulk generation must consider the size of generation units and the two main processes involved in their operation, namely the failure and the restoration processes. A failure in a generating unit results in the unit being removed from service in order to be repaired or replaced; this event is known as an outage, **Dutta,** and **Sharma, 2012**.

Conventional power plants experience unplanned outages, because of mechanical or other malfunction. Episodes such as this are called forced outages. There is always a non–zero probability that any single generating unit will be on forced outage.

Taking all such probabilities from each generator allows the calculation of the probability that enough generator units are on forced outage so that the utility will be unable to meet its load, **Milligan,** and **Parsons, 1997**.

The planning procedure for the expansion of generating capacity by adding new units, based on the criterion that a certain risk level should not be exceeded, is selected largely by economic considerations.

A widely used deterministic criterion is the N-1 criterion, which means that there must be sufficient spinning reserve on the system such that no load will lose power if any one line or any one generator fails. The probabilistic approach is a more realistic one in which a risk index enables a comparison to be made between various operating scenarios. The acceptable risk level is a management decision based on economic requirements.

Once a risk level has been defined, sufficient generation can be scheduled to satisfy this risk level. This process can be done using the concept of unit commitment risk, **Lewis, 1996**.

2. LITERATURE SURVEY

It is valuable to present a review of some studies dealing with the assessment of risk level.

W. Luan, et al., 2006 outline risk assessment method for diesel generation stations based on RISK_A. a model which was developed for assessing station reliability through assigning failure probabilities to all equipment and modeling their relationships. End-of-life failure probability for diesel generation unit has been derived based on its actual maintenance history and age profile.

C. N. Ning, et al., 2006 demonstrated two application examples of probabilistic risk assessment. In the first, a risk based method is proposed to take the uncertainty of contingency occurrence and impacts into account to provide an essential set of contingency cases for a transient stability special protection system (SPS) implementation. In the second, an approach for determining the power transfer limit of a longitudinal electric power system is presented.

M. Cepin, 2006 presented a definition of quantitative risk criteria considering probabilistic safety assessment. Development of risk criteria is considered separately for permanent and temporary changes in the nuclear power plant. Developed criteria can represent a standpoint for risk-informed decision-making.

O.B. Ajadi, et al., 2012 identified that hazards and risks are associated with installation, operation and maintenance of diesel powered generator using a 40kVA generator. Hazards of varying degrees were identified with every section and jobbing of the whole activities. The associated risk was classified, about 60 percent high risk to 40 percent medium risk.

This paper presents a comparative study for the risk criterion of al-Qudus plant for the present and planned cases depending on the technical operating data of 2011 that is provided by Republic of Iraq / MOE/ Training and Development Office / Control and Operation Office, and Generation and Production of Electrical Energy /planning section.

3. BASIS of RISK LEVEL ASSESSMENT

The probabilistic approach to unit commitment considers the size of generation units and the two states model (unit up and down states) where, λ and μ are the failure and repair rates respectively. The long-run failure probability, known as the unavailability of a unit, Un and the long-run success probability, known as the availability of a unit, A can be expressed in terms of unit's failure and repair rates as follows:

$$Un = \frac{\Sigma(\text{down time})}{\Sigma(\text{down time} + \text{up time})} \tag{1}$$

$$A = \frac{\Sigma(\text{up time})}{\Sigma(\text{down time} + \text{up time})} \tag{2}$$

$$Un = \frac{\lambda}{\lambda+\mu} \tag{3}$$

$$A = \frac{\mu}{\lambda+\mu} \tag{4}$$

The unit unavailability is commonly referred to as the 'forced outage rate', FOR.

$$FOR = \frac{\text{forced outage hours}}{\text{in service hours} + \text{forced outage hours}} \tag{5}$$

The step building of a generation model is to combine the capacity and availability of the individual units to estimate available generation in the system. The result is a capacity model; in which each generating unit is represented by its nominal capacity ci and its unavailability index Uni (or forced outage rate).

For each of the (N) generators in the system, the available capacity ci, for i =1…N, is a random variable that can take the value 0 with probability Uni and the value ci with probability $A_i = 1 - Un_i$

Note: (N) is the number of generators in the system.

The individual state probability is:

$$P_{(X)} = \begin{cases} A & xi = ci \\ Un & xi = 0 \end{cases} \tag{6}$$

Where:

$P_{(X)}$: probability of system for state x.

xi: is the state of the i th generator.
The cumulative state probability (or the distribution function) is:

$$P_{(X)}=\begin{cases} 0 & xi < 0 \\ Un & 0 \leq xi < ci \\ 1 & xi \geq ci \end{cases} \qquad (7)$$

The total generating capacity available (effective capacity) in the system is:

$$C_A = \sum_{i=1}^{N} ci$$

As an example consider a system consisting of three 25 MW units, each one having forced outage rates of 0.02. **Table 1.** Shows capacity outage table, **Lewis 1996, Prada 1999, Singh 2008, Ehsani, et al. 2009.**
Computer Matlab programming software is realized for computing the capacity outage probabilities and the flow chart structure of it is shown in **Fig. 1**.

4. AL-QUDUS PLANT DESCRIPTION

Republic of Iraq / MOE/ Training and Development Office / Generation and Production of Electrical Energy /planning section, 2011

The plant consists of the following equipment:
a. Six (6) GE rating of 125MW
b. Four (4) GE rating of 43MW
i.e.
N=10 in Al-Qudus (present state).
The generators have the following nomenclature and rating:

Nomenclature	Rating	Voltage
a. U1-4 Frame 9E	154MVA	15kV
b. U5-8 LM6000	63MVA	11kV
c. U9-10	141MVA	15kV

Units' commission dates are provided below:

Unit name	Day	Month	Year
U1	21	May	2002
U2	5	July	2002
U3	10	August	2004
U4	8	September	2004
U5	29	August	2004
U6	8	June	2005
U7	25	August	2005
U8	11	August	2005
U9	14	May	2009
U10	14	May	2009

Al-Qudus gas power station single line diagram with its planned expansion is shown in **Fig. 2**. Based upon the life expectancy units 1-4 have approximately 8 more years of operation before they need to be given a life extension inspection. Units 9 and 10 have approximately 11 more years of operation prior to being given a life extension inspection.

5. CASE STUDY:

5.1 Present Case

Capacity outage probability table is an array of capacity levels and the associated probabilities of existence. In practical system the probability of having a large quantity of capacity forced out of service is usually quite small because this case requires several units to be out of service.
Risk level assessment of generating plants is of great importance especially for Al-Qudus plant that is part of Baghdad region network which suffers lack in supplying the load demand.
In this work plant generators are divided into groups. Each group consists of “N” units which are identical, i.e., have the same generation capacity, Un or FOR, and A.
For simplicity, it is assumed that each unit has only two states and can be either fully available or fully unavailable with probabilities:
A= 1-FOR and Un = FOR,
The following values of the forced outages; including the forced outages due to the lack in fuel; and availabilities that are calculated for the year 2011 are:
FOR for the units U1, U2, U3, U4, U9, U10= 0.092
i.e. A=0.908.
FOR for the units U5, U6, U7, U8= 0.074
i.e. A=0.926
Al-Qudus capacity outage probability table can be formulated; after calculations; for the present case as shown in **Table 2**.
Fig.3-1 represents the probability graph of available capacity meeting generation capacity, and **Fig.3-2** shows the cumulative probability graph.

5.2 Planned Case

The plan of MOE is to install four more frame engines at this site; i.e. N=14 in Al-Qudus (future state); with capacity of 125MW for each as illustrated in Fig.1 with two rectangles; each rectangle is surrounding two units.
This addition and the planned fuel availability will raise the availability; hence reducing unavailability; of all the plant units and from the experience it is expected to be as follows:
FOR for the units
U1, U2, U3, U4, U9, U10, U11, U12, U13, U14= 0.02
i.e. A=0.98.
FOR for the units
U5, U6, U7, U8= 0.05
i.e. A=0.95
Al-Qudus planned capacity outage probability table can be formulated; after calculations; as shown in **Table 3** which is truncated by omitting states more than 34 state, since it is not in the vision of risk level.
Fig.4-1 represents the probability graph of the planned available capacity meeting generation capacity, and **Fig.4-2** shows the planned cumulative probability graph.

6. RISK CRITERIA RESULTS

Risk is defined as the probability of not meeting the load, thus it is given by the value of cumulative probability corresponding to the outage state one increment below that which satisfies the load.

As an example, consider the previous example mentioned and illustrated in **Table 1**, if the load demand is 50 MW then:

Risk level= Cumulative Probability (when Capacity in is less than 50 MW)

i.e. Risk level= 0.0012

The two probabilistic; i.e. present case and planned case; risk level are determined assuming constant load demand and the future demand growth is neglected to clarify the plant development.

The average load demand at Al-Qudus bus-bar for 2011 was 750 MW, **MOE 2011**, and then the risk in each of the two systems; can be found from tables (2) & (3); are:

Risk in present case= 0.1091

Risk in planned case= 0.003095

7. CONCLUSION:

To reveal the improvement of Al-Qudus plant, the values of risk criteria must be compared; thus as it is found that:

Risk criterion of the present system is: 0.1091

Risk criterion of the planned system is: 0.003095

It is apparent from the comparison between the two results that present risk is (35 times) greater than that in the planned plant; which means that the four additional units is improving the performance of Al-Qudus plant with a good factor.

This result also confirms that the variation in risk criteria depends upon: forced outage rate, number of units, and definitely the load demand.

This study is useful to calculate planned risk criterion improvement which represents the performance upgrading for any plant of all power systems.

REFERENCES:

- Ajadi, O.B., Adekunle, A. A., and Peter, K.O., September 2012, *Identification of Hazards and Risk Assessment for a 40 KVA Diesel Powered Lighting Set*, Greener Journal of Science Engineering and Technological Research, Vol. 2, pp. 39-47.

- Cailliau, M., et al, May 2011, *RES Integration and Market Design*, http://www.eurelectric.org/CatPub/ Document.aspx? Folder ID=1507& Document ID =30399.

- Cepin, M. March 2006, *Development of Risk Criteria in Nuclear Power Plants – Problems and Solutions*, International Journal of Materials & Structural Reliability Vol.4, No.1, pp. 53-63.

- Dutta, S., and Sharma, R., .January 2012, *Optimal Storage Sizing for Integrating Wind and Load Forecast Uncertainties* , IEEE PES conference on innovative smart grid technologies, pp. 928-934**.**

- Ehsani, A., Karimizadeh, A., Fallahi, H., and Jalali, A., 2009, *A Comparison of Deterministic and Probabilistic Methods for Determining the Required Amount of*

Spinning Reserve, World Academy of Science, Engineering and Technology 60, pp. 38-43.

- Lewis, E. E., (1996)," Introduction to Reliability Engineering ", John Wiley and Sons, Inc., second edition.

- Luan, W. , Kheong, S.C. , and Helen, I., June 2006, *Risk Assessment of Rural Diesel Generation*, IEEE Power Engineering Society Meeting.

- M. Milligan, and B. Parsons (1997)," A Comparison and Case Study of Capacity Credit Algorithms for Intermittent Generators", National Renewable Energy Laboratory.

- Ning, C. N., Hsieh, C. A., Hsiao, T. Y., and Lu, C. N., June 2006, *Two Application Examples of Probabilistic Risk Assessment in Power System Operation*", 9th International Conference on Probabilistic Methods Applied to Power Systems KTH, Stockholm, Sweden.

- Prada, J. F., July 1999, *The Value of Reliability in Power Systems - Pricing Operating Reserves* -, MIT Energy Laboratory, Massachusetts Institute of Technology, Report No. EL 99-005 WP**.**

- Republic of Iraq / Ministry of Electricity/ Training and Development Office / Generation and Production of Electrical Energy /planning section, 2011.

- Singh, C., May 2008, *Operational Reliability: Issues, Challenges and Possibilities*, Report No. 973, Beijing**.**

- Zachary, S., and Dent, C.J., February 2012, *Probability theory of capacity value of additional generation*, Journal of Risk and Reliability, (SAGE Publications), vol. 226, pp. 133-143.

Table 1. Example for three-unit system capacity outage [J. F. Prada 1999].

Units out	Capacity out	Capacity in (CA)	Probability P[C = CA]	Cumulative probability P[C ≤ CA]
None	0 MW	75 MW	$(0.98)^3 = 0.9412$	1.000
1 or 2 or 3	25 MW	50 MW	$3*(0.02)(0.98)^2$ =0.0576	1- 0.9412 =0.0588
1,2 or 1,3 or 2,3	50 MW	25 MW	$3*(0.98)(0.02)^2$ = 0.0012	0.0588- 0.0576 =0.0012
1,2,3	75 MW	0 MW	$(0.02)^3$=0.00000	0.0000

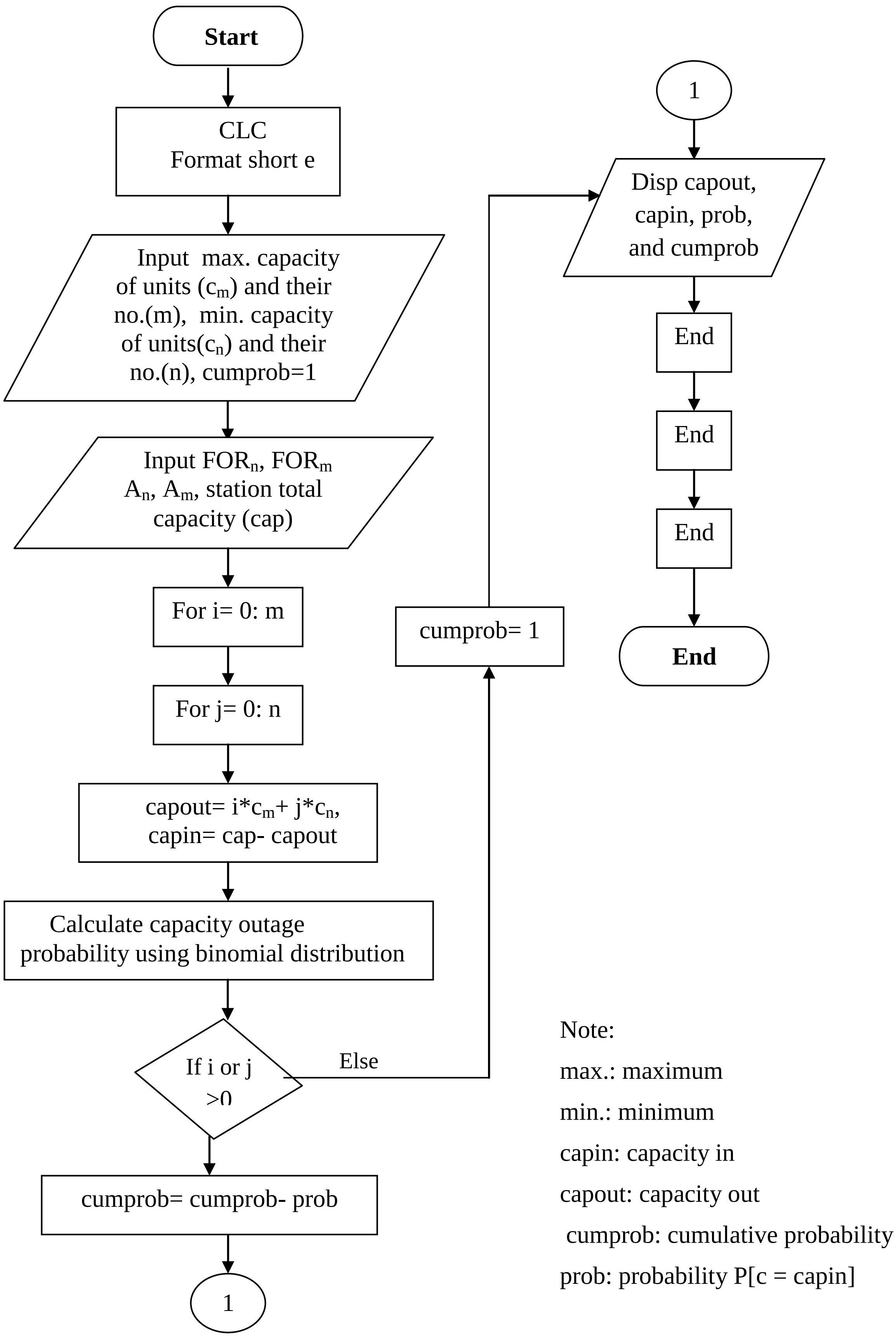

Figure 1. Flow chart structure of the program that computes the capacity outage probabilities.

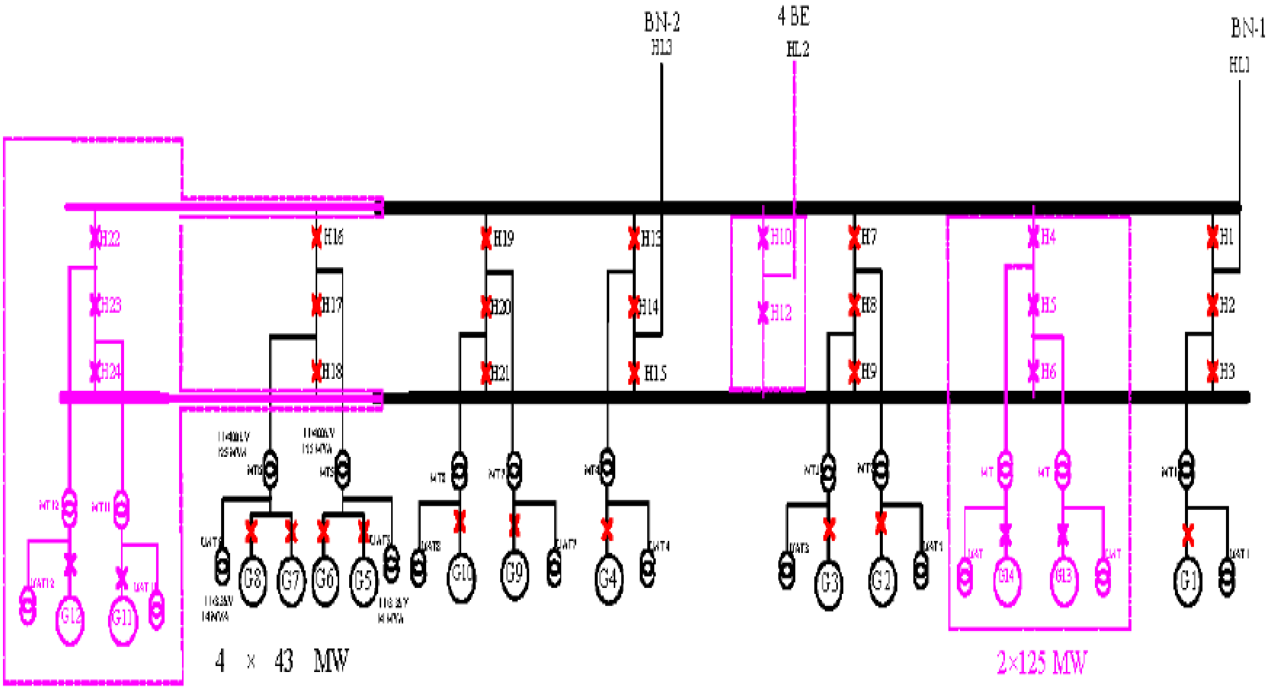

Figure.2. Al-Qudus single line diagram with its planned extension [Republic of Iraq / Ministry of Electricity/ Training and Development Office / Generation and Production of Electrical Energy /planning section, 2011].

Table 2. Present case actual capacity outage of Al-Qudus plant.

State	Capacity out(MW)	Capacity in(MW)	Probability (C=CA)	Cumulative probability
0	0	922	0.4121	1
1	43	879	0.1317	0.5879
2	86	836	0.0158	0.4562
3	125	797	0.2505	0.4404
4	129	793	0.0008412	0.1899
5	168	754	0.0801	0.1891
6	172	750	1.7e-5	0.10917
7	211	711	9.6e-3	0.1091
8	250	672	0.0634	0.0995
9	254	668	5.21e-4	0.0361
10	293	629	0.0202	0.0355
11	297	625	1.02e-5	0.0153
12	336	586	0.0024	0.0153
13	375	547	0.00697	0.0129
14	379	543	1.29e-4	0.00503
15	418	504	0.00217	0.0058608
16	422	500	2.6e-6	0.0036908
17	461	461	2.63e-4	0.0036882
18	500	422	3.91e-4	0.0034282
19	504	418	1.4e-5	0.0030372
20	543	379	1.25e-4	0.0030232
21	547	375	3e-7	0.0028982
22	586	336	1.5e-5	0.0028979
23	625	297	2.64e-5	0.0028829
24	629	293	7.98e-7	0.0028565
25	668	254	5.389e-8	0.002856
26	672	250	1.59e-8	0.002856
27	711	211	1.012e-6	0.002856
28	750	172	4.176e-8	0.002856
29	754	168	5.8e-8	0.002856
30	793	129	7.91e-10	0.002856
31	797	125	1.1e-9	0.002856
32	836	86	1.71e-8	0.002856
33	879	43	8.525e-11	0.002856
34	922	0	1.81e-11	0.002856

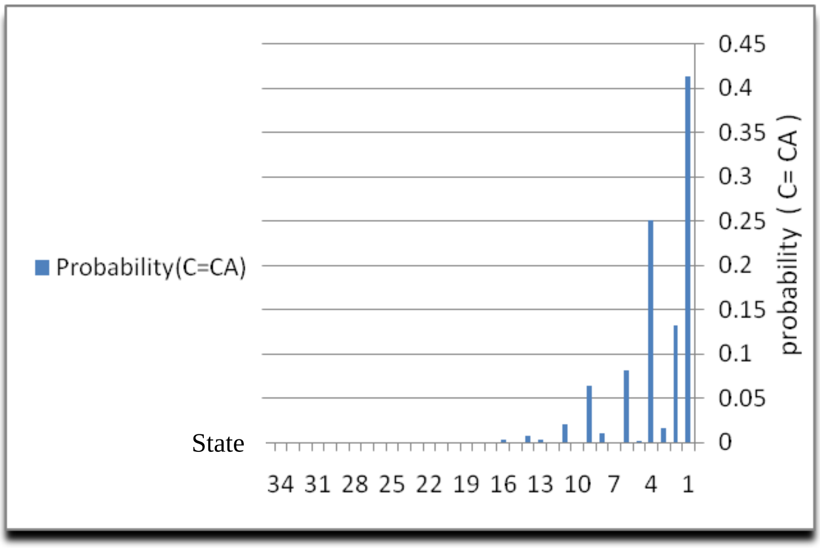

-1-

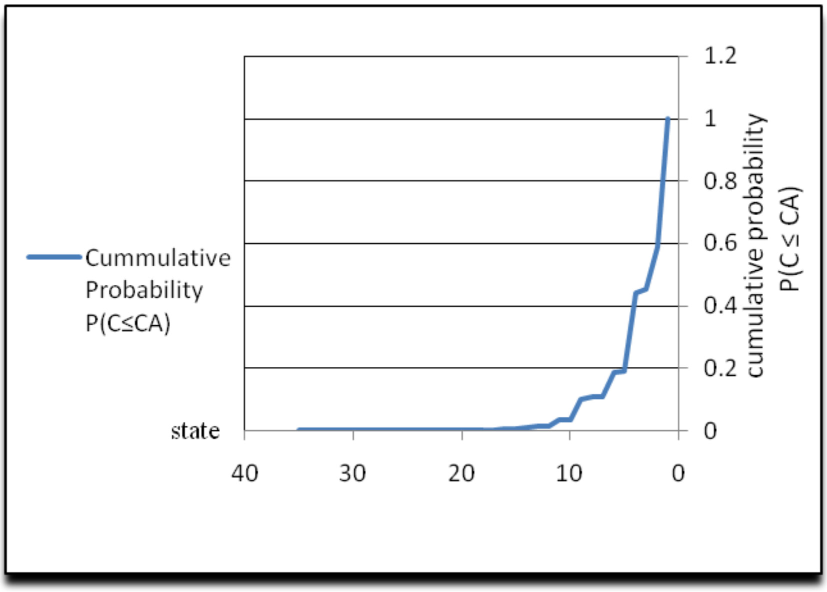

-2-

Figure 3. 1- Present available capacity meeting generation capacity probability.

2- Cumulative probability.

Table 3. Planned capacity outage of Al-Qudus plant.

State	Capacity out(MW)	Capacity in(MW)	Probability (C=CA)	Cumulative probability
0	0	1422	0.6655	1
1	43	1379	0.1401	0.3345
2	86	1336	8.154e-3	0.1944
3	125	1297	0.1358	0.1863
4	129	1293	3.8811e-4	0.0505
5	168	1254	0.0285	0.0501
6	172	1250	5.1067e-6	0.0216
7	211	1211	2.257e-3	0.0216
8	250	1172	0.01247	0.0193
9	254	1168	7.92e-5	0.006879
10	293	1129	2.626e-3	0.006793
11	297	1125	1.0422e-6	0.004167
12	336	1086	2.297e-4	0.004167
13	375	1047	6.788e-4	0.003938
14	379	1043	7.274e-6	0.003259
15	418	1004	1.429e-4	0.003252
16	422	1000	9.571e-8	0.003109
17	461	961	1.88e-6	0.003109
18	500	922	9.697e-6	0.003107
19	504	918	3.9587e-7	0.003097
20	543	879	2.042e-6	0.003097
21	547	875	5.209e-9	0.003095
22	586	836	1.61e-7	0.003095
23	625	797	1.319e-7	0.003095
24	629	793	5.655e-9	0.003095
25	668	754	2.78e-8	0.003095
26	672	750	7.44e-11	0.003095
27	711	711	1.462e-9	0.003095
28	750	672	1.68e-9	0.003095
29	754	668	7.69e-11	0.003095
30	793	629	3.54e-10	0.003095
31	797	625	1.012e-12	0.003095
32	836	586	2.797e-11	0.003095
33	879	543	9.814e-13	0.003095
34	922	500	1.29e-14	0.003095

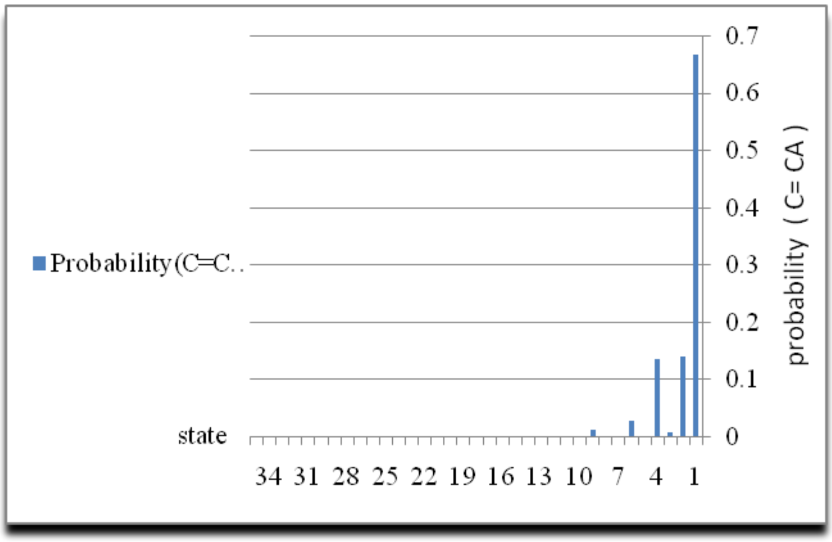

-1-

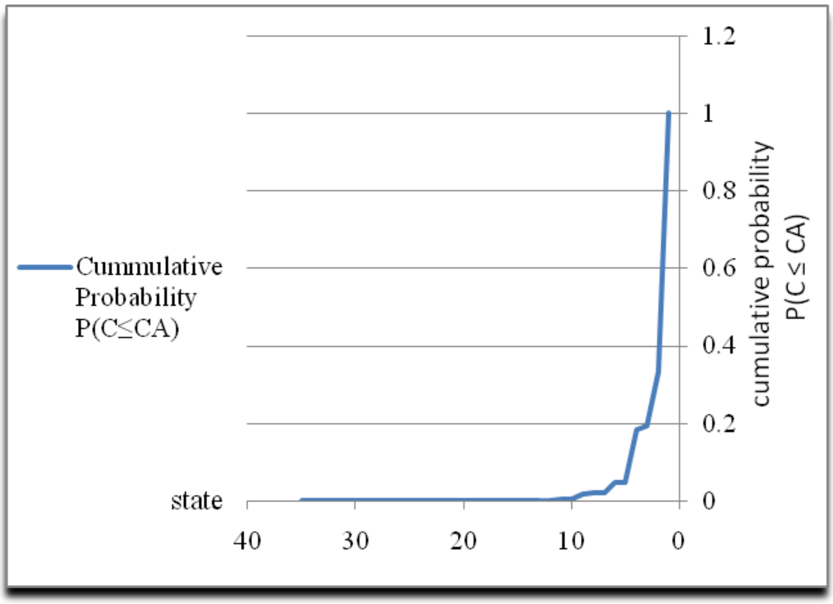

-2-

Figure 4. 1- Planned available capacity meeting generation capacity probability.

2- Planned cumulative probability.

Applying Cognitive Methodology in Designing On-Line Auto-Tuning Robust PID Controller for the Real Heating System

Ahmed Sabah Al-Araji
Assistance Professor
Control and Systems Engineering Dept - University of Technology
E-mail:ahmedsas2040@yahoo.com

ABSTRACT

A novel design and implementation of a cognitive methodology for the on-line auto-tuning robust PID controller in a real heating system is presented in this paper. The aim of the proposed work is to construct a cognitive control methodology that gives optimal control signal to the heating system, which achieve the following objectives: fast and precise search efficiency in finding the on-line optimal PID controller parameters in order to find the optimal output temperature response for the heating system. The cognitive methodology (CM) consists of three engines: breeding engine based Routh-Hurwitz criterion stability, search engine based particle swarm optimization (PSO) and aggregation knowledge engine based cultural algorithm (CA). Matlab simulation package is used to carry out the proposed methodology that finds and tunes the optimal values of the robust PID parameters on-line. In real-time, the LabVIEW package is guided to design the on-line robust PID controller for the heating system. Numerical simulations and experimental results are compared with each other and showed the effectiveness of the proposed control methodology in terms of fast and smooth dynamic response for the heating system, especially when the control methodology considers the external disturbance attenuation problem.

Key words: robust pid controller, cognitive, cultural algorithm, particle swarm optimization, heating system, matlab, labview.

تطبيق المنـهج الإدراكي في تصميم مسيطر تنـاسبي تكاملي تفاضلي متين بتنغيم تلقائي بشكل حي متصل لنظام حراري حقيقي

أحمد صباح عبد الأمير الأعرجي
أستاذ مساعد دكتور
قسم هندسة السيطرة والنظم - الجامعة التكنولوجية

الخلاصة

في هذا البحث, تم تصميم وتنفيذ منهج إدراكي جديد مبتكر لمسيطر تناسبي تكاملي تفاضلي متين بتنغيم تلقائي وبشكل حي متصل لمنظومة حرارية حقيقية. أن الهدف من هذا العمل المقترح هو بناء منهجية السيطرة المدركة والتي تعطي أمثل أشارة سيطرة لنظام الحراري والتي حققت الغايات التالية: كفاءة عالية من حيث السرعة ودقة البحث لإيجاد امثل قيم لعناصر المسيطر وبشكل حي متصل والتي تؤدي لإيجاد أفضل استجابة حرارية للنظام. أن منهج الإدراكي المقترح يتألف من ثلاث محركات: محرك النسل

وأساسه معيارية راوث هيروتز الأستقرارية, ومحرك البحث وأساسه حشد الجسيمات الأمثلية, ومحرك المعرفة المتجمعة وأساسها الخوارزمية الحضارية. لقد تم استخدام حقيبة الماتلاب البرمجية للمحاكاة كأداة لتنفيذ المنهج المقترح لإيجاد وتنغيم القيم الأمثلية للمسيطر التناسبي التكاملي التفاضلي المتين وبشكل حي متصل.
في الزمن الحقيقي تم استخدام حقيبة اللاب فيو البرمجية لتصميم المسيطر التناسبي التكاملي التفاضلي المتين وبشكل حي متصل لنظام الحراري. المحاكاة العددية و النتائج التجريبية قورنت مع بعضها البعض لبيان فعالية المنهج السيطرة المقترح من حيث السرعة والاستجابة الديناميكية الناعمة لنظام الحراري, خصوصا عندما اخذ بنظر الاعتبار مشكلة التضعيف للضوضاء الخارجية.

الكلمات الرئيسية:المسيطر التناسبي التكاملي التفاضلي المتين, الإدراك, الخوارزمية الحضارية, حشد الجسيمات الامثلية, منظومة حرارية, ماتلاب, لاب فيو.

1. INTRODUCTION

Over the past decade, more than 90% of industrial controllers are still implemented based on PID control algorithms as no other controller matches the simplicity, effectiveness, robustness, clear functionality and ease of implementation**, Zhao, et al., 2011.** Several approaches have been used for tuning the parameters of PID controllers such as Ziegler-Nichols method**, Duarte,** and **Jose, 2006.**
In last years, time domain performance, frequency domain performance and robust performance criterion have been used in designing PID controllers where the output of PID controllers (proportional - integral - derivative) are a linear combination of its input i.e. the proportion of the input, the integral of input and the derivative of the input**, Hagglund,** and **Astrom, 1996**.
However, PID controller is sensitive to plant parameter variations and the controller gains must be carefully selected for a desired response, thus the motivation for this work is the robustness which is an important criterion in controller design because most of the real systems are vulnerable to external disturbance, measurement noise and model uncertainty. While many industrial plants are often burdened with problems such as high order, time delays, and nonlinearities; therefore, it has been quite difficult to tune properly the gains of PID controllers. So there are many algorithms to tune the parameters of the PID controller in order to avoid these problems in the prosperities of systems: The comparison of various intelligent techniques used for temperature control of water bath system that consists of different control schemes namely PID, PID using Genetic Algorithms (GA-PID), Fuzzy Logic Control, Neural Network, Adaptive Neuro-Fuzzy Inference System (ANFIS), and GA-ANFIS have been proposed in **Saini,** and **Rani, 2012**.
In addition to that, design and implementation of a temperature control system of the thermal analyzer by combining fuzzy and PID control methods and accomplishing a comparative experiment of conventional PID with fuzzy self-tuning PID control method was explained in **Dong, et al., 2009.**
In **Wei, 2010,** was explained the algorithm that it improves the performance of the temperature control system based on fuzzy self-tuning PID. Also it investigated the applicability of Model Predictive Control (MPC) strategies to heating processes as proposed in**, Sbarciog, et al., 2008,** and used the nonlinear extended prediction self-adaptive control algorithm for the heated tank temperature.
The fundamental essence of the contribution of this work is to overcome the building of robust controller that has high order than that of the system where the controller is not easy to implement for this system in practical engineering application. This difficulty can be solved by the proposed algorithm that built a robust PID controller through applying the cognitive control methodology based CA and PSO technique, the proposed algorithm works as on-line auto-tuning for the PID

controller parameters on the real-time without time consuming as well as no requiring for tedious efforts.
In this paper, experimental investigation is carried out for the appropriate on-line auto-tuning parameters of the robust PID controller that controls the temperature of heating system using cognitive methodology to obtain the best temperature response achieved in real-time based on LabVIEW package.
The remainder of this paper is organized as follows: section two, describes the mathematic model of the heating system. In section three, the proposed cognitive control methodology for robust PID controller is explained. The Matlab simulation results of the proposed control algorithm are presented in section four. Hardware design and real-time results based on LabVIEW package are presented in section five and finally the conclusions are drawn in section six.

2. HEATING SYSTEM MODEL

The heating system model can be derived using the linear heat balance dynamic equation as follows, **Ogata, 2003**:
Heat input – Heat output = Heat accumulation

$$Q_i(t) - Q_{loss}(t) = Q_{Acc}(t) \tag{1}$$

Unsteady equation is:

$$Q_i(t) - hA(T(t) - T_{air}(t)) = Mcp\frac{dT(t)}{dt} \tag{2}$$

Steady equation at t=0 is

$$Q_i(0) - hA(T(0) - T_{air}(0)) = 0 \tag{3}$$

The difference between the Eqs. (2 and 3) becomes Eq. (4).

$$Q_i(t) - hAT(t) = Mcp\frac{dT(t)}{dt} \tag{4}$$

By taking Laplace Transformation for Eq. (4) in order to find the T.F. for the heating system as follows:

$$Q_i(s) - hAT(s) = McpST(s) \tag{5}$$

$$\frac{T(s)}{Q_i(s)} = \frac{1/hA}{Mcp/hAS + 1} \tag{6}$$

$$\frac{T(s)}{Q_i(s)} = \frac{K}{\tau S + 1} \tag{7}$$

where $K = 1/hA$ and $\tau = Mcp/hA$.

The real parameters implemented in the design of heating system are shown in **Table.1**.
After applying the real parameters of the heating system as in **Table 1.** in the T.F. Eq. (7), the model equation for the heating system will be as Eq. (8):

$$\frac{T(s)}{Q_i(s)} = \frac{1.21}{10.2S + 1} \tag{8}$$

3. ROBUT PID CONTROLLER DESIGN

PID control is widely applied in industrial practice because of its simple structure that consists of three terms: proportional, integral and derivative where the standard form of a PID controller is given in the s-domain as Eq. (9), **Zhong, 2006**.

$$Gc(s) = P + I + D = K_p + \frac{K_i}{s} + K_d s \tag{9}$$

where K_p, K_i and K_d are called the proportional gain, the integral gain and the derivative gain respectively.
The PID controller is very important because it is necessary to stabilize the tracking error of the heating system temperature when the output temperature drifts from the desired temperature.
After understanding the profound theoretical fundamental for the PID parameters tuning algorithms and employing these algorithms in designing a robust PID controller especially for system model which has uncertain parameters such as T_{air} which causes the heat loss disturbances that effect on the temperature output of the real system
A novel cognitive control methodology is proposed to find and tune on-line the PID control parameters in order to get a good evaluation of the performance rejection of the heat loss disturbance and uncertain parameter for the real system then to obtain the optimal and robust PID control action.
Thus, the proposed cognitive control methodology has the characteristics of high control ability, strong adaptability, good dynamic characteristic and robustness.
The proposed structure of the on-line auto-tuning robust PID controller of the heating system can be given in the form of block diagram, as shown in **Fig. 1**.

3.1 Cognitive Control Methodology

Cognitive control methodologies have been proven to be a source of inspiration and guidance to overcome current limitations in the controller for complex and adaptive systems by aggregation knowledge and to structure this knowledge autonomously**, Al-Araji, 2012.**
The proposed cognitive control methodology consists of three engines: Aggregation Knowledge Engine, Search Engine and Breeding Engine.
The aggregation knowledge engine based on cultural algorithm (CA) has been developed by modeling how human culture work. Culture is viewed as a vehicle for storing relevant information gathered since the start of the culture, and is available to all the subsequent generations of the society, **Brownlee, 2011,** and **Yan,** and **Wu, 2011.** This information can be useful for the

generations to guide their problem solving activities, at the same time being dynamically modified by new information gathered by each new generation. The CA is modeled using two separate information spaces:

- Population Space.
- Belief Space.

The population space contains the set of possible solutions to the problem available in the present generation and evaluates with a performance function. The belief space models represent the actual cultural aspects. It stores information related to the problem solution that it has been found till the present generation and in turn influences to the evolution of the population space in subsequent generations thus the belief space is composed of a few knowledge sources, normative knowledge and situational knowledge. Communication between the two spaces is handled by a protocol consisting of two functions:

- An acceptance function, which selects the set of individuals that will influence the belief space.
- An influence function, which influences the creation of the next generation.

In addition the belief space requires an update function which is basically responsible for updating the belief space when it is required. The structure diagram of the communication protocol in the cultural algorithm is shown in **Fig. 2**.

The search engine will be used as a pre-search engine to feed the population space in the aggregation knowledge engine with a selected number of the best solution in order to speed up the process of finding and tuning the optimal PID control parameters and reducing the over all number of function evaluation.

In the proposed work, the search engine is based on particle swarm optimization (PSO) as fast and simple technique algorithm. PSO algorithms use a population of individuals (called particles) “flies” over the solution space in searching for the optimal solution**, Fang, et al., 2011,** and **Chiou, et al., 2012**. The particles were mainly utilized to determine three PID controller parameters *kp, ki* and *kd* as a particle *K* by $K = [kp, ki, kd]$ with its dimension being $\mathrm{POP}_{\mathrm{pre}} \times 3$.

where pop_{pre} is the number of pre-search particles.

The search engine will be fed continuously at each time instant by the breeding engine which is used to generate continuous random solutions with two conditions.

The first condition is that all random solutions should be lie within the practical experience values, as follows:

$$\left.\begin{aligned} kp_{\min} \le kp \le kp_{\max} \\ ki_{\min} \le ki \le ki_{\max} \\ kd_{\min} \le kd \le kd_{\max} \end{aligned}\right\} \tag{10}$$

The second condition is that all random solutions should be submitted to Routh-Hurwitz criterion to check the closed-loop system stability. Mean Square Error (MSE) function for heating system is chosen as criterion for estimating the model performance to be minimized, as Eq. (11):

$$MSE = \frac{1}{pop}\sum_{k=1}^{pop}(T_{desired}^{(k)} - T_{output}^{(k)})^2 \tag{11}$$

where
pop is number of particles.
$T^{(k)}_{desired}$ is the desired temperature at *k* iteration.
$T^{(k)}_{output}$ is the output temperature at *k* iteration.
In pre-search, each particle has its own position [*kp*, *ki* and *kd*] and velocity [$\Delta kp, \Delta ki$ and Δkd] to move around the search space.
The previous best value of the particle is called as *pbest*. Thus, *pbest* is related only to a particular particle. It also has another value called *gbest*, which is the best value of all the particles *pbest* in the swarm.
Particles are updated afterwards according to Eqs. (12, 13, 14, 15, 16 and 17):

$$\Delta Kp_m^{k+1} = \Delta Kp_m^k + c_1 r_1 (pbest_m^k - Kp_m^k) + c_2 r_2 (gbest^k - Kp_m^k) \tag{12}$$

$$Kp_m^{k+1} = Kp_m^k + \Delta Kp_m^{k+1} \tag{13}$$

$$\Delta Ki_m^{k+1} = \Delta Ki_m^k + c_1 r_1 (pbest_m^k - Ki_m^k) + c_2 r_2 (gbest^k - Ki_m^k) \tag{14}$$

$$Ki_m^{k+1} = Ki_m^k + \Delta Ki_m^{k+1} \tag{15}$$

$$\Delta Kd_m^{k+1} = \Delta Kd_m^k + c_1 r_1 (pbest_m^k - Kd_m^k) + c_2 r_2 (gbest^k - Kd_m^k) \tag{16}$$

$$Kd_m^{k+1} = Kd_m^k + \Delta Kd_m^{k+1} \tag{17}$$

$m = 1,2,3,.....pop_{pre}$
where
K_m^k is the weight of particle *m* at *k* iteration.
c_1 and c_2 are the acceleration constants with positive values equal to 2.
r_1 and r_2 are random numbers between 0 and 1.
$pbest_m$ is best previous weight of m^{th} particle.
$gbest$ is best particle among all the particle in the population.
It is proposed that 25% from the *pbest* particles of the pre-search engine individuals will be travelled to the aggregation knowledge engine in order to have a cognitive particles re-generation. The cognitive particles are evaluated by using a performance function to see how close they are to the optimal solution. In order to find the optimal set of the PID controller parameters, it needs to update the cognitive particle K_c = [kp_c, ki_c, kd_c] by using the two levels of CA communication through the acceptance function and the influence function. The acceptance function determines which cognitive particles from the current population are selected to impact the belief space. In this work, it is proposed that the acceptance function selects 20% from the cognitive particles depending on a good step response with minimum settling time (t_s), rise time (t_r) and MSE as a performance index in time domain.

Belief space is composed of normative knowledge and situational knowledge components. The normative knowledge component is composed of the upper and lower bounds of (t_s, t_r and MSE) of the variables cognitive particles accepted. The situational knowledge is a set of the elite kp_c, ki_c and kd_c.

Δkp_c, Δki_c and Δkd_c in the cognitive PSO algorithm are influenced by belief space. The direction of changing ('velocity') is determined by the difference between situational knowledge (kp_c)s, (ki_c)s and (kd_c)s in belief space and the checked values of the resolution parameters, as Eq. (18).

$$\left.\begin{aligned} \Delta kp_{c\min} \le \Delta kp_c \le \Delta kp_{c\max} \\ \Delta ki_{c\min} \le \Delta ki_c \le \Delta ki_{c\max} \\ \Delta kd_{c\min} \le \Delta kd_c \le \Delta kd_{c\max} \end{aligned}\right\} \tag{18}$$

If Δkp_c, Δki_c and Δkd_c are too high, cognitive particles might fly past good solutions. If Δkp_c, Δki_c and Δkd_c are too low, cognitive particles may not explore sufficiently beyond local solution. The influence function will lead the evolutionary process for the next generation through the normative knowledge vector that consists of:

- Δkp_c, Δki_c and Δkd_c.
- Cognitive acceleration values c_{c1},c_{c2}.
- Random number function r_{c1},r_{c2} between 0 to 1.
- Inertia weight factor for the velocity Ω_c

In order to update the cognitive particles velocity, Eqs. (19, 20, and 21) are used in the next iteration.

$$\Delta Kp_{cn}^{k_c+1} = \Omega_c(\Delta Kp_{cn}^{k_c}) + c_{c1}r_{c1}(pbest_{cn}^{k_c} - Kp_{cn}^{k_c}) + c_{c2}r_{c2}(gbest_c^{k_c} - Kp_{cn}^{k_c}) \tag{19}$$

$$\Delta Ki_{cn}^{k_c+1} = \Omega_c(\Delta Ki_{cn}^{k_c}) + c_{c1}r_{c1}(pbest_{cn}^{k_c} - Ki_{cn}^{k_c}) + c_{c2}r_{c2}(gbest_c^{k_c} - Ki_{cn}^{k_c}) \tag{20}$$

$$\Delta Kd_{cn}^{k_c+1} = \Omega_c(\Delta Kd_{cn}^{k_c}) + c_{c1}r_{c1}(pbest_{cn}^{k_c} - Kd_{cn}^{k_c}) + c_{c2}r_{c2}(gbest_c^{k_c} - Kd_{cn}^{k_c}) \tag{21}$$

The Eqs. (22, 23 and 24) for updating and next generation of cognitive particles, as follows:

$$Kp_{cn}^{k_c+1} = Kp_{cn}^{k_c} + \Delta Kp_{cn}^{k_c+1} \tag{22}$$

$$Ki_{cn}^{k_c+1} = Ki_{cn}^{k_c} + \Delta Ki_{cn}^{k_c+1} \tag{23}$$

$$Kd_{cn}^{k_c+1} = Kd_{cn}^{k_c} + \Delta Kd_{cn}^{k_c+1} \tag{24}$$

$n = 1,2,3,.....pop_c$

where

pop_c is number of cognitive search of cognitive particles.

$K_{cn}^{k_c}$ is the weight of cognitive particle n at k_c iteration.

$pbest_{cn}$ is best previous weight of n^{th} cognitive particle.

$gbest_c$ is best cognitive particle among all the cognitive particles in the population space.

After updating and generating new cognitive particles of the PID parameters in the population space for the next iteration by using Eqs. (19, 20, 21, 22, 23 and 24), two conditions should be applied; the first condition is checking of the range acceptance of robust PID controller parameters as Eq. (10) for achieving the stability and second condition is applying Eq. (11) in order to estimate the value of the cost function for each particle, if one or two conditions are not true, this mean Δkp_c , Δki_c or Δkd_c violated the normative knowledge and it is forced back into the cognitive search space dictated by the normative knowledge. Else, at the end of each best cognitive particle generation, the normative knowledge is updated with the bounds of the accepted particles and the situational knowledge component is updated if necessary. Then continue the proposed algorithm until finding the optimal values of the robust PID controller parameters.

4. SIMULATION RESULTS

This section discusses the mapping between the real heating system and the numerical simulation by using Matlab package. The signal of the proposed robust PID controller will feed the heater unit of the heating system and this signal has to be within range (0 to 1500)watt because of the specification of real heater actuator ,therefore; will need a linear relationship with saturation transfer function (0-1500) in order to satisfy gain mapping and to limit the heater actuator output for the real heating system modeling.

To show the dynamic behavior of the heating system, the open loop step response of the temperature for the heating system is shown in **Fig. 3**, when applying a 21.49watt as input step change in the heater actuator of system in order to increase the heating system temperature by 1C^o with reference to its temperature at the initial condition which is equal to 25C^o. The settling time for the temperature response of the heating system is equal to 39.83 minute and rise time is equal to 22.33 minute and the time constant is equal to 10.2 hour. The sampling interval for the heating system is chosen to be 1 minute using Shannon theorem.

The proposed robust PID controller scheme, as in **Fig. 1**, is applied to the heating system model and it used cognitive methodology for auto-tuning the parameters of the PID controller on-line to find the best temperature response for the heating system.

The proposed cognitive methodology is set to the following parameters:

Population of pre-search is equal to 100.

Population of cognitive search is equal to 25.

Population of belief space is equal to 5.

Situational knowledge is equal to 5×3.

Normative knowledge is equal to 1×8.

Number of weights in each particle is equal to 3 because there are three parameters for PID controller.

Number of pre-search iteration (k) is equal to 10.

Number of cognitive iteration (k_c) is equal to 20.

Figs. 4a, 4b and **4c** represent the simulation results of the closed loop time response of the temperature control system with on-line auto-tuning robust PID controller based on cognitive methodology with initial temperature 25C^o and with proposed external disturbance function as Eq.

(25) which has been added in order to investigate the robustness and adaptation of the PID controller and to evaluate the performance rejection of the heal loss and model uncertainties.

$$d(t) = 10\sin(10kt) \tag{25}$$

Fig. 4a shows the response of the output temperature of the heating system to a step change, it had no over shoot and the steady-state error was approached to zero value in each step when the desired steps change in temperature were (50, 60 and 70) C^o and the external disturbance effect was very small during sixty samples.
The robust PID control action response is shown in **Fig. 4b** that it had few spikes in response to the desired step change in temperature with very small oscillation in order to keep the temperature output of the heating system within desired range and minimize tracking temperature error of the system and reduce the disturbance effect on the heating system.
Fig. 4c shows the error between the desired temperature and the temperature output of the heating system. The error was small value in the transient at each step change and became much close to zero in steady state with very small oscillation. The optimal parameters kp_c, ki_c and kd_c at each sample for the robust PID controller that have been tuned on-line based on cognitive methodology are shown in **Figs. 5a, 5b** and **5c** respectively.
Fig. 6 shows the optimal "velocity" Δkp_c, Δki_c and Δkd_c at each sample that have been calculated in the belief space in order to influence the particles kp_c, ki_c and kd_c of the next generation.

5. HARDWARE DESIGN AND REAL-TIME RESULTS

In this section, the experimental setup for the real-time heating system temperature control is shown in **Fig. 7**.
The setup of heating system consists of:

- The water tank that has volume (30, 25, 30) cm.
- AC heater actuator that has heat energy range (0-1500) watt.
- Temperature sensor LM134 with operation range (0 to 100) C^o.
- Data acquisition device from National Instrument NI Company type 6009USB with guided LabVIEW package.
- Digital phase controller based AT89C51 micro-controller to control power magnitude.
- AC drive circuit based Triac device.
- Electronic circuit board for signal conditioning based operational amplifier TL064.
- DC power supply that provides power to the circuitry.
- Laptop computer type Pentium dual-core 1.73GHz is used for the real time computation.

In the real-time computer control system based on LabVIEW package, the cognitive methodology has been applied to find optimal parameters for robust PID controller that controlled the temperature of the heating system in the real-time with sampling time equal to 1 minute. The front panel diagram of the control algorithm has been written in the LabVIEW, as shown in **Fig. 8**.
Fig. 9 shows the electronic circuit diagram design for the temperature control system and it consists of multi-stage as follows: the first stage is signal conditioning circuit which includes a voltage follower with unity gain to avoid the attenuation in the feedback signal of the temperature sensor LM134 and the first order low pass filter stage that has a cutoff frequency of 10Hz which will remove possible noise components that occur in the sensor outputs especially within main supply frequency at 50Hz. This filter is built using TL064 quad operational amplifier, **Faulkenberry, 1986**.

The output of this amplifier is fed to the gain amplifier stage that amplified the sensor signal by five times in order to make the sensitivity of this sensor equal to $50mV/C^{o}$ instead of $10mV/C^{o}$ that make the full range of operation (0 to 5) volt then its fed to the analog to digital converter ADC 14 bit high speed low power successive approximation converter of the NI-DAQmx-USB 6009 device with range of input voltage (0 to 5) volt as a second stage.

Inside the personal computer, LabVIEW software instructions compares the sensed temperature signal received via this interface with the set-point desired temperature. The resulting error is given as an input to the robust PID controller and found the optimal parameters of the PID controller by using cognitive control methodology that has been built in the LabVIEW package.

The optimal digital control action generated from the robust PID controller will be sent to the digital phase controller which operates as a phase and magnitude detector for the Alternative Current (AC) by using micro-controller AT89C51, as third stage.

The digital data of control action is sent to the NI-DAQmx-USB 6009 device though the USB connector then the digital data will be sent as eight bits within range (00 - FF)hex to the port two (P2.x) of digital phase controller in order to analyze this data by using the assembly program of AT89C51**, Scott Mackenzie, 1999,** which convert the digital data action (00 - FF)hex to generate the firing angle pulse on the gate of the Traic device BT136 through isolator pulse transformer to control the AC power of the heater actuator (0 – 1500) watt. Assume the AC frequency is equal to 50Hz, the firing angle pulse has range from (0 – 20) msec.

The isolator circuit interface has been used between the DAQ (Data Acquisition) card and the heater actuator to prevent the possibility of any back-flow of AC current to the DAQ card from Triac device controller of heater actuator.

The phase detector control action program has been written in assembly language of AT89C51 microcontroller, as shown below:

```
ORG 000h
        SJMP START
ORG 003H
        MOV IE,#00H
        MOV R0,P2
        CLR TF0
        CLR TR0
Count:  MOV TL0,#0DCH
        MOV TH0,#0FFH
        SETB TR0
Cheak1:   JNB TF0,Cheak1
        CLR TR0
        CLR TF0
        DJNZ R0,Count
        SETB P1.0
        MOV TL0,#18H
        MOV TH0,#0FCH
        SETB TR0
Cheak2: JNB TF0,Cheak2
        CLR TR0
        CLR TF0
        CLR P1.0
        MOV IE,#81H
        RETI
START:    CLR P1.0
```

```
        CLR TF0
        CLR TR0
        MOV TMOD,#01H
        MOV IE,#81H
        MOV IP,#01H
        SETB IT0
Cheak3: SJMP Cheak3
END
```

The temperature response for the heating system in real-time was estimated within one hour, as shown in **Fig.10a**. It can be seen that response has three steps change in the desired temperature (50, 60 and 70) C^o and at steady state, the response has small fluctuation due to convection current of heat transfer in water of the heating tank.

The tracking error between the desired temperature and the actual temperature output of the heating system is shown in **Fig. 10b**. The firing angle signal of the AC heater driver circuit is shown in **Fig. 10c**.

The response of the feedback robust PID control action is shown in **Fig. 10d**. It has spike during the step change in the desired temperature as well as a small oscillation can also be observed. This action of the controller has kept the temperature of the heating system within the desired value with minimum tracking temperature error and it has attempted to reduce the disturbance effect on the heating system.

In fact, there are small differences in results between the numerical simulation and real-time control system because in the real-time state there were accumulation errors such as undesirable characteristics of temperature sensor "non-linearity, drift, and offset", offset in the operational amplifier output, and the quantization error of the analog to digital converter; therefore, the results in the real-time had small fluctuation in the actual temperature output of the heating system.

6. CONCLUSIONS

A robust cognitive PID temperature control methodology for the heating system model has been designed and tested using Matlab package and carried out in real-time using LabVIEW package on the real heating system model.

Simulation and real-time computer control results show evidently that the proposed robust PID controller model has demonstrated effectively the capability of tracking desired temperature as well as evaluating the performance rejection of the heat loss disturbance and uncertain parameter of the real system, especially with regards to the external disturbance effect.

REFERENCES

- Al-Araji, A., 2012, *Design of a Cognitive Neural Predictive Controller for Mobile Robot*, PhD thesis, Brunel University, United Kingdom.

- Brownlee, J., 2011, *Clever Algorithms :Nature-Inspired Programming Recipes*, First Edition. LuLu. Melbourne, Australia.

- Chiou, J-S., Tsai, S-H. and Liu, M-T., 2012, *A PSO-Based Adaptive Fuzzy PID-Controllers*, Simulation Modelling Practice and Theory. Vol. 26, pp. 49-59.

- Dong, Z., Su, Y. and Yan, X., 2009, *Temperature Control System of the Thermal Analyzer Based on Fuzzy PID Controller*, Proceeding of 2009 Ninth International Conference on Hybrid Intelligent Systems, pp. 58-61.

- Duarte, V. and Jose, C., 2006, *Tuning of Fractional PID Controllers with Ziegler – Nichols Type Rules*, Signal Processing. Vol. 86, pp. 2771-2784.

- Fang, H., Chen, L. and Shen, Z., 2011, *Application of an Improved PSO Algorithm to Optimal Tuning of PID Gains for Water Turbine Governor*, Energy Conversion and Management. Vol. 52, pp.1763-1770.

- Faulkenberry, S., 1986, *Introduction to Operational Amplifiers with Linear Circuit Applications*, John-Wiley Inc.

- Hagglund, T. and Astrom, K., 1996, *Automatic Tuning of PID Controllers*, in W.S. Levine (Ed), the Control Handbook, CRC Press, Boca Raton, FL, pp. 817-826.

- Ogata, K., 2003, *Modern Control Engineering*, 4th Edition, by Addison- Wesley Publishing Company.

- Saini, S. and Rani, S. 2012, *Temperature Control Using Intelligent Techniques*, Proceeding of 2012 Second International Conference on Advanced Computing & Communication Technologies, pp. 138-145.

- Sbarciog, M., Keyser, R., Cristea, S. and Prada, C., 2008, *Nonlinear Predictive Control of Processes with Variable Time Delay. A Temperature Control Case Study*, Proceeding of 17th IEEE International Conference on Control Applications Part of 2008 IEEE Multi-conference on Systems and Control San Antonio, Texas, USA, September 3-5,pp. 1001-1006.

- Scott Mackenzie, I., 1999, *The 8051 Microcontroller*, Prentice-Hall. Inc, 3st edition.

- Wei, J., 2010, *Research on the Temperature Control System Based on Fuzzy Self-tuning PID*, International Conference On Computer Design and Applications (ICCDA 2010), pp. 13-15.

- Yan, X. and Wu, Q., 2011, *Function Optimization Based on Cultural Algorithms,* Journal of Computer and Information Technology. Vol. 2, No. 1, pp. 143-149.

- Zhao, S., Iruthayarajan,M., Baskar, S. and Suganthan, P., 2011, *Multi-Objective Robust PID Controller Tuning Using Two Lbests Multi-Objective Particle Swarm Optimization,* Information Sciences, Vol. 181, pp. 3323-3335.

- Zhong, Q., 2006, *Robust Control of Time-Delay Systems*, Springer–Verlag London Limited.

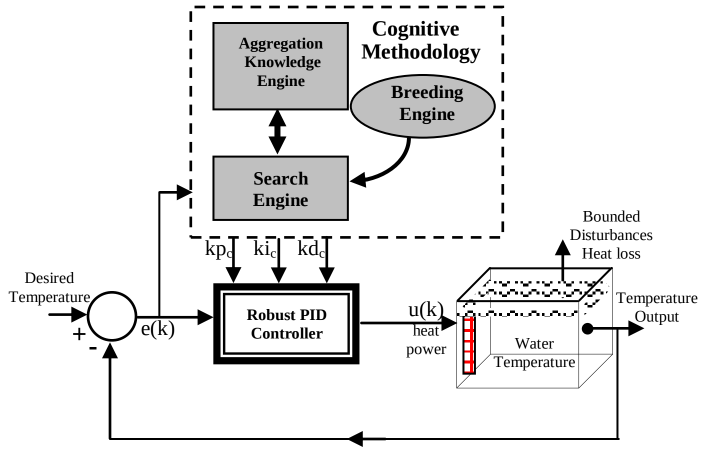

Figure 1. The proposed block diagram of the robust PID controller for heating system.

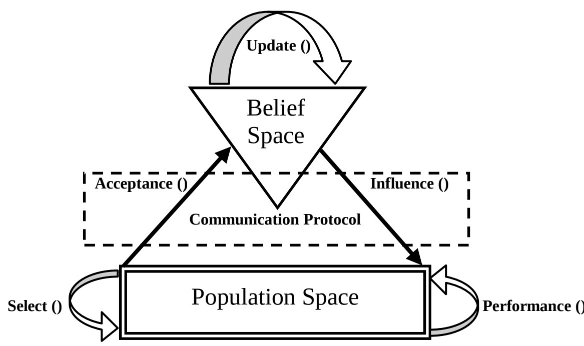

Figure 2. The structure diagram of the communication protocol.

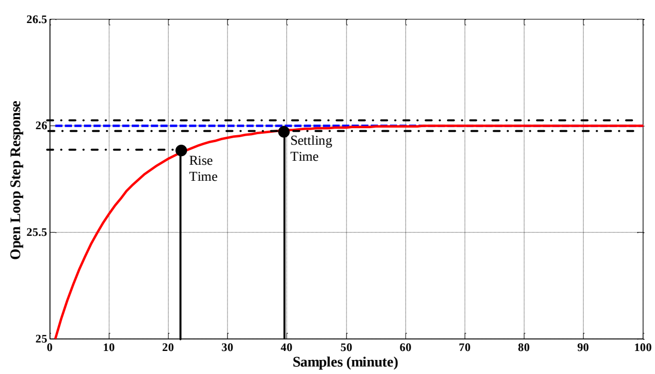

Figure 3. Step response of open loop heating system.

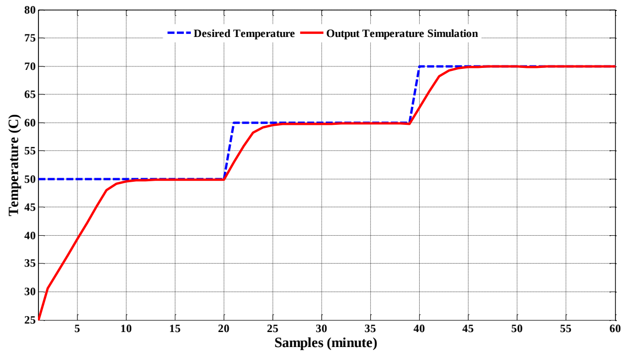

Figure 4a. Heating system output temperature simulation.

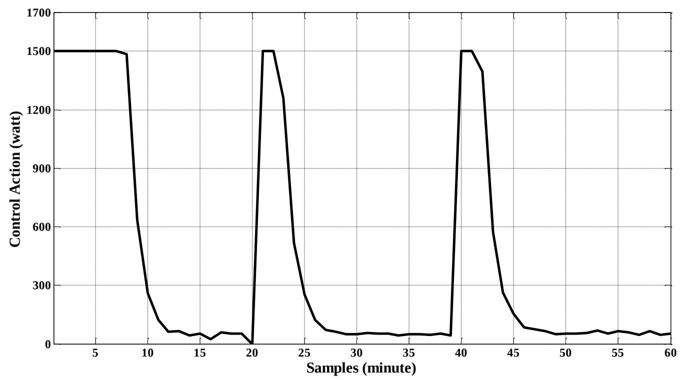

Figure 4b. Control action simulation.

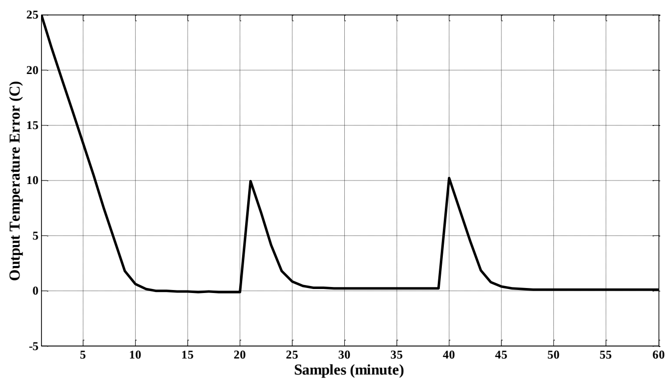

Figure 4c. Output temperature error simulation.

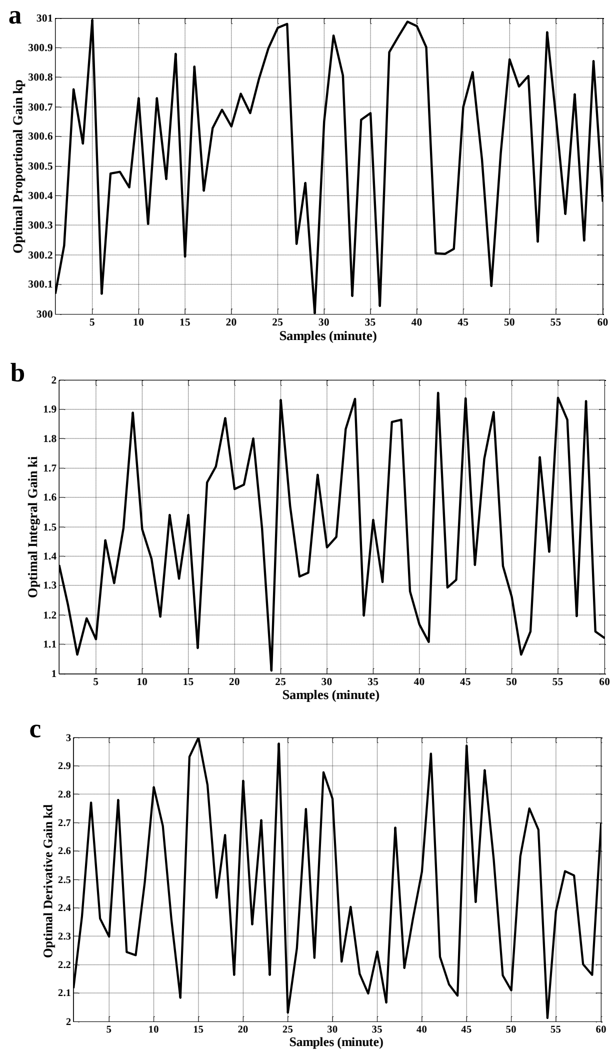

Figure 5. Optimal parameters of robust PID controller: a) Proportional gain; b) Integral gain; c) Derivative gain.

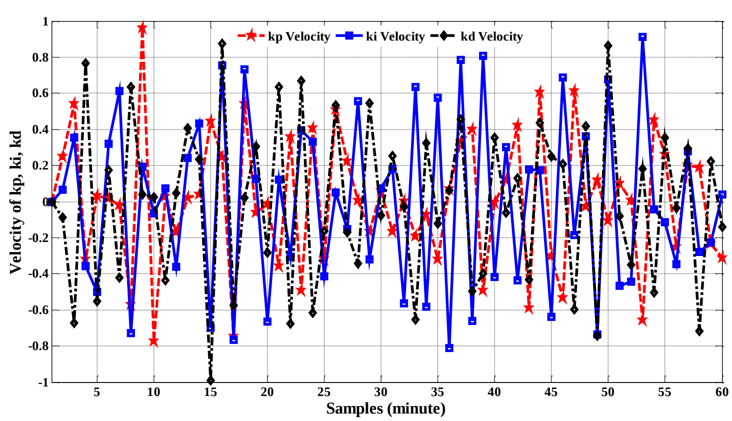

Figure 6. Simulation of the best gains velocity.

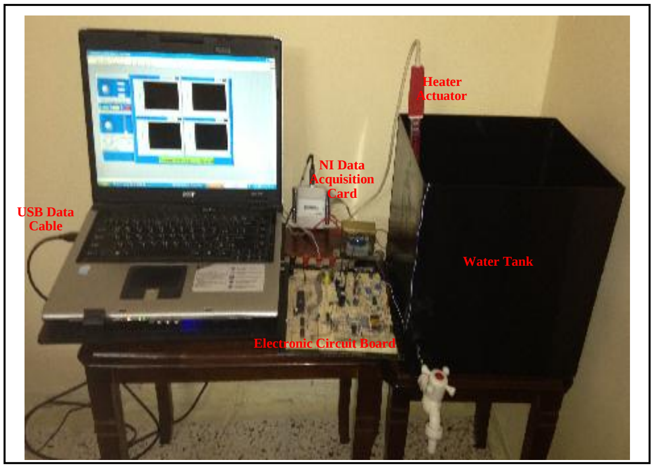

Figure 7. The experimental work in the real-time temperature control system.

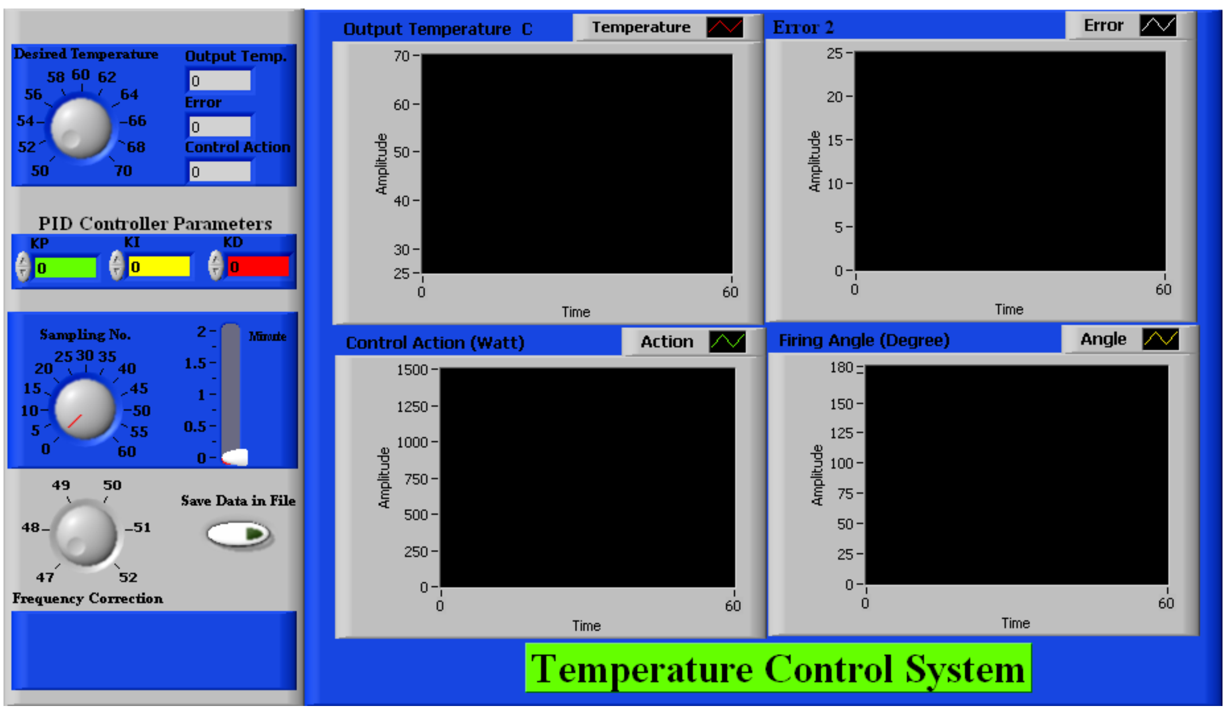

Figure 8. Front panel diagram for control algorithm.

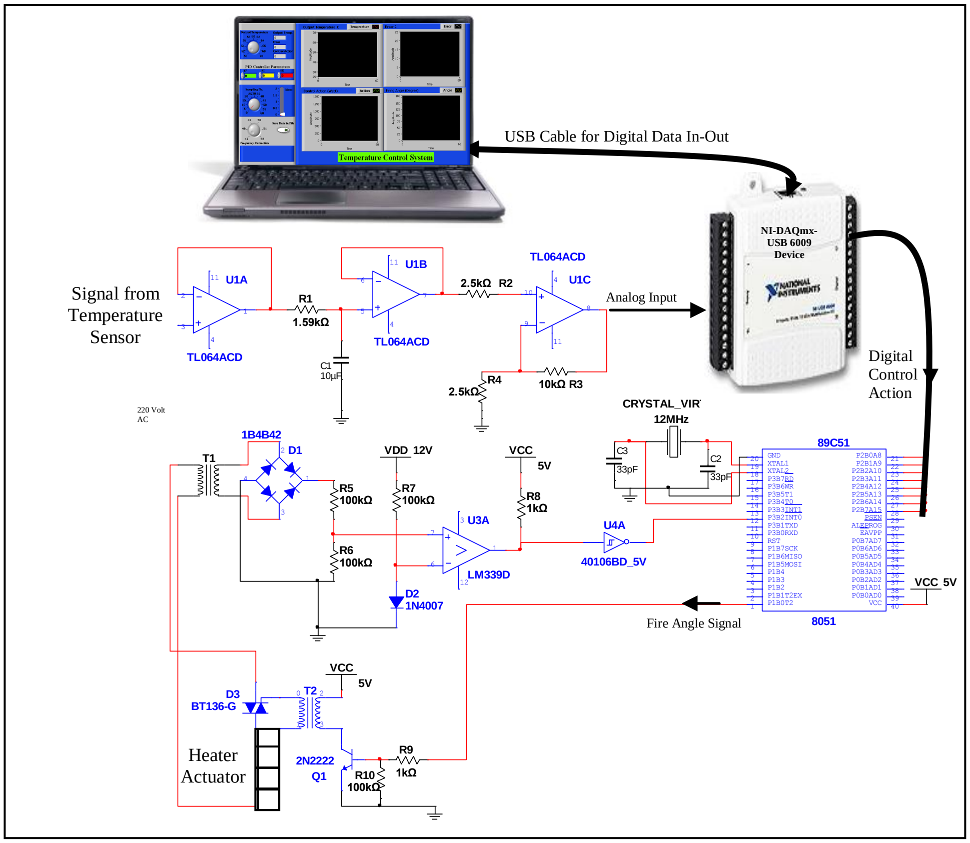

Figure 9. The schematic diagram of the electronic control circuit.

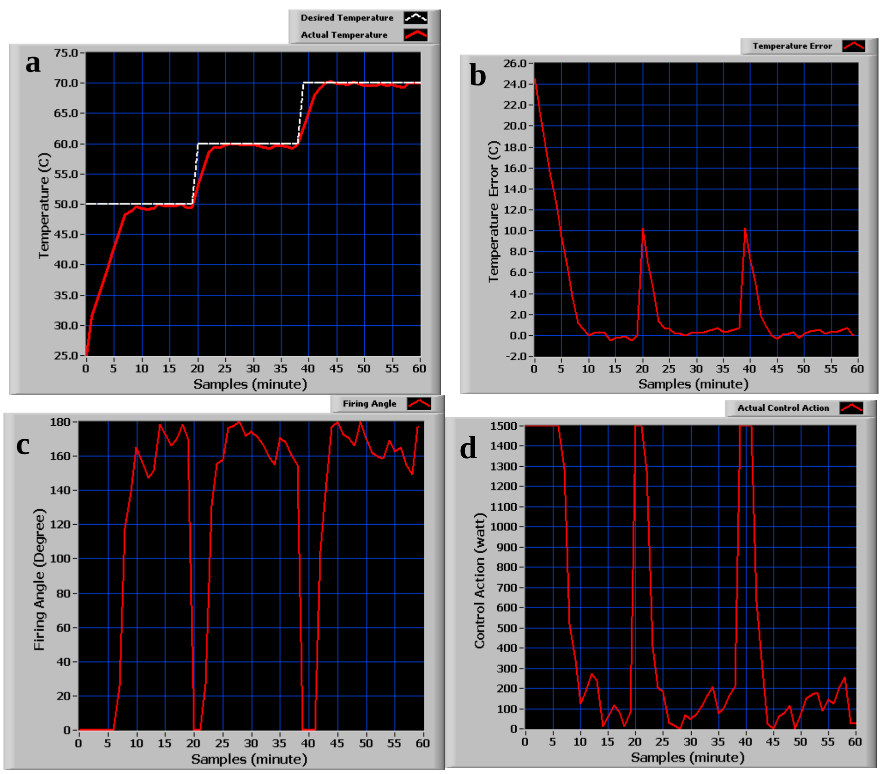

Figure 10. (a) Actual temperature output for heating system; (b) Temperature error; (c) Actual firing angle; (d) Actual control action.

Table 1. Heating system real parameters.

Real parameter	**Values**
A: surface area of the tank	0.075 m^2
h: over heat transfer coefficient	11 $watt/m^2C^o$
M: mass of water in tank	7.5 kg
cp: specific heat of water	4.2 KJ/kgC^o

Remediation of Groundwater Contaminated with Copper Ions by Waste Foundry Sand Permeable Barrier

Ayad Abedalhamza Faisal
Assistant Professor
College of Engineering-University of Baghdad
Email: ayadabedalhamzafaisal@yahoo.com

Maryam Dheyauldeen Ahmed
MSc. student
College of Engineering-University of Baghdad
Email: maryam_dheya@yahoo.com

ABSTRACT

The permeable reactive barrier (PRB) is one of the promising innovative in situ groundwater remediation technologies, in removing of copper from a contaminated shallow aquifer. The 1:1-mixture of waste foundry sand (WFS) and Kerbala's sand (KS) was used for PRB. The WFS was represented the reactivity material while KS used to increase the permeability of PRB only. However, Fourier-transform infrared (FTIR) analysis proved that the carboxylic and alkyl halides groups are responsible for the sorption of copper onto WFS. Batch tests have been performed to characterize the equilibrium sorption properties of the (WFS+KS) mix in copper-containing aqueous solutions. The sorption data for Cu^{+2} ions, obtained by batch experiments, have been subjected to the Langmuir and Freundlich isotherm models. The Langmuir model was chosen to describe the sorption of solute on the solid phase of PRB. COMSOL Multiphysics 3.5a based on finite element method was used for formulation the transport of copper ions in two-dimension physical model under equilibrium condition. Numerical and experimental results proved that the PRB plays a potential role in the restriction of the contaminant plume migration. A good agreement between the predicted and experimental results was recognized with mean error (ME) not exceeded 10 %.

Keywords: groundwater, permeable reactive barrier, waste foundry sand, heavy metal, polution.

معالجة المياه الجوفية الملوثة بايونات النحاس بواسطة حاجز مخلفات رمل المسبك النفاذ

أياد عبد الحمزة فيصل
أستاذ مساعد
كلية الهندسة- جــامـــعـــة بـــغـــداد

مريم ضياء الدين أحمد
طالبة ماجستير
كلية الهندسة - جــامـــعـــة بـــغـــداد

الخلاصة

الحاجز التفاعلي النفاذ من التقنيات الحديثة المبتكرة لمعالجة المياه الجوفية في الموقع في ازالة عنصر النحاس من الطبقات السطحية الملوثة.خلطة مخلفات رمل المسبك ورمل كربلاء بنسبة (1:1) أستخدمت كحاجز تفاعلي نفاذ حيث تمثل مخلفات رمل المسبك المادة الفعالة بينما يستخدم رمل كربلاء لزيادة نفاذية هذا الحاجز .التحليل بأستخدام الاشعة تحت الحمراء أثبت ان مجموعة الكربوكسيل وهاليدات الالكيل هي المسؤولة عن أمتزاز النحاس على مخلفات رمل المسبك. اختبارات الدفعة أنجزت لوصف صفات الامتزاز للخلطة (مخلفات رمل المسبك ورمل كربلاء) في المحلول الحاوي على النحاس . البيانات التي تم الحصول عليها من التجارب بطريقة الدفعة تم تحليلها بواسطة موديلات لانكمير وفريندلج. تم أختيار موديل لانكمير لوصف أمتزاز المحلول على الطور الصلب للحاجز التفاعلي النفاذ. تم أستخدام برنامج COMSOL Multiphysics 3.5 a الذي يعتمد على طريقة العناصر المحددة لوصف انتقال ايونات النحاس بموديل فيزيائي ثنائي الابعاد في ظل حالة التوازن. النتائج المختبرية والعددية أثبتت أن الحاجز التفاعلي النفاذ يلعب دور أساسي في حصر حركة البقعة الملوثة .لوحظ وجود توافق جيد بين النتائج المتوقعة والمختبرية وبمعدل خطأ أقل أويساوي10%.

الكلمات الرئيسية : المياه الجوفية, الحاجز التفاعلي النفاذ, مخلفات رمل المسبك, المعادن الثقيلة, التلوث.

1. INTRODUCTION

Groundwater is water found beneath the surface of the ground. It is primarily water that has seeped down from the surface by migrating through the soil matrix and spaces in geologic formations. Groundwater in aquifers is important for irrigation, domestic and industrial uses . Groundwater contamination can occur either from improper disposal, accidental release ….etc. or from naturally occurring mineral and metallic deposits in rock and soil. A groundwater pollutant is any substance that, when it reaches an aquifer, makes the water unclean or otherwise unsuitable for a particular purpose, **Mason, 2003**.

Heavy metals are among the most dangerous inorganic water pollutants, they can be related to many anthropogenic sources and their compounds are extremely toxic. These metals can be accumulated in the aquatic food web reaching human beings through the food chain, and causing several pathologies. The presence of heavy metals in groundwater is due to water exchange with contaminated rivers and lakes or to leaching from contaminated soils by rainfall infiltration **, Di Natale et al. ,2008.**

The treatment of contaminated groundwater is among the most difficult and expensive environmental problems and often the primary factor limiting closure of contaminated sites. The most common technology used historically for remediation of groundwater has been ex-situ pump-and-treat systems. These systems are still suited for certain site-specific remediation scenarios; however, the limitations of pump-and-treat technologies have also been recognized. Accordingly, there was a necessity to develop other new innovative methods to remediate groundwater contaminated with heavy metals. Over the past decade, permeable reactive barriers (PRBs) have provided an increasingly important role in the passive interception and in-situ treatment of groundwater as a component of remedial action programs. PRBs have been used to remove a wide range of organic and inorganic contaminants from groundwater including petroleum hydrocarbons, chlorinated solvents, nutrients, metals and radionuclides **, Mountjoy et al., 2003.**

Bazdanis et al., 2011, studied the efficiency of PRBs containing organic material and limited quantities of ZVI, fly ash or red mud to remove heavy metals from leachates. Up-flow laboratory column experiments were carried out to study the efficiency in terms of Cu, Zn, Ni and Mn removal. The columns were filled with each reactive mixture and packed slightly to simulate field conditions; synthetic solutions with initial concentration of 50 mg/l of each metal were used. The experimental results showed in most cases adequate metal removal efficiency.

Chalermyanont et al., 2013, described performance of the PRBs on treating heavy-metal contaminated groundwater. ZVI and activated sludge were used as reactive media. Simulation results showed that funnel and gate PRBs have similar performance with the continuous PRBs on treating zinc contaminated groundwater but having less operation time. In additions, both ZVI and activated sludge can be used as reactive material with similar performance. The concentrations of zinc of treated groundwater are less than 5 mg/l.

However, the foundry industry releases large quantities of by-product WFS, which represent both a waste and a pollutant. For example, Nasr Company for Mechanical Industries, Special Steel Foundry / Iraq produced 10 tons of WFS per 8 hours when worked with full capacity. Thus, re-using of this waste as a reactive medium is attractive in terms of sustainable development **,Lee et al., 2004, Siddique et al., 2010 and Oliveira et al., 2011.** Thus, the significance of the present study are: (1) investigation the potential application of WFS as an inexpensive material in PRBs for the removal of copper (Cu^{2+}) from the contaminated groundwater; (2) determining the predominant faunctional groups which are responsible of Cu^{2+} removal in the WFS using Fourier transfer infrared spectroscopy (FTIR) analysis; and (3) characterization the 2D equilibrium transport of Cu^{2+} theoretically, using COMSOL

Multiphysics 3.5a (2008) software which is based on finite element method, and experimentally through simulated subsurface aquifer and WFS barrier under saturated condition for the equilibrium case.

2. MATERIALS AND METHODS

2.1 Materials

The WFS **Table 1** used in the present study had a particle size distribution ranged from 75 μm to 1 mm with an effective grain size, d_{10}, of 180 μm, a median grain size, d_{50}, of 320 μm and a uniformity coefficient, C_u, of 1.94. As the hydraulic conductivity of this sand was very low ($=1x10^{-6}$ cm/s), it is mixed with Kerbala's sand (KS). The 1:1-mixture of (WFS+KS) was used with achieved conductivity equal to $2x10^{-3}$ cm/s. Also, the bulk density and porosity of this tested reactive mixture are 1.48 g/cm^3 and 0.42 respectively.

The sandy soil, with composition and properties shown in **Table 2**, was used as aquifer in the conducted experiments. This soil had a particle size distribution ranged from 75 μm to 2 mm with an effective grain size, d_{10}, of 280 μm, a median grain size, d_{50}, of 240 μm and a uniformity coefficient, $C_u= d_{60}/d_{10}$, of 1.54.

Copper was selected as a representative of heavy metal contaminants. To simulate the water's copper contamination, a solution of $CuSO_4.5H_2O$ (manufactured by Germany) was prepared and added to the specimen to obtain representative concentration.

2.2 Experimental Methodology

2.2.1 Batch experiments

Batch equilibrium tests are carried out to specify the best conditions of contact time, initial pH, initial concentration, (WFS+KS) dosage and agitation speed. Series of 250 ml flasks are employed and each flask is filled with 100 ml of copper solution which has initial concentration of 50 mg/l. One gram of (WFS+KS) was added into different flasks and these flasks were kept stirred in the high-speed orbital shaker at 250 rpm for 4 hours. A fixed volume (20 ml) of the solution was withdrawn from each flask. This withdrawn solution was filtered to separate the sorbent and a fixed volume (10 ml) of the clear solution was pipetted out for the concentration determination of the copper ion still present in solution. The measurements were carried out using atomic absorption spectrophotometer (AAS) (Norwalk, Connecticut (USA)) at the Center for Market Research and Consumer Protection. These measurements were repeated for two times and average value has been taken. However, the adsorbed concentration of metal ion on the (WFS+KS) was obtained by a mass balance.

The effect of various parameters such as initial pH (2, 4, 6.5, and 8), initial Cu^{2+} concentration (50, 100, 150, 200 and 250 mg/l), (WFS+KS) dosage (0.25, 0.5, 1, 3 and 5 g) and agitation speed (0, 50, 100, 150, 200 and 250 rpm) were studied in term of their effect on removal efficiency. The amount of metal ion retained on the (WFS+KS), q_e in (mg/g), was calculated as follows **, Wang et al. 2009**:

$$q_e = (C_o - C_e)\frac{V}{m} \tag{1}$$

where C_o is the initial concentration of copper in the solution (mg/l), C_e is the equilibrium concentration of copper remaining in the solution after the end of the experiment (mg/l), V is the volume of solution in the flask (l), and m is the mass of (WFS+KS) in the flask (g).

Langmuir Eq. (2) and Freundlich Eq. (3) models are used for the description of sorption data as follows **, Watts, 1998**:

$$q_e = \frac{abC_e}{1+bC_e} \quad (2)$$

where a is empirical constant and b is the saturation coefficient (l/mg).

$$q_e = K_F C_e^{1/n} \quad (3)$$

where K_F is the Freundlich sorption coefficient and n is an empirical coefficient.

2.2.2 Continuous experiments

The simulated Cu^{+2} transport was performed in a two-dimensional tank schematically shown in **Fig. 1**. This bench-scale model aquifer is contained within a rectangular 6 mm thick acrylic glass tank (100 cm L × 40 cm W × 10 cm D), including two vertical perforated acrylic glass plates as partitions covered with filter paper. These partitions are provided the lateral boundaries of the sand-filled middle compartment which has dimensions of 80×40×10 cm. The purpose of the two outer compartments, i.e. influent and effluent chambers, was controlling the position of the watertable within the model aquifer deposited in the middle compartment and, in addition, controlling the wetting of this aquifer mass. Each outer compartment has dimensions of 10 cm long, 40 cm width, and 10 cm high. The flow through the model aquifer was accomplished by peristaltic pump discharging copper solution from a storage tank of 10 l volume. One value of flow rate (120 ml/min) was selected here with corresponding interstitial velocity equal to (0.6 cm/min). Sampling plate **Fig. 2** was placed on the top of the glass tank to support the sampling ports. This plate contains 3 columns and 2 rows of sampling ports. Aqueous samples from the model aquifer were collected using stainless needles at specified periods.

The tank was packed with sandy soil as aquifer and (WFS+KS) as barrier in the configuration and alignment (10 cm thickness) illustrated in **Fig. 1**. Monitoring of Cu^{2+} concentration along the length of the tank in the effluent from sampling ports was conducted for a period of 3 days. Water samples of 2 ml volume were taken regularly (after 12, 24, 36…. 72 hours) from these ports. For sampling the ports, six needles were connected to its location in each test. The samples were immediately introduced in test tubes and analyzed by AAS. The filling material in the middle compartment was assumed to be homogeneous and incompressible, and constant over time for water-filled porosity. All tubing and fitting for the influent and effluent lines should be composed of an inert material.

A tracer experiment in the tank described above was performed to determine the effective dispersion coefficient for the sandy soil and (WFS+KS) using the same procedure adopted by **Ujfaludi , 1986.**

A solution of 1 g/l NaCl in distilled water as a tracer was continuously fed into the tank. This tracer has been widely used due to its safety, cheapness, weak propensity to adsorption, not being affected by the liquids density and viscosity, and the easy detection of the concentration changes**.**

3. RESULTS AND DISCUSSION

3.1 Fourier-Transform Infrared (FTIR) Analysis

This analysis has been considered as a kind of direct means for investigating the sorption mechanisms by identifying the functional groups responsible for metal binding **, Chen et al., 2008**. Infrared spectra of WFS samples before and after sorption of Cu^{+2} were examined using (SHIMADZU FTIR, 800 series spectrophotometer). These spectra were measured within the range 4000-400 cm^{-1} as shown in **Fig. 3**. The sorption peaks in the region of 400-750 cm^{-1} can be assigned to –C–R stretching vibrations of alkyl halides group. The carboxylic stretching vibrations can be attributed to sorption peak at 1037.70. The shifts in the IR frequencies support that carboxylic and alkyl halides groups are responsible for the sorption of copper onto WFS**, Doke et al., 2012**.

3.2 Effect of Shaking Time and Initial pH of Solution

Fig. 4 shows the effect of contact time and initial pH of solution on Cu^{+2} sorption using 1 g of (WFS+KS) added to 100 ml of metal solution for batch tests at 25ºC. This figure shows that the sorption rate was very fast initially and it's increased with increasing of contact time until reached the equilibrium time (= 1 h). This may be due to the presence of large number of adsorbent sites available for the sorption of metal ions. As the remaining vacant surfaces decreasing, the sorption rate slowed down due to formation of replusive forces between the metals on the solid surfaces and in the liquid phase **, El-Sayed et al., 2010**. Also, the increase in the Cu^{+2} removal as the pH increases can be explained on the basis of a decrease in competition between proton and metal species for the surface sites which results in a lower columbic repulsion of the sorbing metal. However, further increase in pH values would cause a decreasing in removal efficiency. This may be attributed to the formation of negative copper hydroxides which are precipitated from the solution making true sorption studies impossible. It is clear from this figure that the maximum removal efficiency of copper was achieved at initial pH of 6.5.

3.3 Effect of (WFS+KS) Dose

Fig. 5 illustrates the Cu^{+2} removal efficiency as a function of different weights of (WFS+KS) ranged from 0.25 to 5 g added to 100 ml of metal solution. It can be observed that the removal efficiency improved with increasing (WFS+KS) dosage from 0.25 g to 1 g for a fixed initial metal concentration. This was expected due to the fact that the higher dose of adsorbents in the solution, the greater availability of sorption sites.

3.4 Effect of Agitation Speed

Fig. 6 shows that about 20% of the copper was removed before shaking (agitation speed= zero) and the uptake increases with the increase of shaking rate. There was gradual increase in metal ions uptake when agitation speed was increased from zero to 250 rpm at which about 93% of Cu^{+2} has been removed. This can be attributed to improving the diffusion of ions towards the surface of the reactive media and, consequently, proper contact between ions in solution and the binding sites can be achieved.

3.5 Sorption Isotherms

The sorption isotherms were produced by plotting the amount of copper removed from the solution (qe in mg/g) against the equilibrium metal concentration in the solution (Ce in mg/l) at constant temperature , **Hamdaouia**, and **Naffrechoux**, **2007**and **Kumar**, and **Kirthika**, **2009**. The data of the batch tests are fitted with linearized form of Langmuir and Freundlich models. Accordingly, the equations of these models will be;

$$q_e = \frac{0.9292C_e}{1+0.092C_e} \qquad R^2=0.988 \qquad (4)$$

$$q_e = 3.397C_e^{0.207} \qquad R^2=0.986 \qquad (5)$$

It is clear that these models are provided the best representation of copper sorption onto (WFS+KS) reactive material. However, the Langmuir model was chosen to describe the sorption of solute on solid in the partial differential equation governed the transport of a solute undergoing equilibrium sorption through permeable reactive barrier in the continuous mode.

3.6 Longitudinal Dispersion Coefficient

Results of the experimental runs concerned the measurement of longitudinal dispersion coefficient (D_L) at different values of velocity (V) for soil and (WFS+KS) are taken a linear relationship as follows:
For soil,

$$D_L = 68.16\,V + 0.056 \qquad R^2=0.973 \tag{6}$$

For (WFS+KS),

$$D_L = 73.51\,V + 0.282 \qquad R^2=0.999 \tag{7}$$

These equations are taken the general form of longitudinal hydrodynamic dispersion coefficient as follows:

$$D_L = \alpha_L V + \tau D_o \tag{8}$$

This means that the longitudinal dispersivity (α_L) is equal to 68.16 cm for soil and 73.51 cm for mix.

3.7 2D PRB design-model setup

The contaminant migration in a porous medium is due to advection-dispersion processes; therefore, considering a two dimensional system, the dissolved copper mass balance equation may be written, as follows:

$$D_x \frac{\partial^2 C_{cu}}{\partial x^2} + D_y \frac{\partial^2 C_{cu}}{\partial y^2} - V_x \frac{\partial C_{cu}}{\partial x} = R\,\frac{\partial C_{cu}}{\partial t} \tag{9}$$

where C_{cu} represents copper mass concentration in water and R is known as the retardation factor since it has the effect of retarding the transport of adsorbed species relative to the advection front..

For the flow of contaminated groundwater through the sandy soil, the value of R will be assumed equal to 1 which is reasonable for this type of soils. On the other hand, the sorption of copper on (WFS+KS) barrier is governed by Langmuir sorption isotherm and the retardation factor is expressed as:

$$R = 1 + \frac{\rho_d}{n_{\boldsymbol{B}}}\left(\frac{0.9292}{(1+0.092C_{cu})^2}\right) \tag{10}$$

where n_B is the porosity of the barrier.

To present theoretical verification for tank test described previously, Eq. (9) in combination with initial and boundary conditions **Table 3** can be solved using COMSOL Multiphysics 3.5a. The used mesh discrezation (i.e. number of mesh points, number of elements, and type of elements ….etc) is shown in **Fig. 7**.

Fig. 8 plotted the predicted spatial distribution of copper normalized concentration across the sand aquifer in the presence of (WFS+KS) barrier after 7 days for flow rate equal to 60 and 120 ml/min. It is clear that the propagation of contaminated plume is restricted by this barrier region. Also, the value of applied flow rate, i.e. velocity of flow, plays a significant role in the extent and concentration magnitude of the contaminant plume. Accordingly, the extent of contaminant plume in the longitudinal (x) direction is greater than transverse (y) direction and highest concentrations occur in the sand bed which up-gradient of PRB. The concentration of the contaminated plume reaching the outlet may attain lower than 1.3 mg/l quality limit prescribed for surface water or drinking water **, Hashim et al., 2011**.

Comparisons between the predicted and experimental results at nodes corresponding to monitoring ports during the migration of the Cu^{+2} plume at different periods of time for flow rate equal to 120 ml/min using (WFS+KS) barrier are depicted in **Fig. 9**. Although the spatial and temporal concentration profiles are taken the same trend, concentration values in the ports (1, 2, and 3) located along the centerline of the source area (y=20 cm) are greater than that in the ports (4, 5, and 6) deviated from the centerline by 10 cm (i.e. y=10 cm). Also, it is clear that the (WFS+KS) barrier have a potential functionality in the retardation of the contaminant migration in the down gradient of this barrier (concentration at ports 3 & 6 equal approximately zero). However, a reasonable agreement between the predicted and experimental results can be observed with ME less than 10%.

4. CONCLUSIONS

- Contact time, initial pH of the solution, initial metal ion concentration, (WFS+KS) dose and agitation speed were most the parameters affected on the sorption process between Cu^{+2} ions and (WFS+KS). The best values of these parameters that will achieve the maximum removal efficiency of Cu^{+2} (=93%) were 1 h, 6.5, 50 mg/l, 1 g/100 ml, and 250 rpm respectively.
- The experimental data for copper sorption on the (WFS+KS) were correlated well by the Langmuir isotherm model with coefficient of determination (R^2) equal to 0.986.
- FTIR analysis proved that the carboxylic and alkyl halides groups are responsible for the sorption of copper onto WFS.
- The results of 2D numerical model solved by COMSOL Multiphysics 3.5a under equilibrium condition proved that the (WFS+KS) barrier is efficient technique in the restriction of contaminant plume. However, a good agreement between the predicted and experimental results was recognized with ME not exceeded 10 %.

REFERENCES

- Bazdanis, G., Komnitsas, K., Sahinkaya, E., and Zaharaki, D., 2011, *Removal of Heavy Metals from Leachates Using Permeable Reactive Barriers Filled with Reactive Organic/Inorganic Mixtures*, Proceedings of the 3rdInternational Conference on Environmental Management, Engineering, Planning, and Economics *(CEMEPE 2011) & SECOTOX Conference*, Skiathos island, Greece (19-24 June).

- Chalermyanont, T., Chetpattananondh, P., and Riyapan, N., 2013, *Numerical Modeling of Permeable Reactive Barriers to Treat Heavy-Metal Contaminated Groundwater*, 6th PSU-UNS International Conference on Eng. and Tech. (ICET_2013), Novi Sad, Serbia, University of Novi Sad, Faculty of Technical Sciences.

- Chen, J. P., Wang, L., and Zou, S. W., 2008, *Determination of Lead Bio-sorption Properties by Experimental and Modeling Simulation Study*, Chemical Eng. J., 131, 209-215.

- Di Natale, F., Di Natale, M., Greco, R., Lancia, A., Laudante, C., and Musmarra, D., 2008, *Groundwater Protection From Cadmium Contamination by Permeable Reactive Barriers*, J. Hazard. Mater., 160, 428–434.

- Doke, K. M., Yusufi, M., Joseph, R. D., and Khan, E. M., 2012, *Bio-sorption of Hexavalent Chromium onto Wood Apple Shell: Equilibrium, Kinetic and Thermodynamic Studies*, Desalination and Water Treatment, 50, 170-197.

- El-Sayed, G. O., Dessouki, H. A., and Ibrahim, S. S., 2010, *Bio-sorption of Ni(II) and Cd(II) Ions from Aqueous Solutions onto Rice Straw*, Chem. Sci. J., CSJ-9.

- Hamdaoui, O., and Naffrechoux, E., 2007, *Modeling of Adsorption Isotherms of Phenol and Chlorophenols onto Granular Activated Carbon*, J. Hazard. Mater., 147, 381–394.

- Hashim, M. A., Mukhopadhyay, S., Sahu, J. N., and Sengupta, B., 2011, *Remediation Technologies for Heavy Metal Contaminated Groundwater*, J. of Environmental Management, 92, 2355-2388.

- Kumar, P. S., and Kirthika, K., 2009, *Equilibriumand Kinetic Study of Adsorption of Nickel from Aqueous Solution onto Bael Tree Leaf Powder*, J. Eng. Sci. and Tech., 4, 351-363.

- Lee, T., Benson, C. H.,and Eykholt, G. R., 2004, *Waste Green Sands as Reactive Media for Groundwater Contaminated with Trichloroethylene (TCE)*, J. Hazard. Mater., B109, 25-36.

- Mason, W.R., 2003, *Pollution of Groundwater*, www.encyclopedia.com › ... › Water:Science and Issues › January 2003.

- Mountjoy, K.J., Pringle, E.K., Choi, M., and Gowdy, W., 2003,*The Use of Permeable Reactive Barriers for In-situ Remediation of Groundwater Contaminants*, www.esaa-events.com/remtech/2003/pdf/Mountjoy.pdf.

- Oliveira, P. E. F., Oliveira, L. D., Ardisson, J. D., and Lago, R. M., 2011, *Potential of Modified Iron Rich Foundry Waste for Environmental Applications: Fenton Reaction and Cr(VI) Reduction*, J. Hazard. Mater., 194, 393-398.

- Siddique, R., Kaur, G., and Rajor, A., 2010, *Waste Foundry Sand and its Leachate Characteristics*, Resources, Conservation and Recycling, 54, 1027-1036.

- Ujfaludi, L., 1986, *Longitudinal Dispersion Tests in Non-uniform Porous Media*, Hydrological Sciences - Journal - des Sciences Hydrologiques, 31.

- Wang, S., Nan, Z., Li, Y., and Zhao, Z., 2009, *The Chemical Bonding of Copper Ions on Kaolin from Suzhou, China*, Desalination ,249 ,991–995.

- Watts, R.J., 1998, *Hazardous Wastes: Sources, Pathways, Receptors*, John Wiley and Sons, Inc.

NOMENCLATURE

a: empirical constant , l/g.
b: saturation coefficient , mg/g.
C_{cu}: copper concentration , mg/l.
C_o : initial concentration , mg/l.
C_e : equilibrium concentration , mg/l.
C_u: uniformity coefficient , dimensionless.
D_L: longitudinal hydrodynamic dispersion coefficient , m^2/sec.
D_o: molecular diffusion coefficient , m^2/sec.
D_x: longitudinal dispersion coefficient , m^2/sec.
D_y: lateral dispersion coefficient , m^2/sec.
K_F: freundlich sorption coefficient , m^2/sec.
m :mass of (WFS+KS) in the flask , g.
n: porosity ,dimensionless.
q_e: amount of solute removed from solution , mg/kg.
R: retardation factor,dimensionless.
R^2: coefficient of determination
V : volume of solution in the flask , l.
V_x: actual velocity , m/sec.
τ: tortuosity factor of soil medium
ρ_b: bulk density of the soil , g/cm^3.
α_L: longitudinal dispersivity , cm.

Table 1. Composition and physico-chemical properties of WFS.

Property	**Value**
SiO_2**(%)**	94.36
Al_2O_3 **(%)**	2.82
Fe_2O_3 **(%)**	2.12
Na_2O (%)	0.24
CaO (%)	0.05
TiO_2 **(%)**	0.14
MgO (%)	0.23
K_2O (%)	0.039
Bulk density (g/cm3)	1.44
Particle density (g/cm3)	2.67
Porosity	0.46
Surface area (m2/g)	5.9351
Cation exchange capacity (meq/100 g)	10.94

Table 2. Composition and properties of the soil used in the present study.

Property	**Value**
Particle size distribution (ASTM D 422) Sand (%) Silt and Clay (%)	 99 1
Hydraulic conductivity (cm s^{-1})	$2x10^{-3}$
Cation exchange capacity (meq/100 g)	3.12
pH	8.5
Organic content (ASTM D 2974, %)	0.26
Bulk density (g/cm^3)	1.567
Porosity	0.409
Soil classification	Sand

Table 3. Boundary and initial conditions used in the transport modeling of copper in 2D laboratory scale tank.

Item	Location	Type/ Value
Boundary conditions	Upper boundary	No flux/symmetry
	Lower boundary	No flux/symmetry
	Left side boundary	No flux/symmetry
	Right side boundary	Advective flux
	Line source	Concentration=50 mg/l
Initial condition	(x,y)	Concentration=0

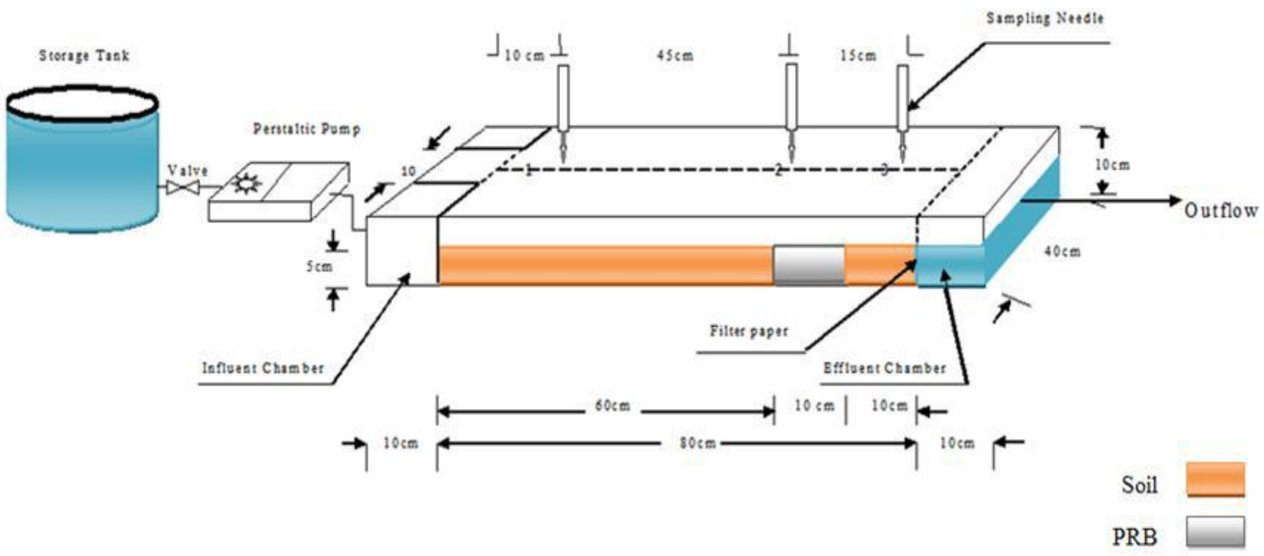

Figure 1. Schematic diagram of the bench-scale model aquifer.

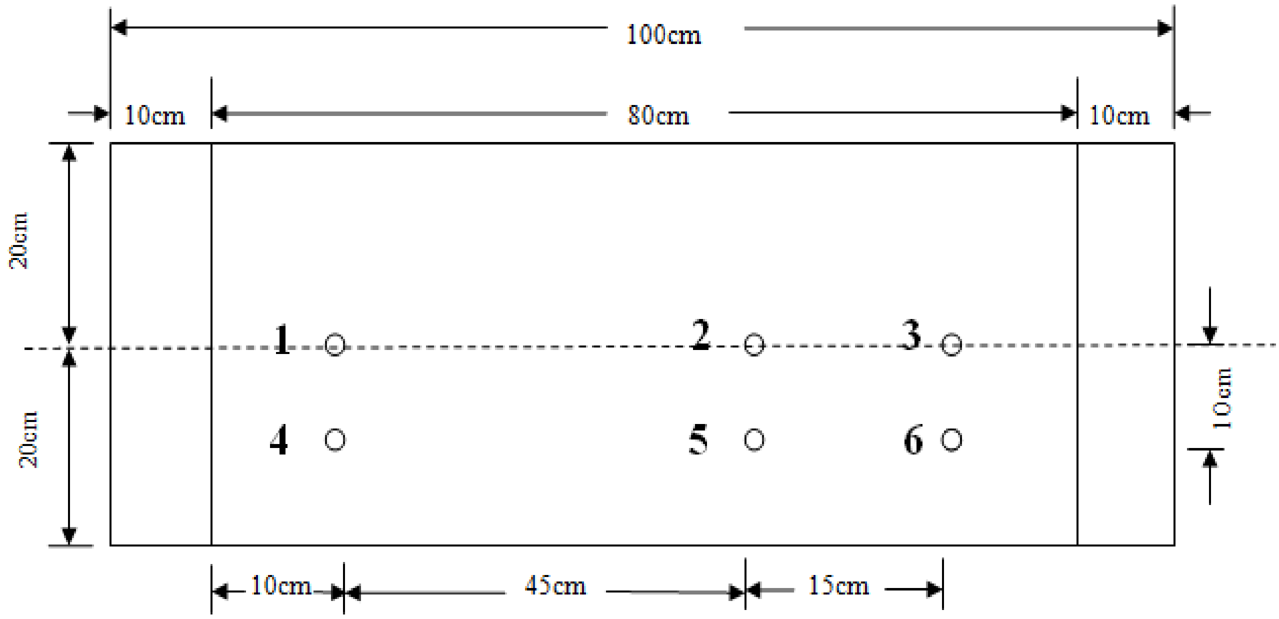

Figure 2. Schematic diagram of the sampling plate and sampling ports.

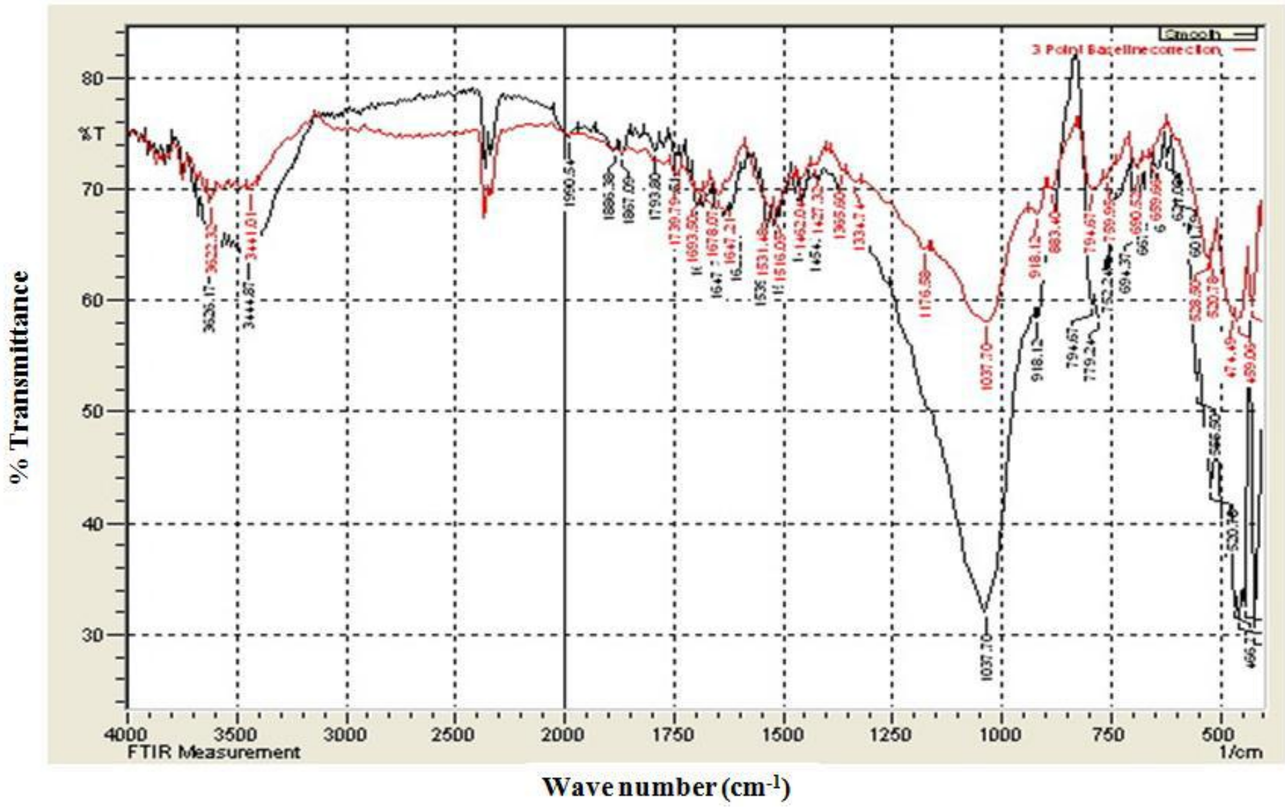

Figure 3. FTIR spectra of WFS (black line) before sorption and (red line) after sorption.

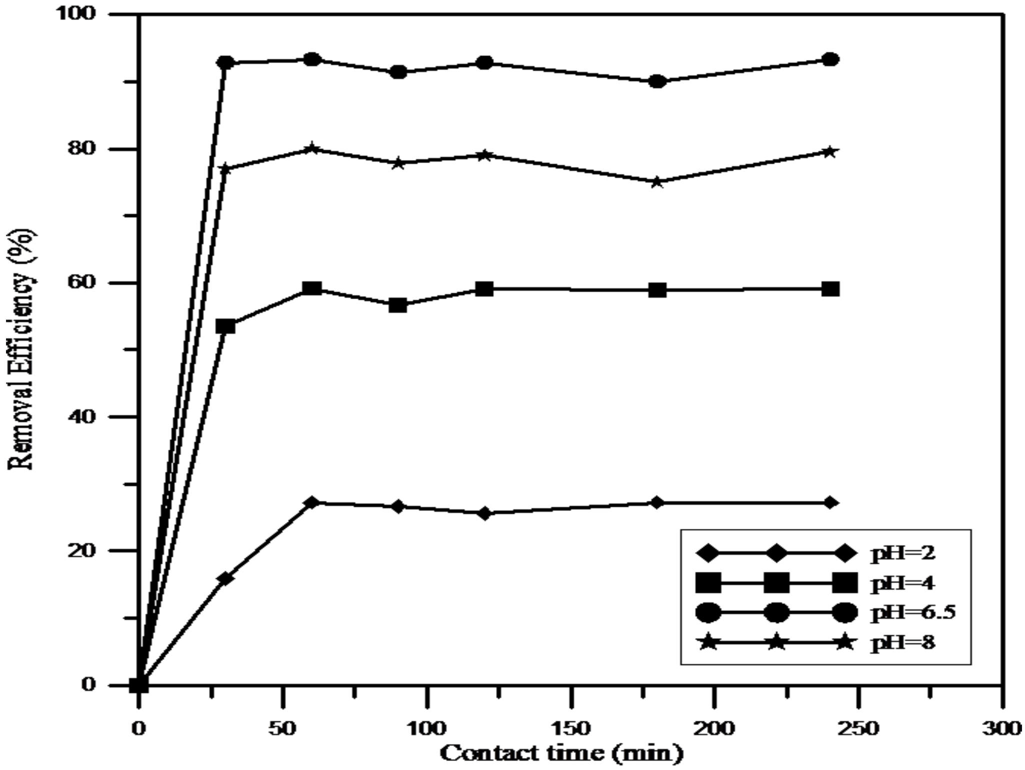

Figure 4. Effect of initial pH on removal efficiency of copper by (WFS+KS) as a function of contact time (C_o= 50 mg/l; (WFS+KS) dose= 1 g/100 ml; agitation speed= 250 rpm; T= 25^{o}C).

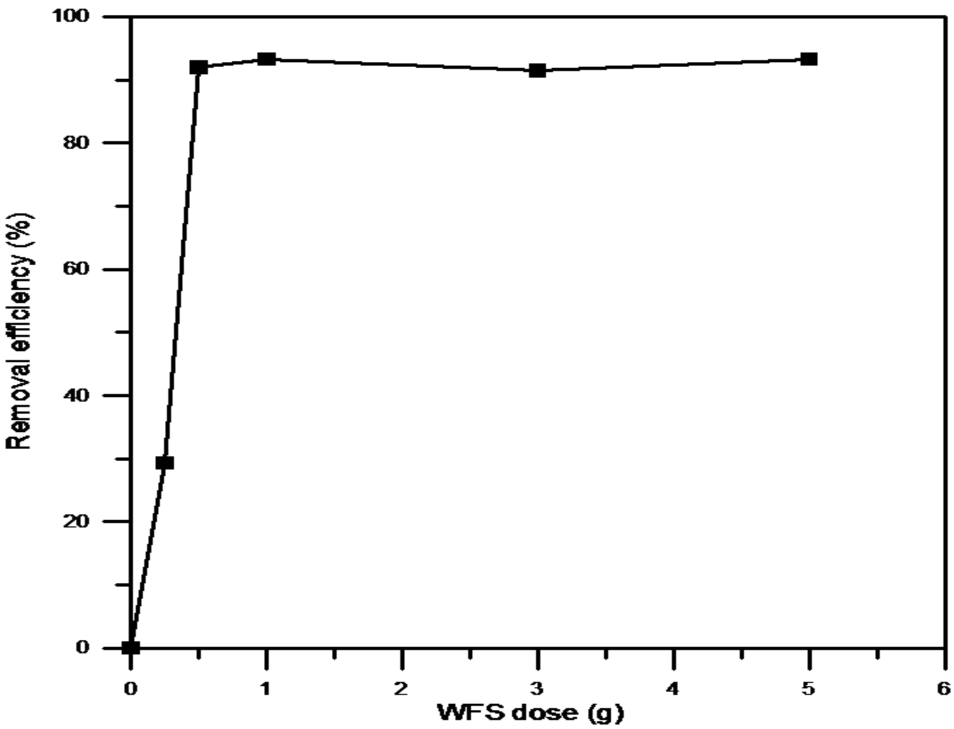

Figure 5. Effect of WFS dosage on removal efficiency of copper (C_o=50 mg/l; pH=6.5; agitation speed= 250 rpm; contact time=1 h; T= 25^{o}C).

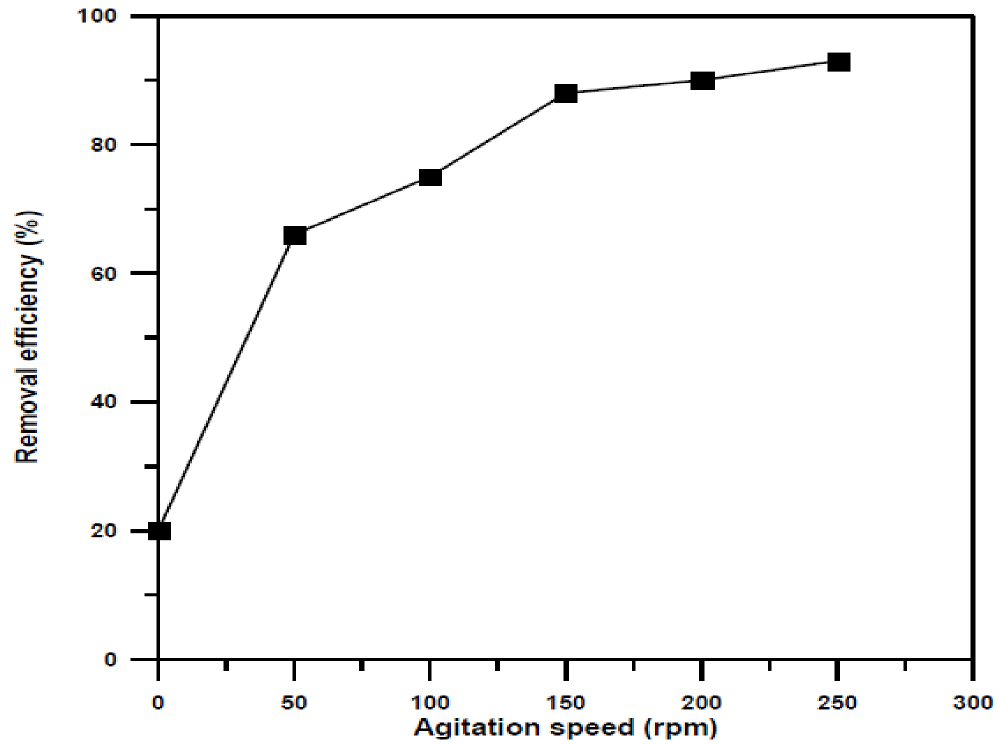

Figure 6. Effect of agitation speed on removal efficiency of copper as a function of contact time (C_o=50 mg/l; pH=6.5; WFS dose= 1 g/100 ml; T= 25^{o}C).

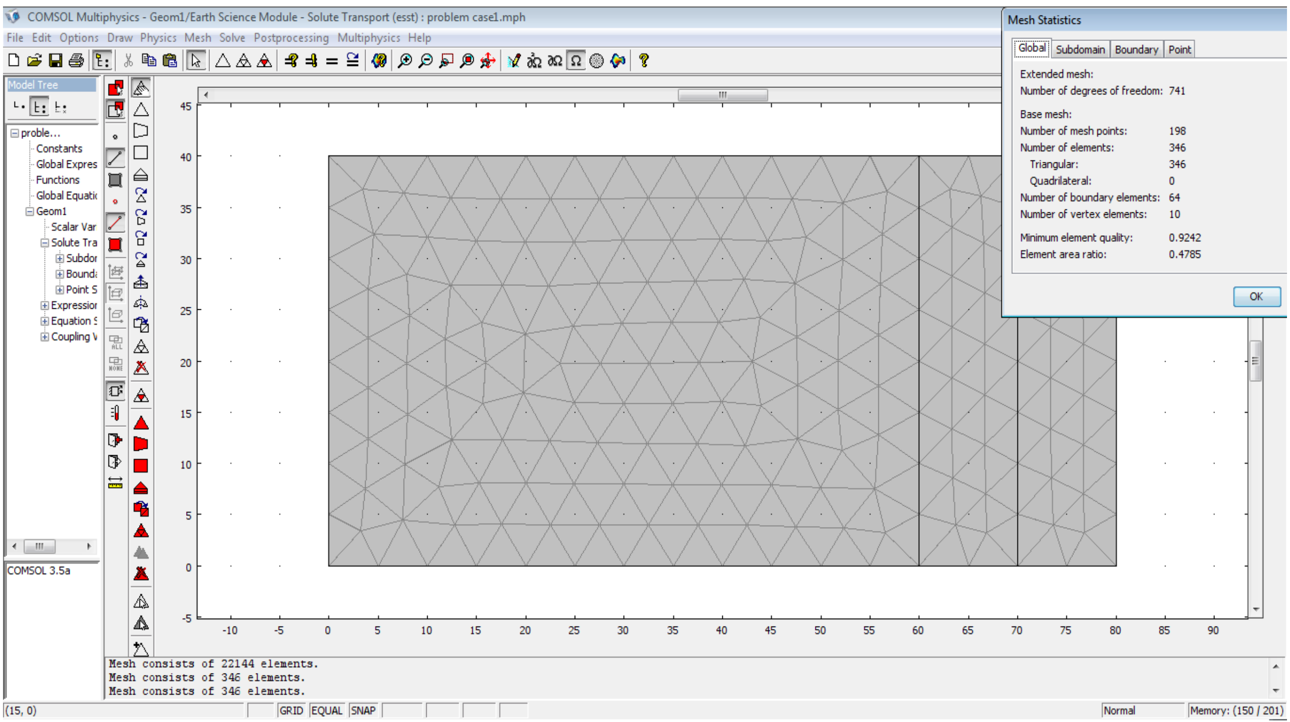

Figure 7. Domain discrezation and mesh statistics of 2D model (all dimensions in cm).

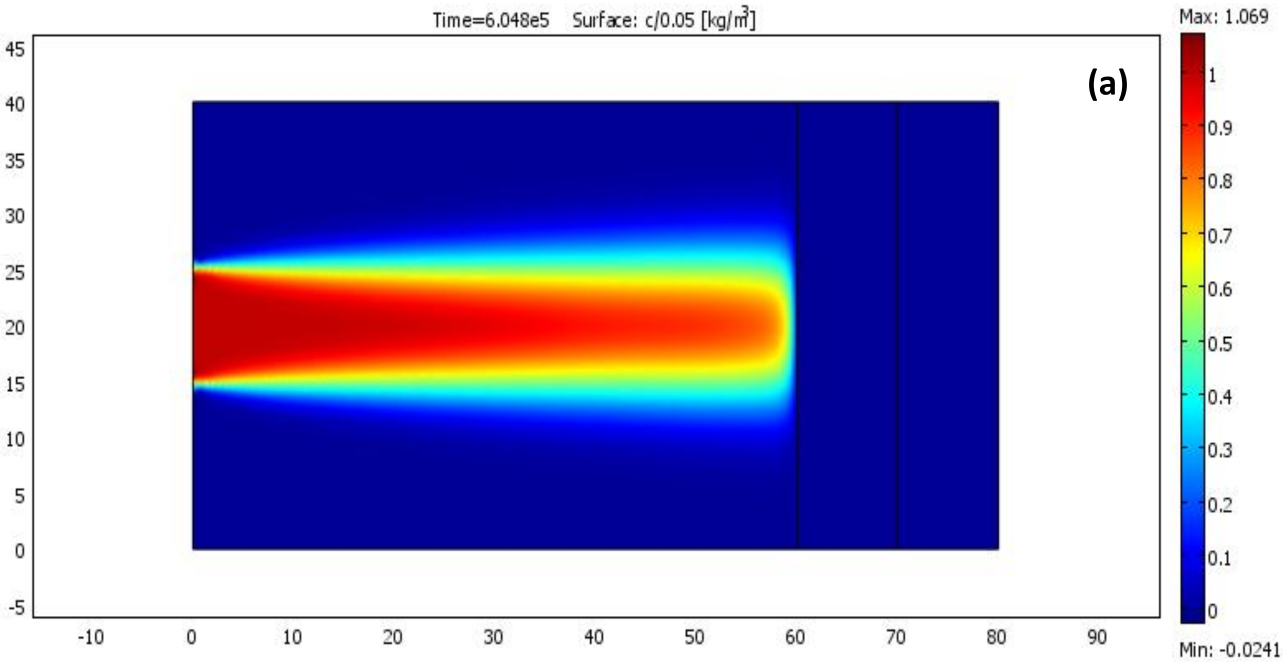

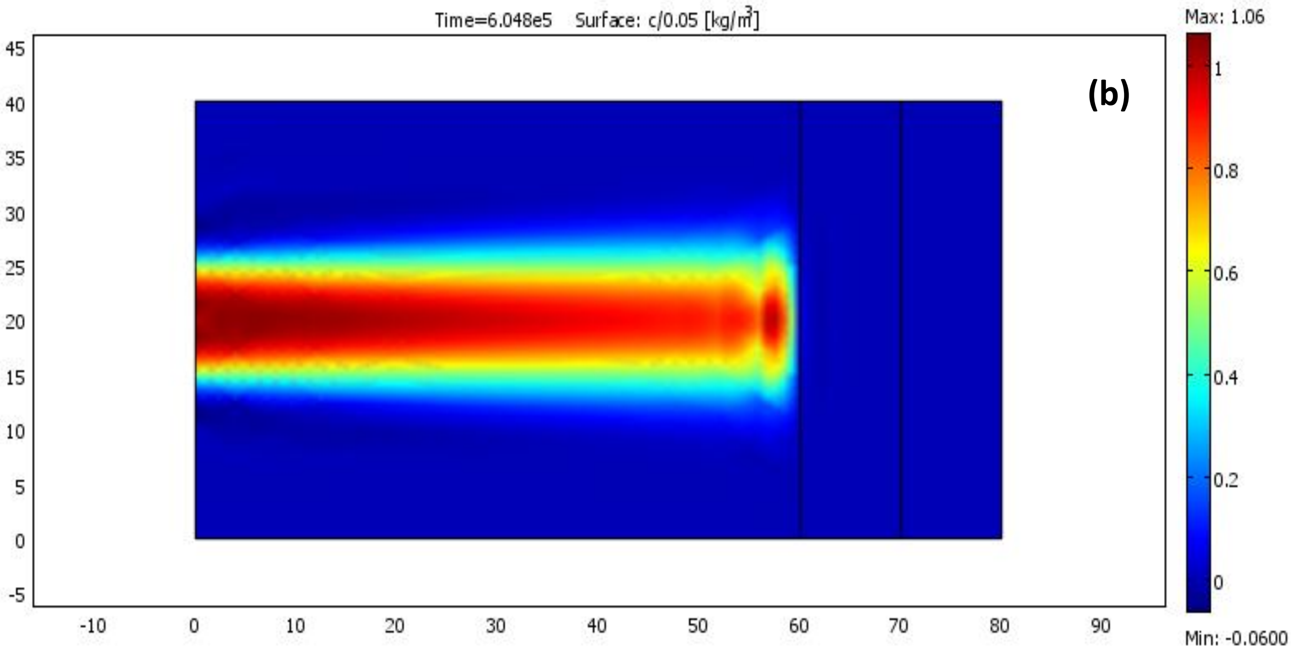

Figure 8. Distribution of copper concentration after 7 days for flow rate equal to (a) 60and (b) 120 ml/min.

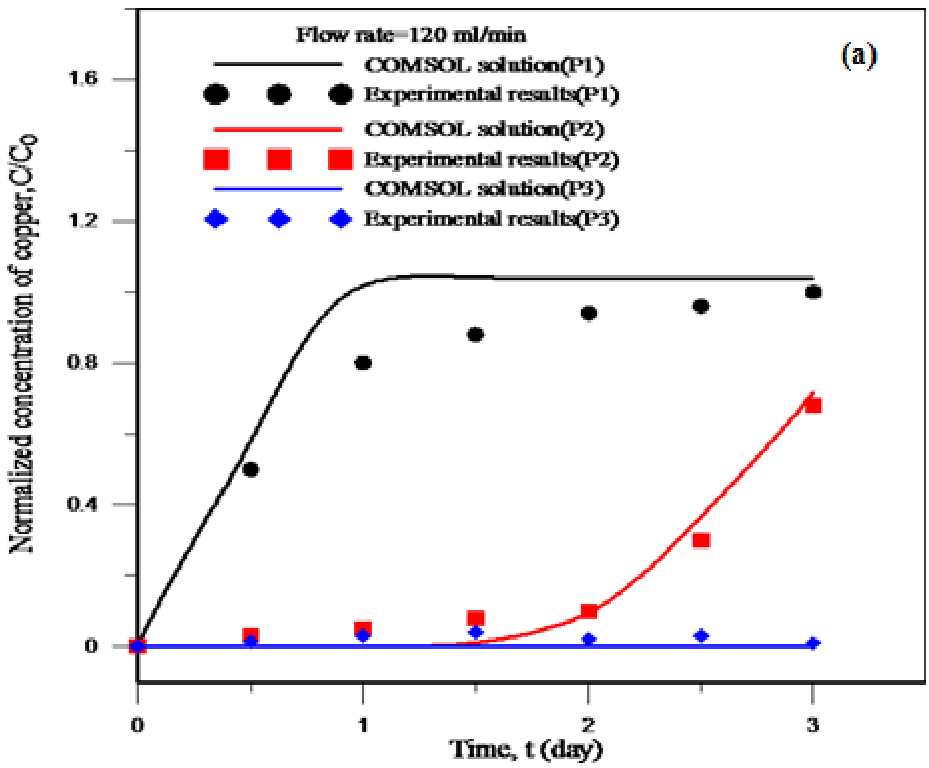

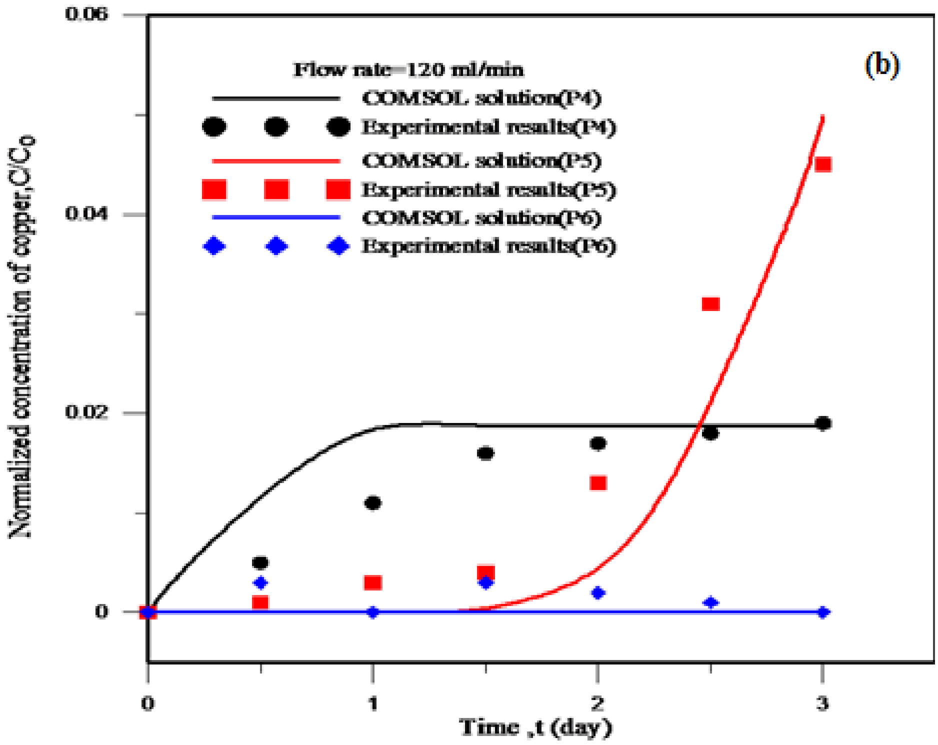

Figure 9. Breakthrough curves as a result of the copper transport at different ports located at (a) y=20 and (b) y=10 cm for flow rate=120 ml/min.

MR Brain Image Segmentation Using Spatial Fuzzy C- Means Clustering Algorithm

Dr. Safa Soud Mahdi
Medical Engineering Department
Engineering Collage- Nahrain University
email: dr_safaisoud@yahoo.com

Reem Shakir Mahmood
Medical Engineering Department
Engineering Collage- Nahrain University
email: reem_altameemi@yahoo.com

ABSTRACT

A conventional FCM algorithm does not fully utilize the spatial information in the image. In this research, we use a FCM algorithm that incorporates spatial information into the membership function for clustering. The spatial function is the summation of the membership functions in the neighborhood of each pixel under consideration. The advantages of the method are that it is less sensitive to noise than other techniques, and it yields regions more homogeneous than those of other methods. This technique is a powerful method for noisy image segmentation.

Keywords: fuzzy c-means; spatial information; image segmentation; clustering; mri brain image.

تجزئه صور الرنين المغناطيسي باستخدام المنطق المضبب المكاني (sFCM)

دكتور صفاء سعود مهدي
قسم الهندسة الطبيه
كلية الهندسة -جامعة النهرين

ريم شاكر محمود
قسم الهندسة الطبيه
كلية الهندسة- جامعة النهرين

ألخلاصه

ان خوارزميه المنطق المضبب الاعتياديه (FCM) لاتستخدم جميع المعلومات المكانيه للpixel وذلك يوثر سلبا في تقسيم الصوره بسبب وجود الضوضاء. في هذه البحث نستخدم خوارزميه (Spatial Fuzzy C-Mean) التي تتطلب تضمين المعلومات المكانيه للمعادله العضويه(membership function) للpixel التي تستخدم في تجزئه الصوره, والتي تحسب من خلال جمع ال(membership function)- في محيط كل pixel .فائده هذه الطريقه هي قله التحسس للضوضاء الذي في الصوره بالنسبه لبقيه طرق التجزئه ,وتكون المجاميع الناتجه عن هذه الطريقه متجانسه بحيث تعتبر هذه الخوارزميه هي الطريقه الفعاله لتجزئه الصور المشوشه.

الكلمات الرئيسية: المنطق المضبب , المعلومات المكانيه , تجزئة الصوره, التقسيم , صور الدماغ الرنينية

1. INTRODUCTION

The underlying objective of medical image segmentation is to partition it into different anatomical structures, thereby separating the components of interest, such as Brain tumors, from their background. Computerized medical image segmentation is a challenging problem, due to poor resolution and weak contrast. Moreover the task is often made more difficult by the presence of noise and artifacts, due to instrumental limitations, and patient movement.

In this paper, segmentation process is applied on Magnetic resonance imaging (MRI) Brain images, MRI is a noninvasive method for imaging internal tissues and organs, and it represents crucial diagnostic imaging technique for the early detection of abnormal changes in tissues and organs. It possesses fairly good contrast resolution for different tissues, and high spatial resolution and slice selection at any orientation.

Fuzzy c-means (FCM) is an unsupervised clustering technique that has been successfully applied to feature analysis, clustering, and classification in the fields such as astronomy, geology, medical imaging, target recognition, and image segmentation. An image can be represented in various feature spaces, and the FCM algorithm classifies the image by grouping similar data points in the feature space into clusters. This clustering is achieved by iteratively minimizing a cost function those dependents on the distance of the pixels to the cluster centers in the feature domain.

The pixels on an image are highly correlated, i.e., the pixels in the immediate neighborhood possess nearly the same feature data. Therefore, the spatial relationship of neighboring pixels is an important characteristic to improve the performance of FCM, many techniques have been developed.

Wang, et al., 2004. proposed a feature-weight assignment method is improved the performance of FCM clustering. **Mohamed, et al., 1999.** modified the fuzzy c-mean (MFCM) clustering algorithm where the membership value was chosen to tolerate the resistance. In this method, the spatial influence on the center pixel is considered as an explicit modification of its membership value to tolerate the resistance. **Liew, et al., 2000.** presented a spatial fuzzy clustering algorithm that exploits the spatial contextual information into image data, where the influence of the neighboring pixels is suppressed in nonhomogeneous regions of the image. **Das, et al., 2006.** proposes a particle swarm based segmentation algorithm for automatically grouping the pixels of an image into different homogeneous regions using spatial information.

The aim of this research is to introduce an improved segmentation method for FCM clustering. In a standard FCM technique, a noisy pixel is wrongly classified because of its abnormal feature data. Improved method incorporates spatial information, and the membership weighting of each cluster is altered after the cluster distribution in the neighborhood is considered. This scheme greatly reduces the effect of noise and biases the algorithm toward homogeneous clustering.

2. SPATIAL FUZZY C-MEANS CLUSTERING

Clustering techniques are mostly unsupervised methods that can be used to organise input data into groups based on similarities among the individual data items. The Fuzzy C-Means algorithm (often abbreviated to FCM) is an iterative algorithm that finds clusters in data and which uses the concept of fuzzy membership. Instead of assigning a pixel to a single cluster, each pixel will have different membership values on each cluster. This method was developed by Dunn in 1973 and improved by Bezdek in 1981 and it is widely used in image segmentation.

The Fuzzy C-Means attempts to find clusters in the data by minimizing an objective function given in the equation below **Chuang,et al., 2006.**

$$J = \sum_{j=1}^{N} \sum_{i=1}^{c} u_{ij}^{m} \parallel x_{j-} v_i \|^2 \quad (1)$$

J is the objective function and it reduces at each iteration. It means the algorithm is converging or getting closer to a good separation of pixels into clusters. N is the number of pixels in the image, C is the number of clusters used in the algorithm, (m >1) is a weighting factor that controls the fuzziness of the resultant segmentation, in this research m = 2, u_{ij} represents the membership function of pixel X_j in the ith cluster, V_i is the ith cluster center, , and $\| X_j - V_i \|$ is the Euclidean distance between X_j and V_i .the membership functions are subject to the following constraints: $\sum_{i=1}^{c} u_{ij}$=1; 0≤ $u_{ij} \leq 1$; 0< $\sum_{j=1}^{N} u_{ij} < N$

The cost function is minimized when pixel closes to the centeroid of their clusters are assigned high membership values, and low membership values are assigned to pixels with data far from the centeroid. The membership function represents the probability that a pixel belongs to a specific cluster. In the FCM algorithm, the probability is dependent on the distance between the pixel and each individual cluster center in the feature domain. The membership functions and cluster centers are updated iteratively **Li, et al., 2011.**

$$u_{ij} = \sum_{k=1}^{c} \left(\frac{\| x_j - v_i \|}{\| x_j - v_k \|} \right)^{\frac{-2}{(m-1)}} \quad (2)$$

And

$$v_i = \frac{\sum_{j=1}^{N} u_{ij}^{m} x_j}{\sum_{j=1}^{N} u_{ij}^{m}} \quad (3)$$

One of the problems of standard FCM algorithms in image segmentation is the lack of spatial information. Since image noise and artifacts often impair the performance of FCM segmentation, because neighboring pixels possess similar feature values, and the probability that they belong to the same cluster is great so it would be attractive to incorporate spatial information into a standard FCM algorithm **Chuang, et al., 2006.**

To exploit the spatial information, a spatial function is defined as

$$h_{ij} = \sum_{k \in NB(x_j)} u_{ij} \quad (4)$$

Where NB (x_j) represents a square window centered on pixel x_j in the spatial domain. A 5x5 window was used in this research. Just like the membership function, the spatial function h_{ij} represents the probability that pixel x_j belongs to *i*th cluster. The spatial function of a pixel for a cluster is large if the majority of its neighborhood belongs to the same cluster. The spatial function is incorporated into membership function as follows:

$$u'_{ij} = \frac{u_{ij}^{p} h_{ij}^{q}}{\sum_{k=1}^{c} u_{ij}^{p} h_{ij}^{q}} \quad (5)$$

where p and q are parameters to control the importance of both functions. In a homogenous region, the spatial functions fortify the original membership, and the clustering result remains unchanged. However, for a noisy pixel, this formula reduces the weighting of a noisy cluster by the labels of its neighboring pixels. As a result, misclassified pixels from noisy regions can easily be corrected. The spatial FCM with parameter p and q is denoted $\mathrm{sFCM}_{p,q}$.Note that $\mathrm{sFCM}_{1,0}$ is identical to the conventional FCM **Soesanti, eta al.**

The flow chart of the sFCM algorithm is shown in **Fig. 1**

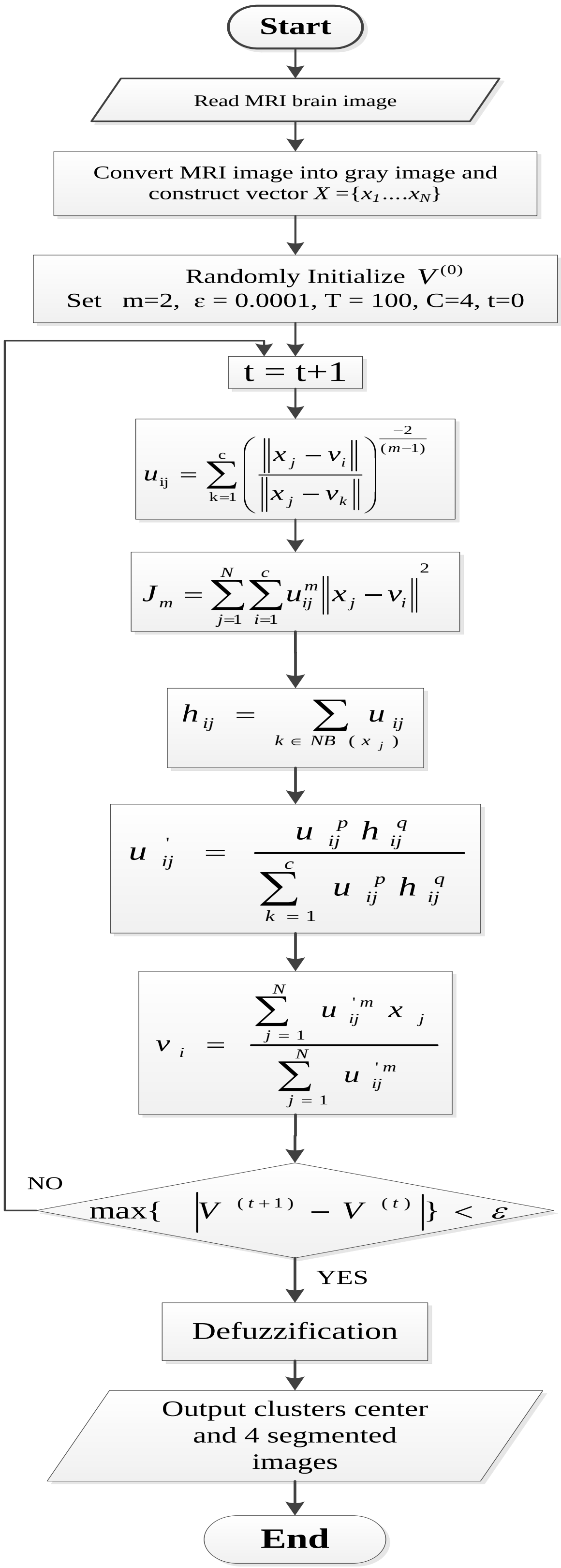

Figure 1. The flow chart of sFCM algorithm.

3. VALIDITY FUNCTIONS FOR FUZZY CLUSTERING

1. Clustering validity functions based on partition coefficient and partition entropy.

Fuzzy partition used in this paper to evaluate the performance of clustering in a quantitative way. The representative functions for the validity function based on the fuzzy partitions are partition coefficient Vpc and partition entropy Vpe which are defined as follows **Sayadi, et al., 2007.** :

$$V_{pc}=\frac{\sum_j^N \sum_i^c u_{ij}^2}{N} \tag{6}$$

and

$$V_{pe}=\frac{-\sum_j^N \sum_i^c \,[u_{ij} * \log u_{ij}]}{N} \tag{7}$$

The idea of these validity functions is that the partition with less fuzziness means better performance. In both equation (6) and (7), u_{ij} (i = 1, 2,…c; j = 1, 2,… N) is the membership of data point j in cluster i. As a result, the good clustering is achieved when ($\frac{1}{c} \leq v_{pc} \leq 1$) and ($0 \leq v_{pe} \leq 2$), the best clustering is when the value V_{pc} is maximal or V_{pe} is minimal **Xiao, et al., 2010.**

2. Clustering validity functions based on geometric sample structure.

The idea of validity functions based on measuring geometric data structure is that samples within one partition should be compact and samples between different clusters should be separate. To quantify the ratio of total variation within clusters and the separation of clusters, Xie and Beni proposed Xie-Benie validity function V_{xb} and it is defined as follows **Xiao, et al., 2010.**

$$V_{xb}=\frac{-\sum_j^N \sum_i^c \, u_{ij}^2 \, \|x_j - v_i\|^2}{N * (\, \min_{i \neq k} \{ \|v_k - v_i\|^2\})} \tag{8}$$

An optimal clustering result generates samples that are within one cluster and samples that are separated between different clusters. Minimised V_{xb} is expected to lead to a good partition.

Partition coefficient and partition entropy is a class of validation functions that uses only the membership function to evaluate the partitioning of the clusters. Their disadvantages are that it does not take into account the geometrical properties of the data and it depends monotonically on the number of clusters while Xie-Beni validity function however quantifies the performance of the clustering by taking into account the total variation within each clusters and the separation between-cluster.

4. RESULT AND DISCUSSION

A complete program using MATLAB programming language and CPU Core 2 Duo (1.83 GHz) for this process. **Fig. 2** shows the 512 x 416 grayscale original MRI Brain image with tumor.

The spatial function modifies the membership function of a pixel according to the membership statistics of its neighborhood. Both sFCM techniques reduce the noise effect, because no similar cluster is present in the neighborhood, the weight of the noisy cluster is greatly reduced with sFCM. Furthermore, the membership of the correct cluster is enhanced by the cluster distribution in the neighboring pixels. As a result, both sFCM techniques effectively correct the misclassification caused by the noise and makes the segmented images more homogeneous.

The MR images used in this paper are obtained from AL-KADEMYA HOSPITAL for male patient (year birth:1950).

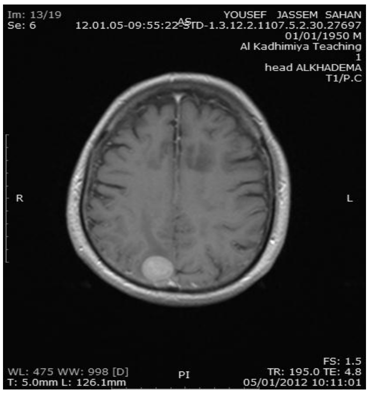

Figure 2. T1 weighted image.

Fig.3 to **Fig.6** shows the result of segmentation of image shown in **Fig. 2** by applying spatial FCM algorithm with parameter (p=1,q=1) on T1 weighted image.

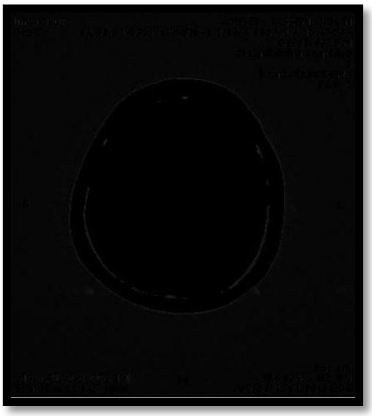

Figure 3. Cluster 1 of $\mathrm{FCM}_{1,1}$ algorithm.

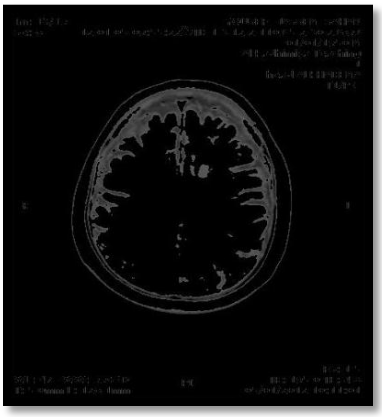

Figure 4. Cluster 2 of $FCM_{1,1}$ algorithm.

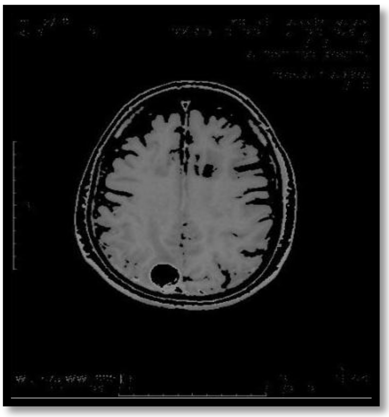

Figure 5. Cluster 3 of $\mathrm{sFCM}_{1,1}$ algorithm.

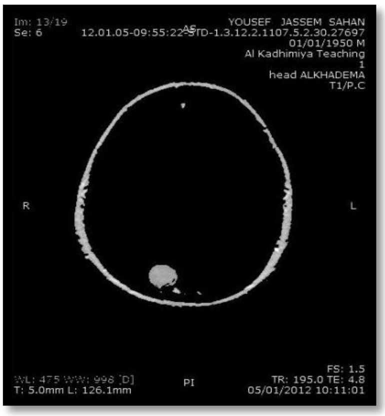

Figure 6. Cluster 4 of $\mathrm{FCM}_{1,1}$ algorithm.

Different gray levels were taken for initialization of the clusters centers as shown in table 1 while table 2 shows the optimized clusters centers obtained from the iteration of the $FCM_{1,1}$ algorithm.

Table 1. Selected clusters centers.

40	90	140	200

Table 2. optimized clusters center.

7.2124	68.1943	112.0011	187.8991

The plot shown in **Fig .7** shows how the iterative optimization of the objective function is carried out with the up-dating of the membership function u_{ij} and the clusters centers c_{ij}.

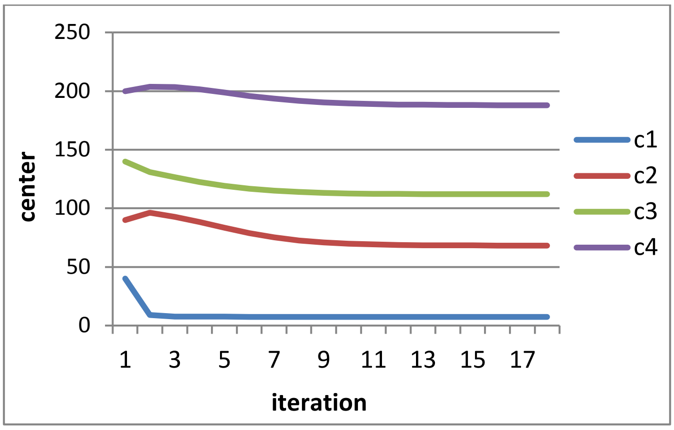

Figure 7. Iterative optimization of cluster center for $\mathrm{FCM}_{1,1}$ algorithm.

Fig. 8 shows the bars graph of the four clusters.

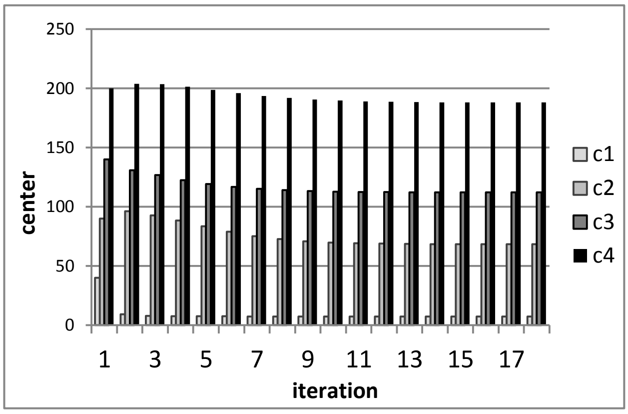

Figure 8. Bar graph for cluster variation in each iteration for $\mathrm{FCM}_{1,1}$ algorithm.

Fig.9 to **Fig.12** shows the result of segmentation of image shown in **Fig. 1** with parameters (p=0, q=2).

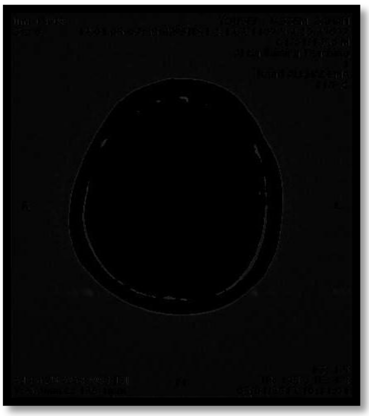

Figure 9. Cluster 1 of $FCM_{0,2}$ algorithm.

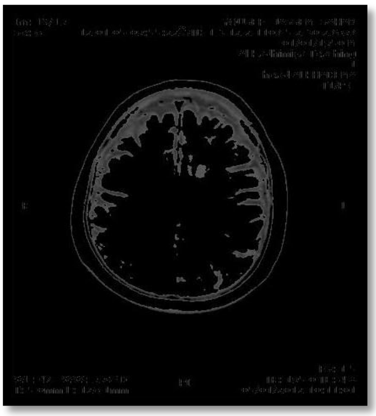

Figure 10. Cluster 2 of $FCM_{0,2}$ algorithm.

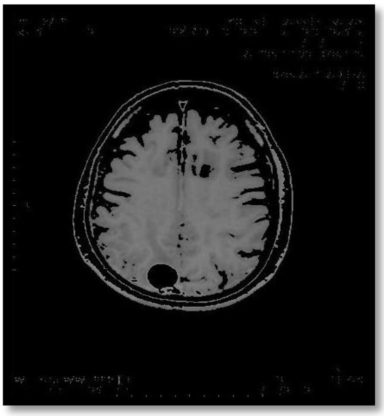

Figure 11. Cluster 3 for $s\mathrm{FCM}_{0,2}$ algorithm.

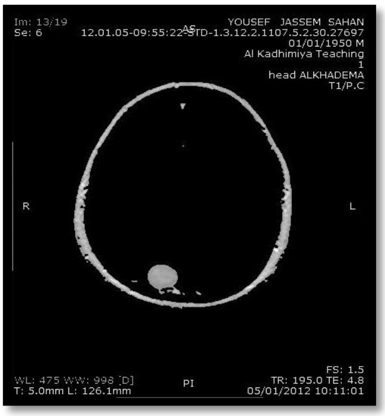

Figure 12. Cluster 4 of $FCM_{0,2}$ algorithm.

In table 3 shown Deferent gray levels were taken for initialization of the clusters centers while table 4 shows the optimized clusters centers obtained from the iteration of the $FCM_{0,2}$ algorithm.

Table 3. Selected clusters centers.

40	90	140	200

Table 4. Optimized clusters center.

11.3708	69.9816	110.8312	165.8091

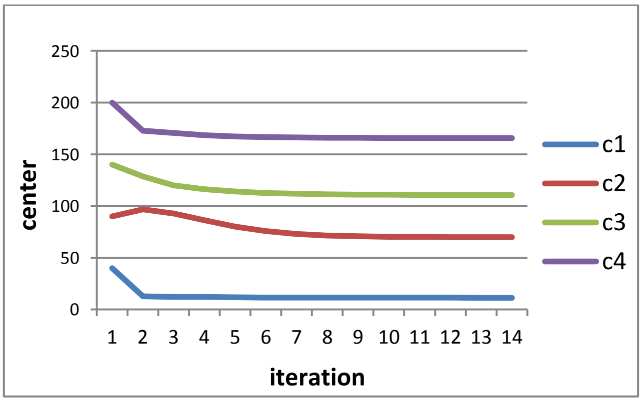

Figure 13. Iterative optimization of cluster center for $sFCM_{0,2}$ algorithm.

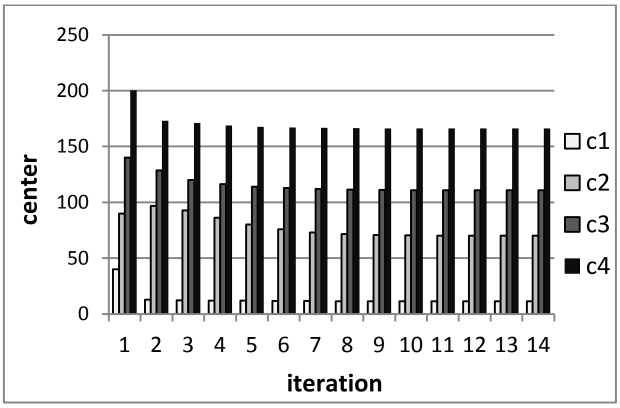

Figure 14. Bar graph for cluster variation in each iteration for $sFCM_{0,2}$ algorithm.

Three basic tissue classes found on a healthy brain MR image: white matter (WM), gray matter (GM) and cerebrospinal fluid (CSF).

Both sFCM techniques reduce the overlap of gray matter with white matter cluster, because the spatial function modifies the membership statistics of its neighborhood. Such neighboring effect biases the solution toword piecewise-homogeneous labeling, this make the segmented images more homogeneous. The sFCM algorithm with a higher q (>1) parameter shows a better smoothing effect, but disadvantages of using higher spatial weighting (q) are the blurring of some of fine details. This is difficult to judge from the results so used the cluster validity functions. Table.5 tabulates the validity functions used to evaluate the performance of sFCM clustering. In this cases, the validity functions based on the fuzzy partition were better for the $sFCM_{1,1}$ (p=1, q=1) than $sFCM_{0,2}$ (p=0, q=2). For V_{pc} (V_{pe}), the $sFCM_{1,1}$ is greater (smaller) than $sFCM_{0,2}$, and the validity function based on feature structure showed increased for $sFCM_{0,2}$. V_{xb} Measured the compactness in the feature domain. The sFCM modifies the partition on the basis of spatial distribution and causes deterioration of compactness in feature domain so V_{xb} is increased for $sFCM_{0,2}$ more than $sFCM_{1,1}$.

Table5. Cluster validity function.

Type	Vpc	Vpe	Vxb
$\mathbf{sFCM_{1,1}}$	**0.9622**	**0.0675**	**0.0041**
$\mathbf{sFCM_{0,2}}$	**0.9377**	**0.1125**	**0.042**

5. CONCLUSIONS

In this paper, spatial fuzzy c mean was applied in segmenting an actual MRI data set. This method improved the segmentation result, by incorporates the spatial information into the membership function to improve the segmentation results. The membership functions of the neighbors centered on a pixel in the spatial domain are enumerated to obtain the cluster distribution statistics; these statistics are transformed into a weighting function and incorporated into the membership function. This neighboring effect reduces the noise effect and makes the clustering more homogeneous.

The result of $sFCM_{1,1}$ (p=1, q=1)algorithm shows good segmentation result better than $sFCM_{0,2}$ because higher spatial weighting (q) cause blurring of some fine details, also using cluster validity function to evaluate the performance of both method show the best clustering is achieved using $sFCM_{1,1}$ algorithm with maximum value of V_{pc} (1.28% larger than $sFCM_{0,2}$), and minimum value of V_{pe} (25% less than $sFCM_{0,2}$), minimum value of V_{xb} (82.21% less than $sFCM_{0,2}$)

The results show that the method effectively segmented MRI brain images with spatial information, and the segmented abnormal MRI brain images can be analyzed for diagnosis purpose.

6. REFERENCES

- Chuang, K., Tzeng, H., Wu, J., and Chen, T., 2006, *Fuzzy C-Means Clustering with Spatial Information for Image Segmentation*," Elsevier Ltd. Computerized Medical Imaging and Graphics, vol. 30, pp. 9-15.

- Das, S., Abraham, A., and Konar, A., 2006, *Spatial Information Based Image Segmentation Using a Modified Particle Swarm Optimization Algorithm*' ISDA, vol. 2, pp. 438-444.

- Li, B., Chui, C., Chang, S., and Ong, S. H., 2011, *Integrating Spatial Fuzzy Clustering With Level Set Methods for Automated Medical Image Segmentation*, Elsevier Computers in Biology and Medicine, vol. 41, pp.1–10.

- Liew, A.W.C., Leung, S. H., and Lau, W. H., 2000, *Fuzzy Image Clustering Incorporating Spatial Continuity*, IEEE Proceedings-Vision, Image and Signal Processing', pp.185-192.

- Mohamed, N.A., Ahmed, M.N., and Farag, A., 1999, *Modified Fuzzy C-Mean in Medical Image Segmentation*, Proc. Int. Conf. Acoustics, Speech, and Signal Processing, pp. 3429-3432.

- Sayadi, M., Tlig, L., and Fnaiech, F., 2007, *A New Texture Segmentation Method Based on The Fuzzy C-Mean Algorithm and Statistical Features*," Applied Mathematical Sciences, Vol. 1, pp. 2999 – 3007.

- Soesanti, I., Susanto, A., Widodo, TH. S., and Tjokronagoro, M., *MRI Brain Images Segmentation Based on Optimized Fuzzy Logic and Spatial Information*, International Journal of Video & Image Processing and Network Security ,Vol .11 No (04), 6-11.

- Supot S., Thanapong, C., Chuchart, P., and Manas, S., *Segmentation of Magnetic Resonance Images Using Discrete Curve Evolution and Fuzzy Clustering*," IEEE International Conference on Integration Technology, pp. 697-700.

- Wang, X., Wang, Y., and Wang, L., 2004, *Improving Fuzzy C-Means Clustering Based on Feature weight Learning*, Pattern recognition letters, vol. 25, (10), pp. 1123- 1132.

- Xiao, K., Ho, S. H., and Bargiela, A., 2010, *Automatic brain MRI segmentation scheme based on feature weighting factors selection on fuzzy c-means clustering algorithms with Gaussian smoothing*, Int. J. of Computational Intelligence in Bioinformatics and Systems Biology, vol. 1, pp. 316-331.

7. NOMENCLATURE

C	Cluster Number
h_{ij}	Spatial Function
J_m	Objective Function
m	Fuzziness Factor
N	No. Of Pixels In Image
NB (x_j)	A Square Window Centered On Pixel
P, q	Parameter control the importance of spatial function and membership function
t	Iteration
T	Max Number Of Iteration
X	Vector Of Data Set
x_j	Individual Pixel
μ_{ij}	Membership Function Of Pixel
μ'_{ij}	Membership Function With Spatial Information
v_i	Cluster Center

Laminar Forced Convection of Dusty Air through Porous Media in a Vertical Annulus

Asst. Prof. Dr. Manal Hadi salh AL-Hafidh
Engineering College-Baghdad University
Email: manal hadi2005@yahoo.com

Salman Hameed Obaid
Engineering College-Baghdad University
E-mail: moment_1989@yahoo.com

ABSTRACT

An experimental and numerical study has been carried out to investigate the forced convection heat transfer by clean or dusty air in a two dimensional annulus enclosure filled with porous media (glass beads) between two vertical concentric cylinders. The outer cylinder is of (82 mm) outside diameters and the inner cylinder of (27 mm) outside diameter. Under steady state condition; the inner cylinder surface is maintained at a high temperature by applying a uniform heat flux and the outer cylinder surface at an ambient temperature. The investigation covered values of input power of (6.3, 4.884, 4.04 and 3.26 W), Reynolds number values of (300, 700, 1000, 1500, and 2000) and dust ratio values (density number N) of (2, 4, 6 and 8). A computer program in MATLAB has been built to carry out the numerical solution by writing the governing equation in finite difference method. The local Nusselt number, the average Nusselt number, the contours of temperature field and velocity field were presented to show the flow and heat transfer characteristics. The results show that when clean air flow, the wall temperature gradually increases along the cylinder length in the direction of flow and decrease as Reynolds number increase while it increases with input power. For dusty air flow results show that the wall temperature gradually increases along the axial direction and increase with Reynolds number and with input power, and the maximum reduction in heat transfer will be 30 % for N=8 at Re=2000. Comparison was made between the present experimental and numerical results and it gives good agreement. The experimental and numerical Nusselt number follows the same behavior with a mean deviation of 12%.

Key words: laminar, dusty air, forced convection, two dimensional, vertical annulus enclosure, glass beads.

الحمل القسري الطباقي لهواء مترب خلال وسط مسامي في محتوى حلقي عمودي

الاستاذ المساعد د. منال هادي الحافظ
كلية الهندسة - جامعة بغداد

سلمان حميد عبيد
كلية الهندسة - جامعة بغداد

الخلاصة

أجريت في هذا البحث دراسة عملية ونظرية لإنتقال الطاقة الحرارية بالحمل القسري بواسطة الهواء النقي أو المترب في فجوة حلقية ثنائية الأبعاد مملؤة بوسط مسامي (كرات زجاجية) بين أسطوانتين عموديتين متحدتي المركز. القطرالخارجي للأسطوانة الخارجية (82mm) والقطر الخارجي للأسطوانة الداخلية (27 mm). تحت شروط حالة الإستقرار تم حفظ سطح الأسطوانة الداخلية بدرجة حرارية ثابتة وعالية بتسليط فيض حراري منتظم وتم حفظ سطح الأسطوانة الخارجية بدرجة حرارة الجو.شملت الدراسة قيم القدرة المدخلة (6.3, 4.884, 4.04 and 3.26 W) وعدد رينولد Re (300, 700, 1000, 1500, and 2000) وقيم نسب التراب N(2, 4, 6 and 8. تم بناء برنامج بلغة mat lab لتنفيذ الحل العددي باستخدام طريقة الفروق العددية. وتم

تمثيل عدد نسلت الموقعي وعدد نسلت المتوسط ومخططات المجال الحراري ومجال السرعة لتوضيح خواص الجريان وانتقال الطاقة الحرارية. أظهرت النتائج في حالة جريان الهواء النقي أن درجة الحرارة تزداد تدريجيا على طول الأسطوانة باتجاه الجريان وتقل بزيادة عدد رينولد بينما تزداد بزيادة القدرة المدخلة. نتائج جريان الهواء المترب بينت أن درجة الحرارة تزداد تدريجيا في الإتجاه المحوري وتزداد بزيادة عدد رينولد و القدرة المدخلة وأن أقصى انخفاض بانتقال الطاقة الحرارية يساوي % 30 لقيمة N=8وRe=2000. قورنت النتائج العملية والنظربة للبحث الحالي وأظهرت توافق جيد. نتائج عدد نسلت العملية والنظرية أظهرت السلوك ذاته بنسبة إنحراف 12%.

كلمات رئيسية : الطباقي, حمل قسري, هواء مترب, ثنائي الابعاد, محتوى حلقي عمودي, كرات زجاجية.

INTRONDUCTION

Fluid flow in a porous medium is a common phenomenon in nature, and in many fields of science and engineering. Important every day flow phenomena include transport of water in living plants and trees, and fertilizers or wastes in soil. Moreover, there is a wide variety of technical processes that involve fluid dynamics in various branches of process industry. The importance of improving our understanding of such processes arises from the high amount of energy consumed by them. In oil recovery, for example, a typical problem is the amount of unrecovered oil left in oil reservoirs by traditional recovery techniques ,**Aaltosalmi, 2005**. Flow through Convective heat transfer in porous medium has been intensively studied over the past two decades. This is because of its wide applications in geothermal energy engineering, ground-water pollution transport, nuclear waste disposal, chemical reactors engineering, insulation of buildings and pipes, storage of grain coal, **Kaurangini and Basant, 2009**.A lot of experimental and numerical study had been carried out in pure air and dusty air to investigate the heat transfer by forced convection by , **Cheng et al, 1988.** Analyzed the problem of a thermally developing forced convective flow in a packed channel heated asymmetrically. The flow in the packed channel was assumed to be hydrodynamically fully developed and was governed by the Brinkman-Darcy-Ergun equation with variable porosity taken into consideration. A closed - form solution based on the method of matched asymptotic expansions was obtained for the axial velocity distribution, and the wall effect on pressure drop was illustrated.

Al Zahrani and SuhilKiwan, 2008. investigated numerically the steady-state, laminar, axisymmetric, mixed convection heat transfer in the annulus between two concentric vertical cylinders using porous inserts. The inner cylinder was subjected to constant heat flux and the outer cylinder was insulated. A finite volume code was used to numerically solve the sets of governing equations. The Darcy–Brinkman–Forschheimer's model along with Boussinesq's approximation was used to solve the flow in the porous region. The Navier–Stokes equation was used to describe the flow in the clear flow region. The dependence of the average Nusselt number on several flow and geometric parameters was investigated. These include: convective parameter, λ, Darcy number, Da, thermal conductivity ratio, *K*r, and porous-insert thickness to gap ratio *(H/D)*. It was found that, in general, the heat transfer enhances by the presence of porous layers of high thermal conductivity ratios. It was also found that there is a critical thermal conductivity ratio on which if the values of Kr are higher than the critical value the average Nusselt number starts to decrease. Also, it found that at low thermal conductivity ratio $(K\mathrm{r} \approx 1)$ and for all values of λ the porous material acts as thermal insulation.

Kumar et al., 2011. studied the effect of Dusty fluid on MHD free convection flow past a vertical porous plate with heat and mass transfer taking Viscous and Darcy resistance terms into account and the constant permeability of the medium numerically and neglecting induced magnetic field in

comparison to applied magnetic field. The velocity, temperature, concentration and skin friction distributions are derived. It is observed that velocity of dusty fluid and dust particles increases with the increase in Gr (Grashof number), K (Permeability parameter), B (Dusty fluid parameter) and B1 (Dust particles parameter), but it decreases with the increase in M (Magnetic parameter).
In the present work an experimental and numerical investigation had been done to study the 2–dimensional laminar convection heat transfer in an annulus of two concentric vertical cylinders with clean or dusty air as working fluid. The annulus contains porous media (glass beads) and the inner cylinder heated to a constant wall temperature using constant heat flux. The outer cylinder kept at atmospheric temperature. In the numerical method the finite difference approximation is applied and a MATLAB program is built to solve these equations.

EXPERIMENTAL STUDY

The test section in the present work is indicated diagrammatically in **Fig.1.** A centrifugal blower (AUGUSTO CATTANI) of (2.5 cm) diameter was used to supply the air to the system. The dust concentrations were determined during tests by using electronic balance with an accuracy of 0.001 g**.** Dust concentration was calculated by measuring the difference in glass wool weight before and after test.
The dust was stored in a storage tank with a capacity accommodate a large amount of dust. The storage tank has three holes, One of these holes is used for air to inter the tank and then to balance the pressure between the test pipe and the dust storage tank which is called equilibrium pipe, the second hole used to feed the test system with fine dust, while the last one was closed tightly and used to refill the storage tank with dust. The storage tank is connected with a dust control valve to control the concentration of dust before entering the test system**.** The glass wool filter is a cylindrical vessel shaped of 2 cm thick and 12 cm inside diameter and 15 cm height. Glass wool filter was used to retention dust and to determine the concentration of dust. A flow meter was used in the range of (0 – 10 m^3/hr.) and linked with a plastic tube with a diameter of (1.9812cm)**.** Dusty air valve opened after measuring the dust concentration and the dusty air allowed passing to test section.
The test section consists of a Aluminum outer cylinders of (82 mm) outside diameters, (4 mm) thick and (260mm) long to which Aluminum inner cylinders of (27mm) outside diameter, (260 mm) long and (5 mm) thick; yield into radius ratios of 0.365 mm Aluminum was chosen because of its high thermal conductivity, available, cheap and for its easy machinability. The holder and the test rig are connected together and balanced to be vertical so that the inclination angle indicates to read zero. The inner cylinder was heated by passing an alternating current through a (0.25 mm) in diameter, (5m) long, 97 – ohm Nichrome wire coiled as spiral inside glass tube where glass tube was of (8mm) in diameter and (250 mm) long**.** The heater (i.e. the glass tube and the Nichrome wire) was mounted concentrically by two Teflon pieces. Teflon piece drilled to pass the working fluid and thermocouples wires, The inner cylinder was heated by passing an alternating current to a heater inside the inner cylinder and the outer cylinder was subjected to the surrounding temperature. The inner cylinder surface temperatures were measured at six locations using thermocouples type (K). The investigation covered values of input power of (6.3, 4.884, 4.04 and 3.26 W), Reynolds number values of (300, 700, 1000, 1500, and 2000) and dust ratio values (density number N) of (2 to 8).

MATHEMATICAL MODEL

The geometry and coordinate system of the problem considered are shown in **Fig. 2**. Convective heat transfer through a saturated porous media with dusty air flow is considered. The research is based on a series of concepts; such concepts include porosity, permeability of the porous medium, speed of dusty air through porous media, and the quantity of dust particles (called density number) in the fluid flowing through the medium. In order to model the incompressible flow in the porous medium of the steady-state equations. The governing equations are given as follow:

Mass conservation

The properties of both the fluid and saturated solid matrix are taken as constant, except the fluid density which defined the buoyancy in the momentum equation. Then the mass conservation can be written as **Shyamanta, 1998**.

$$\frac{1}{r}\frac{\partial}{\partial r}(r\,u)+\frac{\partial v}{\partial z}=0 \tag{1}$$

Momentum Equation

The equations of motion of a steady viscous incompressible fluid with uniform distribution of dust particles in a porous medium are given by, **Shyamanta, 1998 and AL-Sumaily et al., 2011.**

In R direction

$$\frac{u}{\in}\frac{\partial u}{\partial r}+\frac{v}{\in}\frac{\partial u}{\partial z}=-\frac{1}{\rho}\frac{\partial P}{\partial r}+\frac{\upsilon_{eff}}{\in}\left(\frac{\partial}{\partial r}\left[\frac{1}{r}\frac{\partial}{\partial r}(ru)\right]+\frac{\partial^2 u}{\partial z^2}\right)+\frac{k}{\rho}N\times u-\frac{\upsilon}{K}u \tag{2}$$

In z direction

$$\frac{u}{\in}\frac{\partial v}{\partial r}+\frac{v}{\in}\frac{\partial v}{\partial z}=-\frac{1}{\rho}\frac{\partial P}{\partial z}+\frac{\upsilon_{eff}}{\in}\left(\frac{1}{r}\frac{\partial}{\partial r}\left[r\frac{\partial v}{\partial r}\right]+\frac{\partial^2 v}{\partial z^2}\right)+\frac{k}{\rho}N\times v-\frac{\upsilon}{K}v \tag{3}$$

Energy Equation:

The most important law applied here is the first law of thermodynamic, and according to the assumptions the energy equation is , **AL-Sumaily et al., 2011.** :

$$\frac{\rho\,c_p}{\in}\left(u\frac{\partial T}{\partial r}+v\frac{\partial T}{\partial z}\right)=k_{eff}\left[\frac{1}{r}\frac{\partial}{\partial r}\left(r\frac{\partial T}{\partial r}\right)+\frac{\partial}{\partial z}\left(\frac{\partial T}{\partial z}\right)\right] \tag{4}$$

Where

C_p is specific heat of fluid at constant Pressure ($\frac{kJ}{kg.K}$).

Dimensionless Governing Equations

The advantage of non dimentionalization is that the minimum number of characteristic parameters results. Also the problem variables may be at the same time normalized. All spatial dimensions are nondimensionalized with respect to the gap D as follow ,**Shyamanta, 1998:**

$$V = \frac{v}{v_\infty} \quad R = \frac{r}{Dh} \ , \quad Z = \frac{z}{Dh} \quad P = \frac{p}{\rho v_\infty{}^2} \quad \theta = \frac{(T - T_\infty)}{(T1 - T_\infty)} \ Re = \frac{v_\infty Dh}{\upsilon} \ U = \frac{u}{v_\infty}$$

$$N^* = \frac{C}{R_t}, \quad C = \frac{m \quad N}{\rho} \quad R_t = \frac{m \ u_\infty}{k \ Dh} \ \gamma = \frac{\upsilon_{eff}}{\upsilon} \ , Da = \frac{K}{Dh^2}, R_K = \frac{k_{eff}}{k_f}$$

Where:

C = dust particle concentration.

R_t= relaxation time parameter of dust particle, **Shyamanta, 1998**.

Taking curl of momentum equations to eliminate pressure terms, the momentum and the energy equation will be:

$$\frac{1}{\in}\frac{\partial(U\omega)}{\partial R} + \frac{1}{\in}\frac{\partial(V\omega)}{\partial Z} = (N^* \in - \frac{\in}{\operatorname{Re} Da})\omega + \frac{\gamma}{\operatorname{Re}}\left(\frac{\partial}{\partial R}\left(\frac{1}{R}\frac{\partial(R\omega)}{\partial R}\right) + \frac{\partial^2 \omega}{\partial \ Z^2}\right) \tag{5}$$

$$\frac{1}{R \in}\left[\frac{\partial\Psi}{\partial Z}\frac{\partial\theta}{\partial R} - \frac{\partial\Psi}{\partial R}\frac{\partial\theta}{\partial Z}\right] = \frac{R_K}{\operatorname{Re}\ \Pr}\left[\frac{1}{R}\frac{\partial}{\partial R}\left(R\frac{\partial\theta}{\partial R}\right) + \frac{\partial^2\theta}{\partial Z^2}\right] \tag{6}$$

$$V = -\frac{1}{R}\frac{\partial\psi}{\partial R} \tag{7}$$

$$U = \frac{1}{R}\frac{\partial\psi}{\partial Z} \tag{8}$$

$$-\omega = \frac{1}{R}\left(\frac{\partial^2\psi}{\partial R^2} - \frac{1}{R}\frac{\partial\psi}{\partial R} + \frac{\partial^2\psi}{\partial \ Z^2}\right) = \nabla^2\psi \tag{9}$$

Dimensionless Hydraulic Boundary Conditions for stream lines

At R=$\frac{r_{in}}{Dh}$ and R=$\frac{r_{out}}{Dh}$

$$\psi(i,k) = \frac{4}{3}\psi(i,k+1) - \frac{1}{3}\psi(i,k+2)$$

At $Z = 0, \ L$

$$\psi(i,k)=\frac{4}{3}\psi(i+1,k)-\frac{1}{3}\psi(i+2,k)+\frac{2}{3}R(k)\Delta R$$

Dimensionless Thermal Boundary Conditions

At $R=\frac{r_{in}}{Dh}$ $\theta_{(i,k)}=1$

At $R=\frac{r_{out}}{Dh}$ $\theta(i,k)=\theta_2$

At Z=0 $\theta(i,k)=0$

At Z=L $\theta(i,k)=\theta_{av}$

Calculation of Average Nusselt Number

The average Nusselt number on the walls cylinder can be calculated from the equation below:

$$N\bar{u}=-\frac{1}{l}\int_0^l Nu\ dZ \tag{10}$$

Computational Technique

Eqs.(5, 6 and 9) were transformed into the finite difference equations, where the upwind differential method in the left hand side of the energy Eq. (6) and the centered – space differential method for the other terms were used, and solved by using (SOR) method ,**Wang and Zhang 1990**. A computer program was built using MATLAB to meet the requirements of the problem. The value of the stream line will be calculated at each node, in which the value of stream line is unknown, the other node will appear in the right hand side of each equation. As an initial value of iteration, zero is chosen for the stream line field, while a conduction solution is adopted for temperature field. The index (n) was used to represent the nth approximation of temperature denoted by Θ^n and substituted into the approximated equations, which were solved to obtain the nth –approximation of vorticity ω then substituted Eq.(5) to obtain stream line Ψ, then Ψ was substituted into Eq. (6) to obtain Θ^{n+1}. A similar procedure is repeated until the prescribed convergence criterion given by inequality:

$$Max\left|\frac{\theta^{n+1}-\theta^{n}}{\theta^{n}}\right| \le 10^{-8}$$

The number of grid points used was 41 grid points in the R– direction and 301 in the Z – direction which seems reasonable and will be used in the present study. **Fig.3** illustrates the numerical grid in two planes.

Calculation of Local Nusselt Number

The local Nusselt number (Nu_l) on the walls can be found from the equation below:

$$Nu_l = \frac{h \times w}{k} \tag{11}$$

The value of (h) can be found by making heat balance in the wall ,**Singh, 2003** as follow

$$q_{cond.} = q_{conv.} \tag{12}$$

$$h(T_1 - T_\infty) = -k\left(\frac{\partial T}{\partial r}\right)_{r=0} \tag{12}$$

Then:
From Nusselt number definition and dimensionless magnitudes:

$$Nu = -\left(\frac{\partial \theta}{\partial R}\right) \tag{13}$$

The local Nusselt number *Nu* on the inner walls was expanded in form of finite difference approximation using backward difference scheme, **Anderson et al., 1984.**

$$Nu = \frac{-3\theta_{i,k} + 4\theta_{i-1,k} - \theta_{i-2,k}}{2\,\Delta R} \tag{14}$$

RESULTS AND DISCUSSION

Fig.4 shows the temperature distribution for the case of clean air (N=0) through porous media for different values of Re. This figure illustrates that the temperature decreases with the Increase of (Re) and this is because increasing (Re) yields faster flow through the porous media over the heated wall .When the case of dusty air flow (for different values of dust ratio (N)) through porous media in the annulus and it is clear increase the temperature and increasing the dust ratio (N) leads to an additional increase in temperature. The porous medium affecting flow and heat transfer characteristics and it represents an additional resistance to the flow when compared with clear fluid flows.

Fig.5 shows the Z – component of the streamlines, in the (R-Z) plane for the cases of clean air and dusty air respectively. it is clear that intensity of streamlines increases in upper and lower surfaces of the annulus due to increase in Reynolds number (Re) and the intensity of streamlines decrease when the concentration of dusty air increase. Contours of velocity field in the (R-Z) plane are illustrated in **Fig.6** along the length of the annulus in (Z) direction. Flow illustrates symmetry in both sides of annulus and it is clear that its value in the bottom of the annulus is positive and in the upper is negative.

Fig.7 illustrates the case of dusty air flow through porous media in the annulus and it is clear that increasing the Reynolds number for constant dust ratio leads to increase the temperature and increasing the dust ratio (N) leads to an additional increase in temperature.

Fig.8, shows that the average Nusselt number for clean air increase with the increase of Reynolds number Re at constant heat flux. The average Nusselt number for dusty air decrease with Re and increasing the dust ratio cause an addition decrease in Nu as discussed previously.
The local Nusselt number depends on the temperature distribution along the cylinder length. **Fig.9** show that the local Nusselt number decreases gradually with the axial distance of the heated wall to about halve the length then became constant. The local Nu begin with high value at the inlet of entry length region due to the high difference between the air and the heated wall temperature, then progressively the difference between air and heated wall decreases. In experimental results **Fig.10** illustrates for the dusty air flow in annulus that the Nusselt number decreases with the increase of Reynolds number at constant heat flux and dust ratio. as well as the Nusselt number decreases with the increase of dust ratio at the same value of Reynolds number for constant heat flux.and it is clear that the Nusselt number increase with the increase of Reynolds number at constant dust number for different heat flux values and it is clear that as the heat flux increase the Nusselt number increase.
In **Fig.11** a comparison between the experimental and numerical results of the present work had been done for the variation of the Nusselt number with Reynolds number for clean air and dusty air with different dust ratios. The results of comparison show that the present experimental results follow the same behavior as the numerical results, with a deviation of (12%).

CONCLUSIONS

1. When clean air flow the wall temperature in the radial direction decreases as Reynolds number increases and the heat transfer decreases. For dusty air the wall temperature in the radial direction increase as Reynolds number increases and an addition increase was observed when dust number N increase.
2. The maximum percent reduction in heat transfer is 14.1 for N=8 at Re=2000.
3. The local Nusselt number decrease gradually along the length of the cylinder.
4. The average Nusselt number increases as the Reynolds number increases for clean air flow at constant heat flux.
5. The average Nusselt number decrease as the Reynolds number increases for dusty air flow at constant heat flux.
6. Comparison shows good agreement between the present and previous works.

REFERENCES

- Aaltosalmi U ,2005 *Fluid Flow in Porous Media with the Lattice – Boltzmann Method* PhD. Thesis, University of Jyväskylä on July 29, .

- Al-Sumaily Gazy F , John Sheridan, Mark C. Thompson,2012. *Analysis of forced convection heat transfer from a circular cylinder embedded in a porous medium* International Journal of Thermal Sciences 51 - 121-131.

- Al Zahrani and SuhilKiwan ,2008. *Mixed Convection Heat Transfer in the Annulus Between Two Concentric Vertical Cylinders Using Porous Layers* , J. of Transp Porous Med 76:391–405.

- Anderson A. A., Tannehill,C. J. and Pletcher H. R.1984, *Computational Fluid Mechanics and Heat Transfer*, McGraw – Hill book company/ Hemisphere Publisher.

- Cheng P., Hsu C.T. and Chowdhury A.,1988, *Forced Convection in the Entrance Region of Packed Channel with a Symmetric Heating* , Transactions of the ASME, Vol. 110, pp. 946 - 954.

- Kaurangini M.L. andBasant . K, 2009, *Mixed Convection Flow in A Vertical Annulus Filled with Porous Material Having Constant Porosity* , Techno Science Africana Journal, Volume 3 Number 1, June.

- Kumari M. and. Nathb G.,2008, *Unsteady Natural Convection from a Horizontal Annulus Filled with a Porous Medium*, Int. J. of Heat and Mass Transfer, Vol, 51, pp. 5001–5007. www.elsevier.com.

- Shyamanta, 1998, *MHD Flow and Heat Transfer of A Dusty Viscoelastic Stratified Fluid Down an Inclined Channel in Porous Medium Under Variable Viscosity*, Theoretical and applied mechanics ,vol.26,PP.1-14 .

- Singh N. P. and Ajay Kumar Singh, 2003, *MHD Free Convection and Mass Transfer Flow Past a Flat Plate*, the Arabian Journal for Science and Engineering, vol. 32, number 1A .

- Wang Bu – Xuan and Zhang Xing,1990 "*Natural Convection in Liquid Saturated Porous Media Between Concentric Inclined Cylinders*" Int. J. Heat and Mass Transfer Vol. 33. No 5, pp. 827-833.

NOMENCLATURE

Letter	Description	Units
C_p	Specific heat at constant pressure	kJ/kg °K
d_o	Outer diameter of the inner cylinder	M
dg	Diameter of glass bead	mm
Da	Darcy number $Da=K/Dh^2$	-
D_i	Inner diameter of the outer cylinder	m
D_h	Annulus diameter ($D_i\_ d_o$)	m
h_i	The convection heat transfer coefficient on the inner cylinder (hot surface)	W/m^{2}K
$K_{eff.}$	Effective thermal conductivity of the porous media	W/m K
k_f	Thermal conductivity of the fluid	W/m K

k_s	Thermal conductivity of the solid	W/m K
K	Permeability	m^2
l	Cylinder length	m
L	Dimensionless cylinder length	-
N	Dust ratio	g/min
N^*	Dimensionless dust ratio	-
Nu_1	Local Nusselt number on the inner cylinder $Nu_1 = -\left(\frac{\partial \theta}{\partial R}\right)_1$	-
p	Pressure	N/m^2
P	Dimensionless pressure	-
Q	Input power	W
Q	Convective heat transfer rate	W
$Q_{cond.}$	Heat loss by conduction	W
r	Radial coordinate	m
r_{in}	Radius of the inner cylinder	m
r_{out}	Radius of the outer cylinder	m
R	Dimensionless radial coordinate	m
Re	Reynolds number	$Re = \frac{V\ \ Dh}{\upsilon f}$
Rr	Radius ratio $Rr=r_{in}/r_{out}$	-
Pr	Prandtl number($Pr=\nu/\alpha$)	—
T	Temperature	K
T_∞	Ambiant temperature	K
T_1	Temperature of the inner cylinder surface	K
T_2	Temperature of the outer cylinder surface	K
T_{ave}	Average temperature((T_{1+} T_2)/2)	K
u	Radial velocity component	m/s

v	Axial velocity component	m/s
v_∞	Velocity of air in Axial direction	m/s
U	Dimensionless velocity component in R -direction	-
V	Dimensionless velocity component in Z -direction	-
w	Gap width ($r_{out} - r_{in}$)	m
x, y, z	Cartesian coordinate system	m
Z	Dimensionless axial coordinate	-

Greek Letters

Letter	Description	Units
α	Thermal diffusivity	m^2/s
$\alpha_{eff.}$	Effective thermal conductivity of the porous media	m^2/s
β	Volumetric thermal expansion coefficient	1/K
ε	Porosity	-
θ	Dimensionless temperature	-
γ	Dimensionless kinematic viscosity	-
R_K	Dimensionless thermal conductivity	-
μ_f	Dynamic viscosity of fluid	$N.s/m^2$
ρ_f	density of fluid	kg/m^3
t	Time	s
υ_f	Kinematic viscosity of the fluid	m^2/s
ψ	Streamline	-
ω	Dimensionless vorticity	-
ΔR, ΔZ	Distance between the grid points	-

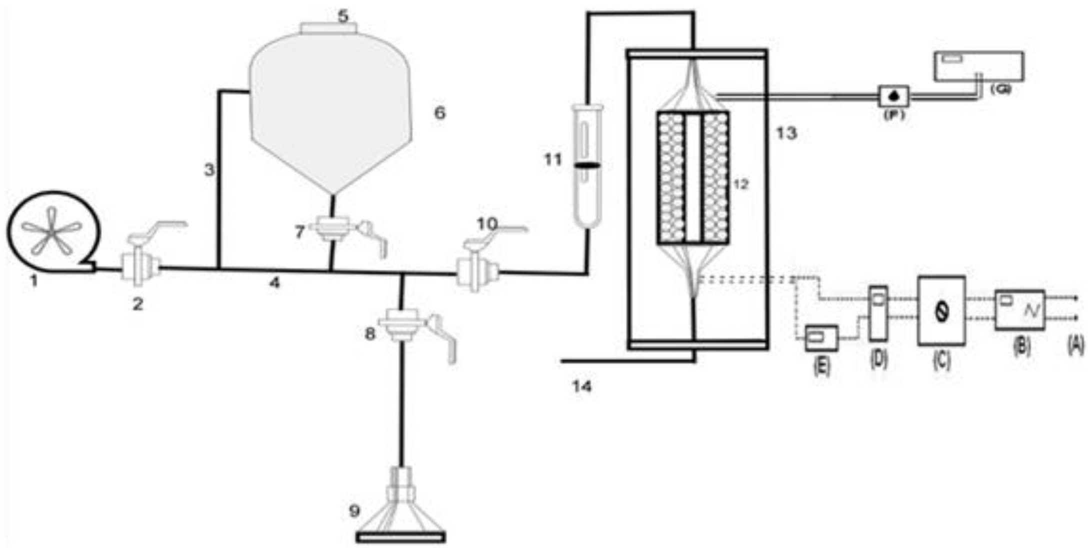

1-Blower 2- flow control valve 3- equilibrium pipe 4- main pipe 5- hole to refill dust
6- dust storage tank 7- dust control valve 8- retention dust valve 9- glass wool filter
10- dusty air valve 11- flow meter 12- vertical annulus With porous media
13- Outer cover 14- outlet pipe A- power supply B- stabilizer C- variac
D- Voltmeter E- Ammeter F- selector switch G- digital thermometer ,
-------- Heater Circuit , ———— Thermocouple Circuit

Figure 1. Schematic diagram of experimental apparatus.

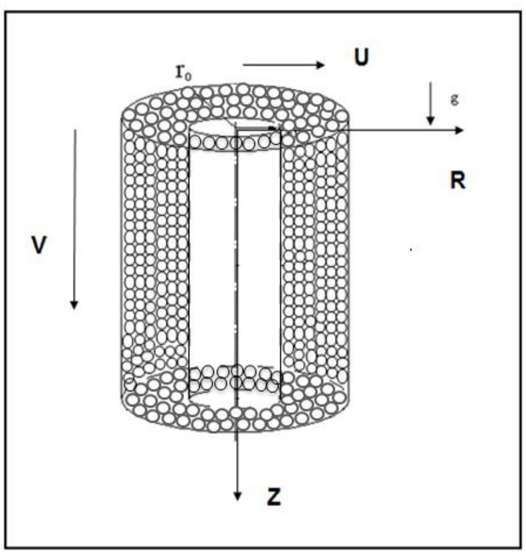

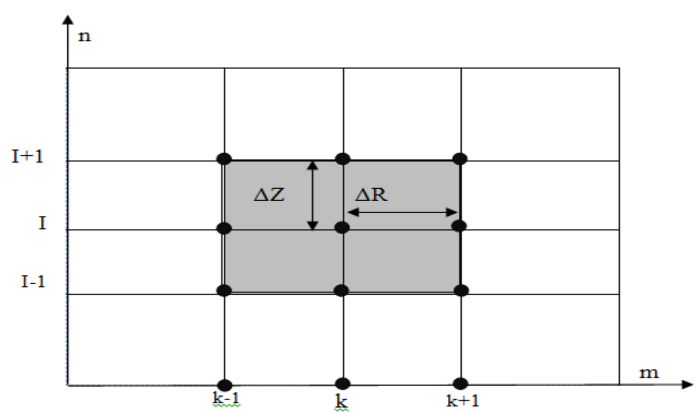

Figure 3 . A Plot of two dimensional discretized domains.

Figure 2 . Geometry and coordinates system.

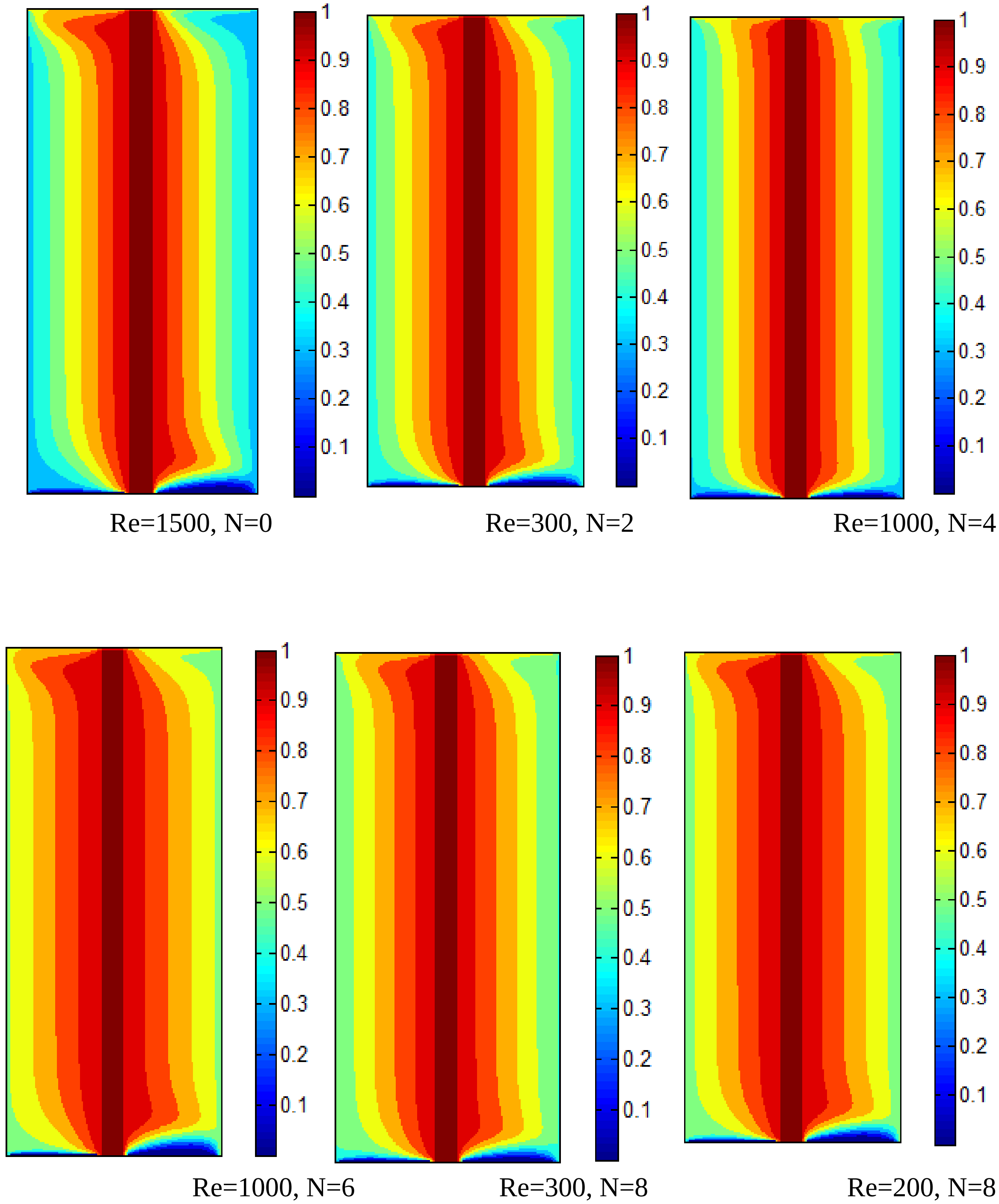

Figure 4. Temperature distributions.

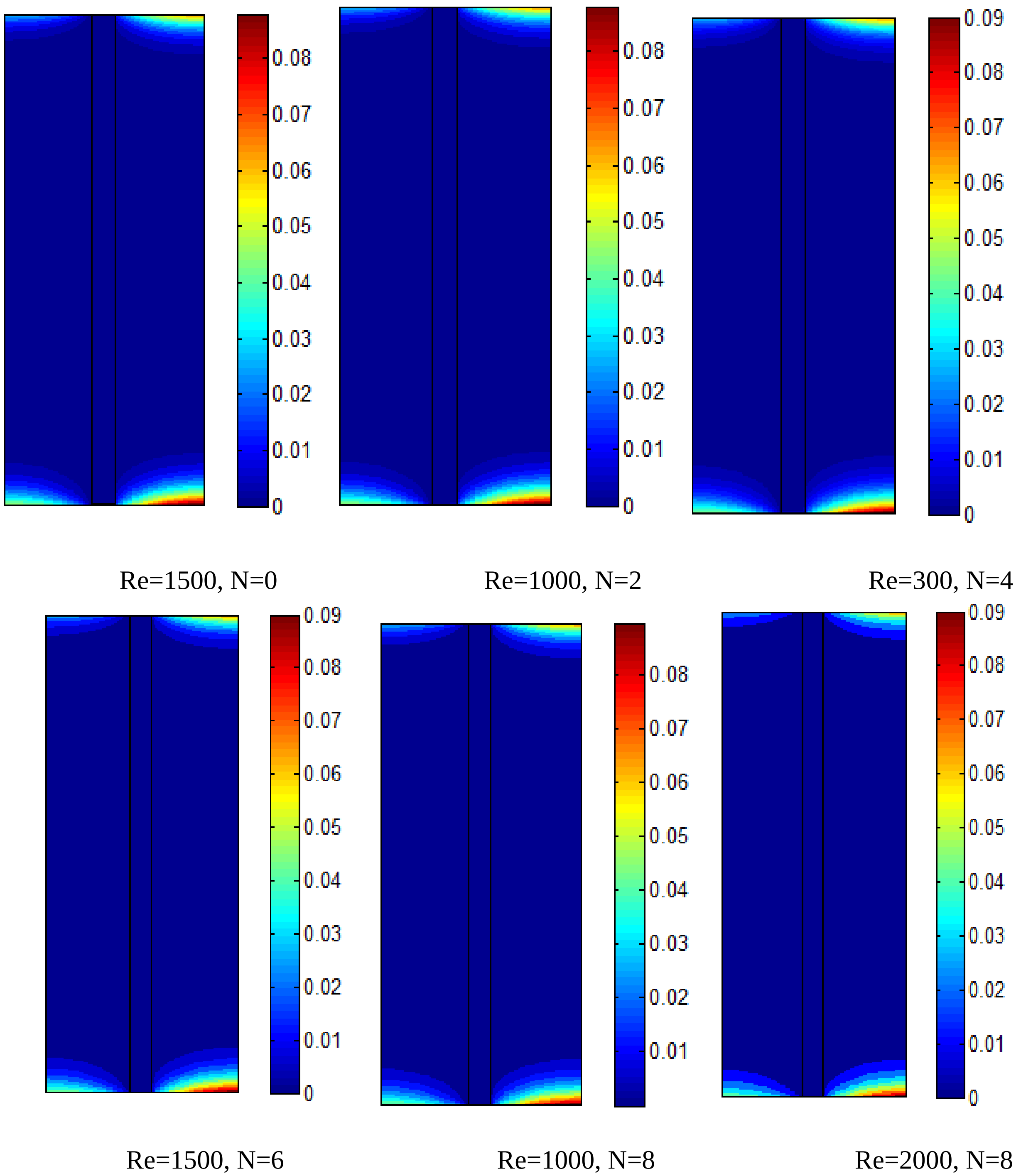

Figure 5. Contours of streamlines (ψ).

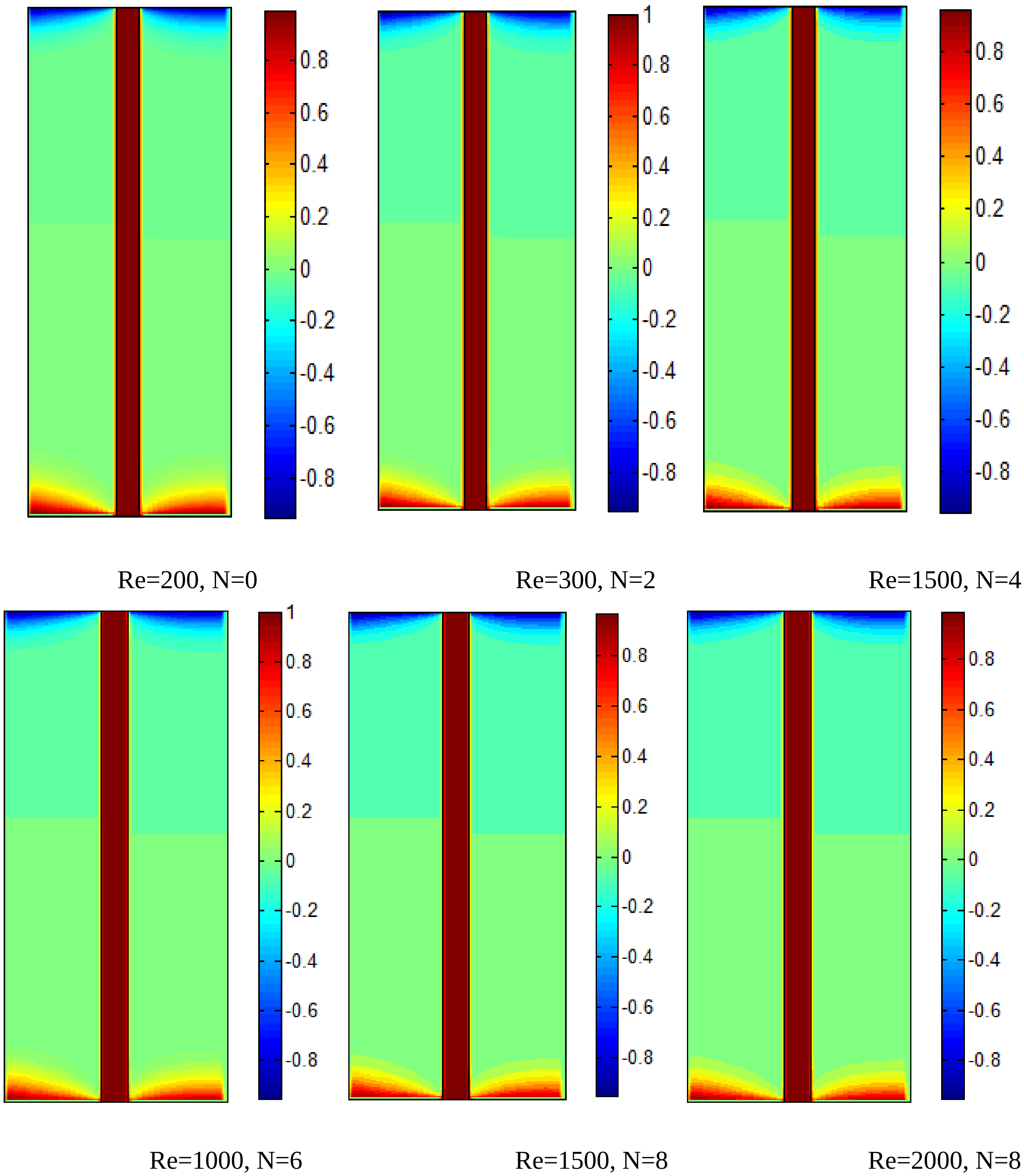

Figure 6 . Velocity field (V) in axial direction.

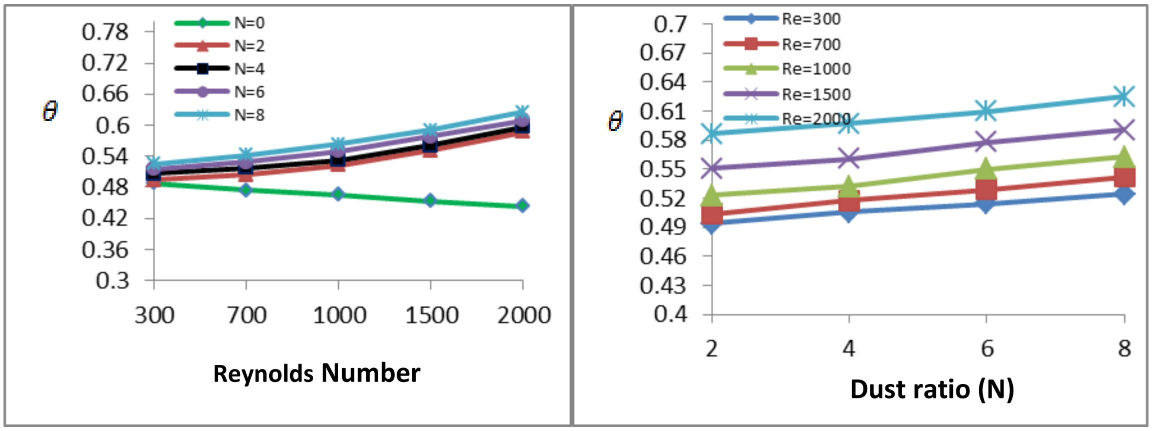

Figure 7. Variation of (θ) with (N) and with (Re).

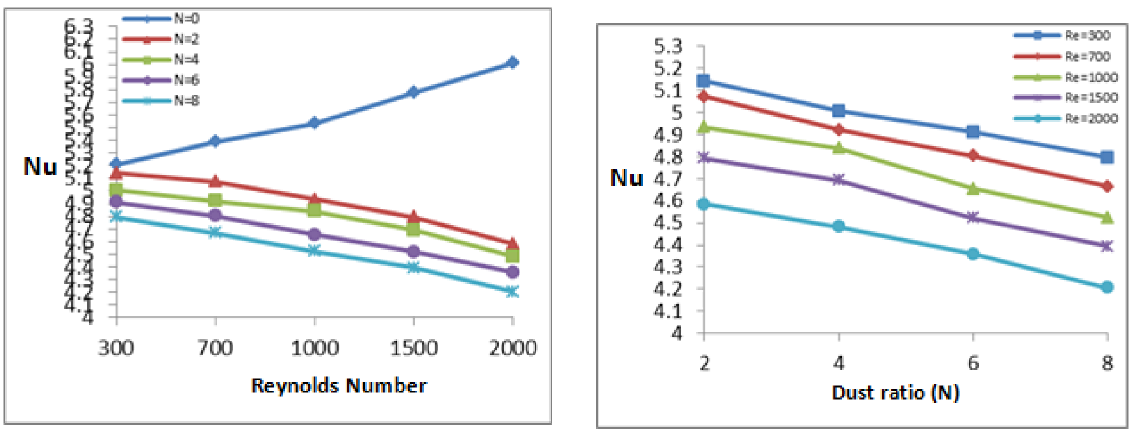

Figure 8. Variation of (Nu) with (N) and with (Re).

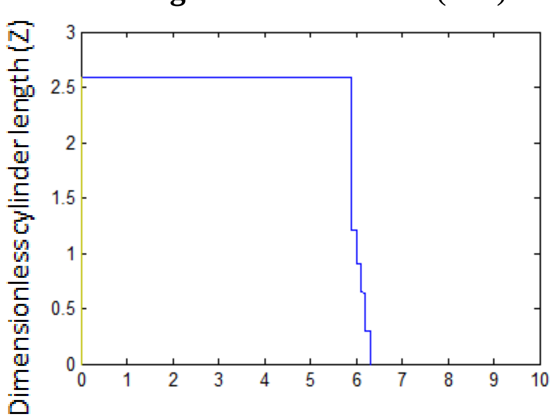

Local Nusselt number(N=0, Re=1000)

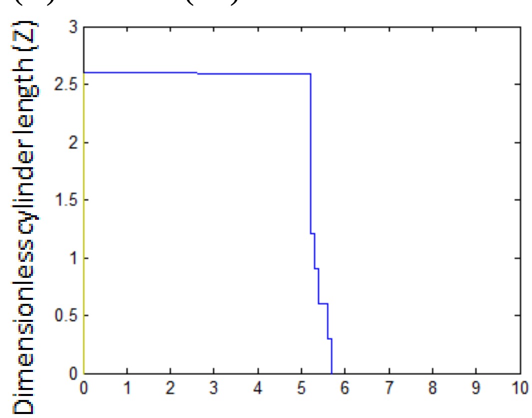

Local Nusselt number(N=0, Re=2000)

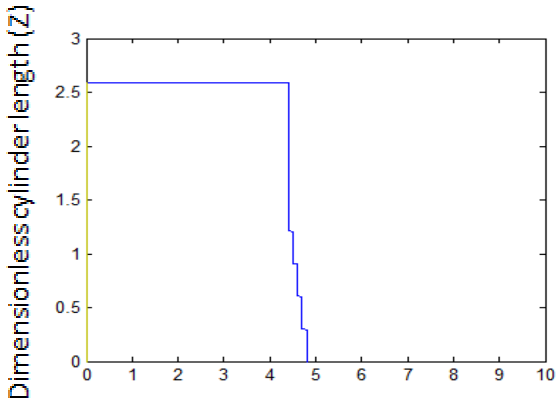

Local Nusselt number(N=4, Re=700)

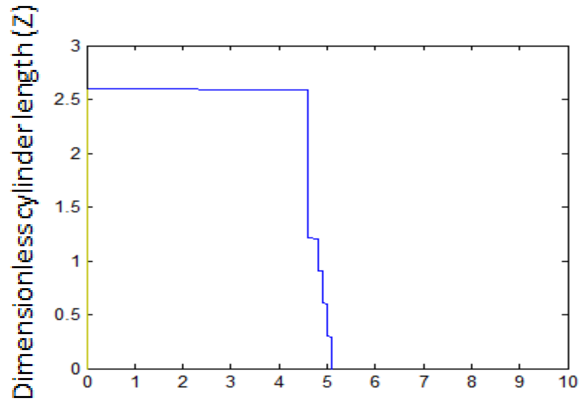

Local Nusselt number(N=8, Re=1000)

Figure 9. Variation of local Nusselt number in (Z – Direction) along the hot cylinder.

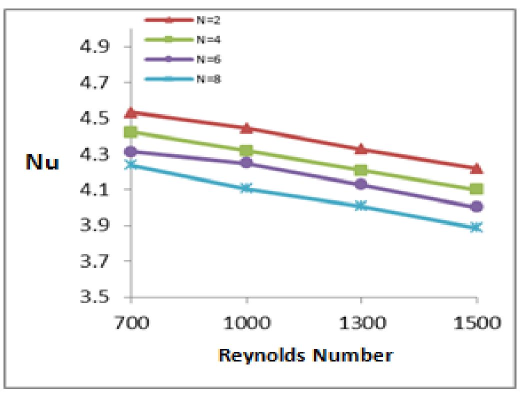

Q=6.3W

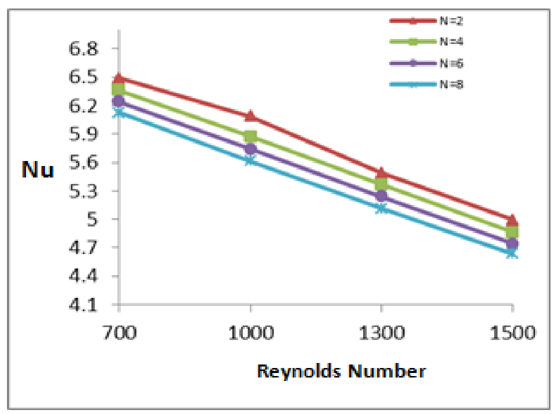

Q=4.884W

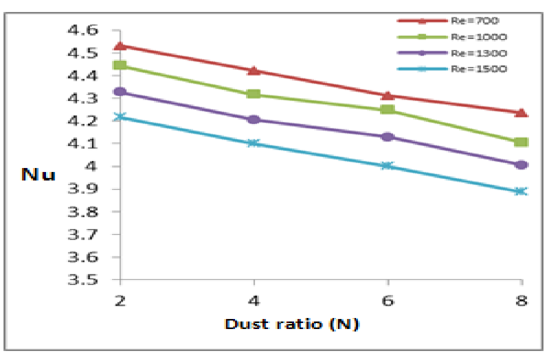

Q=6.3W

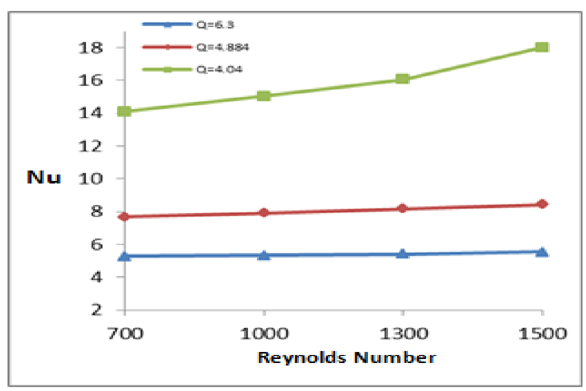

clean air (N=0)

Figure 10. Experimental variation of average Nusselt number with Reynolds number and Dust ratio.

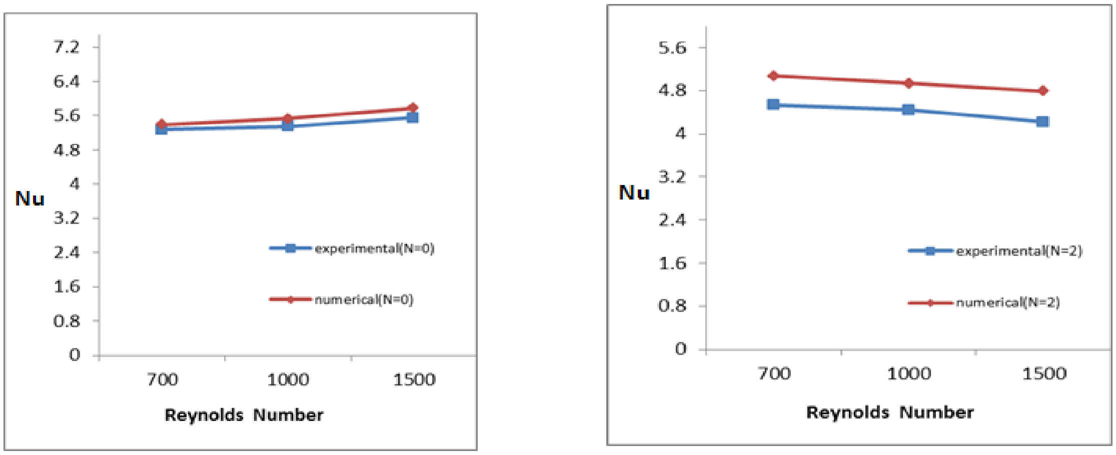

Figure 11. Comparison of Experimental and Numerical Results.

An Investigation into Thermal Performance of Mist Water System and The Related Consumption Energy

Asst. Prof. Dr. Najim Abid Jassim
Mechanical Engineering Department, College of Engineering, University of Baghdad
najmosawe@yahoo.com

Eng. Firas Adel Abdulkareem Haris
Sc. Student, Mech. Eng. Dept., College of Engineering, University of Baghdad
firasalharis@yahoo.com

ABSTRACT

Experimental tests were conducted to investigate the thermal performance (cooling effect) of water mist system consisting of 5µm volume median diameter droplets in reducing the heat gain entering a room through the roof and the west wall by reducing the outside surface temperature due to the evaporative cooling effect during the hot dry summer of Baghdad/Iraq. The test period was Fifty one days during the months May, June, and July 2012. The single test day consists of 16 test hours starting from 8:00 am to 12:00 pm. The results showed a reduction range of 1.71 to 15.5℃ of the roof outside surface temperature and 21.3 to 76.6% reduction in the daily heat flux entering the room through the roof compared with the case of not using water mist system. Also the results show a reduction range of 1.3 to 18.8℃ in the wall outside surface temperature. Finally numerical simulation with ANSYS-FLUENT.14 was conducted to compare its results with the experimental results of the roof and wall tests.

Keywords: energy saving, water spraying, water mist, evaporative cooling techniques, air conditioning

دراسة الاداء الحراري لمنظومة رذاذ الماء و تاثيرها في استهلاك الطاقة

الأستاذ المساعد الدكتور نجم عبد جاسم
قسم الهندسة الميكانيكية \ جامعة بغداد

المهندس فراس عادل عبد الكريم حارس
طالب ماجستير موائع و حراريات\قسم الهندسة الميكانيكية \جامعة بغداد

الخلاصة

تم اجراء اختبارات عملية من اجل دراسة الاداء الحراري لمنظومة رذاذ الماء بقطيرات بمعدل قطر 5 مايكرون , في تقليل الحمل الحراري الداخل الى غرفة من خلال السقف و الجدار الغربي لها بخفض درجة حرارة السطح الخارجي نتيجة التاثير التبريدي التبخيري خلال فترة الصيف الحار و الجاف في بغداد/العراق. فترة الاختبارات كانت لمدة واحد و خمسون يوما خلال اشهر ايار و حزيران و تموز من العام 2012 , و تضمن يوم الاختبار 16 ساعة من الاختبارات ابتداءا من الساعة الثامنة صباحا و حتى الساعة الثانية عشرة ليلا. اظهرت النتائج العملية هبوط بمقدار 1.71 الى 15.5 درجة مئوية في حرارة السطح العلوي للسقف, و هبوطا بمقدار 21.3 الى 76.6 % من الحمل الحراري اليومي الداخل للغرفة من السقف. كذلك و بالنسبة للجدار الغربي فقد اظهرت النتائج هبوطا بمقدار 1.3 الى 18.8 درجة مئوية في حرارة السطح الخارجي للجدار. اخيرا تم استعمال برنامج المحاكاة الهندسي ANSYS-FLUENT.14 من اجل مقارنة النتائج العملية للسقف و الجدار مع النتائج النظرية المتولدة من هذا البرنامج.

الكلمات الرئيسية : توفير الطاقة, تذرية الماء, رذاذ الماء, تقنيات التبريد التبخيري, تكييف هواء.

1- INTRODUCTION

One of the most important problems that face the HVAC engineers is how to overcome the cooling load that is penetrated through the roof and the outside walls specially the ones that are exposed to the sun for a number of hours during summer days. In a country like Iraq where the weather is so hot and the temperature can exceed 50 ℃ in many days during summer, it is so important to find any new solutions to reduce the effect of these loads, and because the weather is dry beside it is hot in summer, it is very axiomatically to think that the evaporating cooling can be the most effected solution for this problem. Furthermore, by attacking at the roof surface, evaporative cooling is utilized where temperatures are highest (due to greater exposure to radiation) and relative humidity is lowest (air will hold more water vapor at higher temperatures). As a result, solar impacts on the roof surface can be negated before any of the other building's defense mechanisms come in to play, **Bachman1985.** By evaporating just enough water on the roof to drive the air to saturation (100% RH)**,** the roof surface and the air film against it approach the wet bulb temperature. The radiant energy which raised the roof temperature (sensible heat) has been relieved by causing a phase change (latent heat) from liquid to vapor. The only issue then, is control of spray sufficient to maximize evaporative cooling of the building skin yet not so much as to allow standing water. And this control is largely what distinguished the successfully designed systems. Evaporative roof systems are not without drawbacks, however, unlike insulation, roof spray contributes to comfort and energy conservation only during the cooling season. Final evaluation of the alternatives should take a lifecycle look at all of the assumptions of cost and benefit, energy savings and roof life. Perhaps the most important objection to roof spray systems is the attendant consumption of water, an increasingly depleted natural resource.

In 1940 interest in (roof spray cooling) had grown sufficiently to merit an ASHRE, study at the Pittsburgh Experiment Station. "Summer Cooling Load as Affected by Heat Gain through Dry, Sprinkled and Water Covered Roofs" by **Houghton et al 1940**, they compared time and heat flow relationships through nine different roof constructions for dry, sprinkled and ponded surfaces. Their conclusions indicated that the sprinkler system was, in all constructions, the most effective measure of reducing heat flow into the building. The results for concrete asphalt roof were as in **Table 1**.

Carrasco et al. 1986, performs an experimental study of the use of a roof spray system. The study was done on a building belong to A&M university in the hot and humid weather of central Texas USA in July 1986. The roof was of wood with thin layer of tar and gravel on top. The experimental results showed that there was a 60 % reduction in the heat transfer through the roof and 20 % (13.8℃) reduction in the roof top surface also a 2.3 to 3.4℃ reduction in the inside air temperature.

Narumi et al. 2007, conducted experimental tests and numerical simulations in order to investigate the effect of misting technologies on reducing urban heat flux and saving energy. An apartment house in Osaka Japan was used as the test building in an investigation of three types of evaporative cooling techniques: "Rooftop spraying", "Veranda spraying" and "Spraying to the outdoor unit of room air conditioner". The test period was from 10 August to 27 September 2007. For Rooftop spraying, the experiments show that a lowering effect was obtained even after cessation of spraying, with the whole-day average falling by 16.4°C. The indoor environment showed a fall of 1.2°C at 120 cm above floor level, while a larger temperature lowering effect was obtained closer to the ceiling.

2- EXPERIMENT PROCEDURE

1) **Test Building**, The experimental tests were carried out in the room located in the second story of a house in alkarkh Baghdad/Iraq. The house was built at the beginnings of the seventeenth of the 20^{th} century. The room inside dimensions were (5.5m length ,4m width, 2.85 height) it has two (1.18m height, 0.96m width) Iron frame windows one at the east wall and the other is at the west wall, and one wooden door with dimension of (1.97m height by 0.98m width) at the north partition **Fig.1**.

2) **Test Period,** The roof and wall experiments days were conducted during the months of May, June & July 2012 which represent the starting of summer in May, till reaching the peak temperatures of summer in Baghdad / Iraq in July. The days of experiments types were divided as in **Table 2**; Fifty one days of experiments were done to study these effects. The single experiment day consisted of

generally pump operation from 8:00 am to 9:00 pm with some exceptions when the stopping time was earlier (7:00 pm - 8:00 pm) especially in May when the water flooded over the upper roof surface at evening because of low temperature which caused reducing of evaporating. Taking the readings of the thermocouples and other measuring instruments was from 8:00 am to 12:00 pm generally**.**

3) **Test Apparatus,** An experimental test Apparatus has been built, in a way that give a flexibility in changing the parameters to be suitable for different types of the tests that is expected to be done. The components of this apparatus can be seen in **Fig.2** to **Fig.4**. The main parts are High pressure reciprocating pump 10 to 100 bar, specialized mist nozzles (size 0.006", which can give droplets of median diameter of 5 µm), piping network.
The parameters to be tested, consisted of Different pump operation methods (continuous or by intervals), different pump pressures, Different mist direction (upward or downward) and different levels from the surface.

4) **Test Procedure** The main idea of this research is using a high pressure water pump (reciprocating pump) to force the water liquid through a very small orifice nozzle (special mist nozzle), with pressure that can reach 100 bar, to get the water in a very small droplets (can be less than 5µm in Volume median Diameter VMD) that can be effectively evaporate without wetting the surface or body that it is expose to it (flash evaporating). This process of evaporation requires energy to be completed. The energy is taken from the air in the form of heat. The result is a temperature reduction, depending on the ambient temperature and the relative humidity of the air. Concerning the roof and the wall tests, Experiments were done to investigate the effects of changing controlling parameters on the important variables which are:
a) Room Roof outside surface temperature.
b) Room Roof inside surface temperature.
c) Room wall outside surface temperature.
d) Room wall inside surface temperature.
e) The room temperature **Fig.5**.
The tests were conducted by using a network of twelve (size 0.006") mist nozzles as shown in **Fig.4**. The inside and outside temperatures of the roof and the west wall were used to calculate the heat flux through the roof and the west wall during the day hours were calculated by the Eq.(1) and Eq.(2)

$$q_r = \frac{(T_{ro} - T_{ri})}{\sum_1^n \frac{t_n}{k_n}} \tag{1}$$

$$q_w = \frac{(T_{wo} - T_{wi})}{\sum_1^n \frac{t_n}{k_n}} \tag{2}$$

3- RESULTS AND DISCUSSION

a) From the roof tests of different months a comparisons have been made between wet and dry test days which are of close dry temperatures during the day long (specially the peak temperature), and close relative humidity. The **Fig.6** to **Fig.8** shows comparison between two days 12-May (dry test) and 20-June (wet test) for the roof top temperatures and heat flux cross the roof in each case. We can see the reduction in the roof heat flux curve in **Fig.8**, and how it came to the negative values (cooling effect) earlier than the case of dry ones **Fig.7**. Another comparison where made between the dry and wet part of the same roof at the same day. **Fig.9** shows a sample of this comparison for the roof top temperatures of the test day 2-July. **Fig.10** shows a comparison for the roof test day's heat flux during June and July. The final conclusions for the roof tests were as listed in **Table 3**.

b) From the wall tests of different months, a comparisons have been made between wet and dry test days which are of close dry temperatures during the day long (specially the peak temperature), and close relative humidity. **Fig.11** shows comparison of two wet days' 29-May, and 9-June with dry test 13-May for the west wall outside surface temperatures. **Fig.12** shows a comparison for the west wall test day's heat flux in July. The low insulated wall behaved as a cooling surface during most of the test days. The final conclusions for the west wall tests were as listed in **Table 4**.

c) The downward misting operation for the roof (from 90 cm height) is more effective in cooling the roof than that of upward misting (mist network on roof surface) by 7.37%. The result of down misting caused the roof to be a cooling surface for more Time (hours) than upward misting.

d) The interval operating methods of the pumps (2-min on and 2- min off) reduce the water consuming. Although that the continuous operating method or semi continuous operating method (continuous operating for an hour time and then interval operating for a half an hour) can increase the cooling effect but it can cause bad effect on the building construction because of water specially at the evening and at the high level of relative humidity, and more water consuming. The best method of operating is the continuous or semi continuous operating method at the peak temperature time (from 11:00 am to 4:00 pm) and interval operating during the other hours. This caused in a thin film of water (only fog during peak temperature) over the roof surface to produce the cooling effect without the harmful effect of water spilling.

e) The using of mist water reduces the outdoor air temperature, the experimental tests shows a reduction of 12.4 to 21.2℃ during the day hours. The number of temperatures reduced depends on the relative humidity and the pump pressure, which will increase the water being misted.

f) This method can be used safely in buildings because most of the water mist will evaporates directly (flash evaporating) and don't spilled on the surface, therefore do not cause any damage of any type to the building. Although a surface humidification can happen during the high relative humidity days or at the morning and the evening, but this effect can be reduced by using the interval operating and the changing the intervals time.

g) Concerning the use of ANSYS-FLUENT.14 software, Two days for each test type (roof or wall) were selected to compare the results of the experimental work with the fluent software results, and to compare the wet and dry results generated by FLUENT. The simulation was conducted by using the software to solve three dimensions transient heat transfer problem. The results were in the form of static temperature contours of two surfaces at the middle of the room. The deviation between experimental and fluent results is 0.2 to 5.8%. **Fig.13** shows a comparison between the experimental and fluent results for the days 20-July (dry) and 15- July (wet) wall tests .**Fig.15** shows the contours of these cases generated by Fluent for the hour 11:00 pm.

4- COMPARISON OF THE PRESENT WORK RESULTS WITH A PREVIUOS WORK RESULTS

Comparison can be made with **Carrasco et. al. 1986** experimental results in July 1986 in Bryan city, Texas they reported that the roof evaporating cooling can reduce the roof-top temperature by up to 25˚F (13.89℃) or about 20%. To make a comparison with the present work, we can compare Carrasco results of 19 July 1986 which was one of the biggest reduction values that was conducted during the experiments as it shown in the result curves of Carrasco paper (5 to 10℃ reduction of the roof top temperature for the period from 1:00 pm to 4:30 pm), with a chosen roof test day in July of the present work which is 4 July 2012 (clear sky with moderate temperature of July in Baghdad).**Fig.14** shows that The present test results show a reduction of the top surface temperature for the same time period of range 5.1 to 11℃, and this is a close result to Carrasco one, although that the weather of Texas is less in temperature levels from that of Baghdad according to (National Oceanic and Atmospheric Administration in the United tate of America) which shows a maximum temperature of 29 July 1986 in Bryan city was 38℃, compared with the temperature of 4 July 2012 of Baghdad which was 44℃. But the high relative humidity of Bryan city that day (average 50%, max 96% and compared with Baghdad in 4

July which was about max. of 27%) may have been the reason of the close results (increasing the humidity will decrease the evaporating process). Knowing that, the wind speed was almost the same for the two cases of the present and Carrasco (about 3m/s).

5- CONCLUSIONS

1) From the experimental work we can confirm that the water mist system can reduce the outside surface temperature of the roof and the west wall of the room by 1.71 to 15.5℃ for the roof and 1.3 to 18.8 ℃ for the wall.
2) The tests confirm that this system can reduce the heat gain entering the building throughout the roof and the west wall by 21 to 76%.
3) The tests showed that, the using of mist water can reduce the outdoor air temperature by 12.4 to 21.2℃ during the day hours.

REFERENCES

- ANSYS, Inc, April 2009, *ANSYS FLUENT 12.0 Theory Guide*.

- Carrasco, A., Pittard, R., Kondepudi, S. N., and Somasundaram, S. Mechanical Engineering Department, Texas A&M University, College Station,1987, *Evaluation of a Direct Evaporation Roof-Spray Cooling System*, Proceedings of the Fourth Symposium on Improving Building Systems in Hot and Humid Climates, Houston, TX, September 15-16, 1987.

- Daisuke Narumi, Kentaro Shigemitsu and Yoshiyuki Shimoda, Osaka University Suita City, Osaka Pref., Japan , 2007 , *Effect of the Evaporative Cooling Techniques by Spraying Mist Water on Reducing Urban Heat Flux and Saving Energy in Apartment House*, PLEA 2009 - 26th Conference on Passive and Low Energy Architecture, Quebec City, Canada, 22-24 June 2009.

- Houghten, F.C., Olsen, H.T. & Gutberlet, C., 1940, *Summer Cooling Load as Affected by Heat Gain Through Dry Sprinkled and Water Covered Roofs,* American Society of Heating and Ventilation, (ASHVE Transactions) Engineers Transcripts,June,1940, Vol. 46, pp. 231.

- Leonard R. Bachman AIA President Building Climate Interface , Inc. Houston, Texas, 1985 , *Rain on the Roof-Evaporative Spray Roof Cooling*, Proceedings of the Second Symposium on Improving Building Systems in Hot and Humid Climates, College Station, TX, September 24-26, 1985.

- National Oceanic and Atmospheric Administration in the United State of America, http://www.ncdc.noaa.gov

6-NOMENCLATURES

k : thermal conductivity of the roof or the wall materials W/m℃
n: the number of the roof or wall layers
q_r :heat flux through the roof at the wet part (sprayed part) W/m^2
q_{rd} :heat flux through the roof at the dry part (not sprayed part) W/m^2
q_w :heat flux through the west wall at the wet part (sprayed part) W/m^2
q_{wd} : heat flux through the west wall at the dry part (not sprayed part) W/m^2
t : roof or Wall Layer Thickness m
T_{ri} : roof inside surface temperature ℃
T_{rm} : room average temperature ℃
T_{ro} : roof outside surface temperature at the wet part (sprayed part) ℃
T_{rod} :roof outside surface temperature at the dry part (not sprayed part) ℃
T_{wi} : wall inside surface temperature ℃
T_{wo} : wall outside surface temperature at the wet part (sprayed part) ℃

7-TABLES AND FIGURES

Table 1. The Results of Houghton et al. for Concrete Asphalt Roof.

	With spray	Without spray
Max. heat flow, w/m^2	6.6	56.7
Min. heat flow, w/m^2	-12.9	-7.24
Avg. heat flow, w/m^2 over 24 hour	-3.84	18.3
Length of time with zero or negative heat flow hour	16	8

Table 2. The roof and wall experimental days.

No.	Test name	No. of days
1	Dry test	9
2	Wet roof test (nozzle misting up)	18
3	Wet roof test (nozzle misting down)	7
4	Wet wall test	17
Total test days		51

Table 3. Final conclusions of roof tests.

	Range	Average
Tro peak reduction at 2:00Pm, ℃	4 – 11.14	7.57
Tro day hours range reduction ℃	1.71 – 15.5	8.6
Tri peak reduction at 8:00Pm, ℃	0.5 – 1.91	1.2
Tri day hours range reduction ℃	0.2 - 2	1.1
Roof heat flux day hours range reduction w/m^2	1.1 - 22	11.55
Daily total roof heat flux range reduction %	21.3 – 76.6	48.95*

* This result is for upward spraying, the daily total roof heat flux becomes negative (cooling) in many case with downward spraying

Table 4. Final conclusions of wall tests.

	Range	Average
Two peak reduction at 3:00-4:00Pm, ℃	2.2 – 18.75	10.5
Two day hours range reduction ℃	1.3 – 18.8	10
Twi peak reduction at 7:00Pm, ℃	2.54 – 5.83	4.2
Twi day hours range reduction ℃	0.8 – 6.83	3.8
Daily total wall heat flux range reduction %	**	**

** The daily total wall heat flux became negative (cooling)

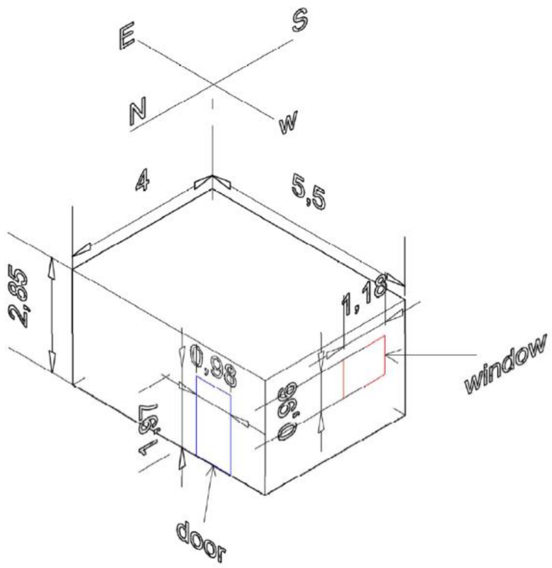

Figure 1. Test room dimension.

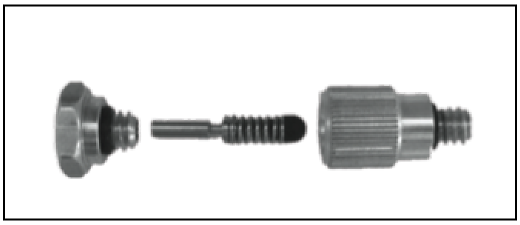

Figure 2. Mist nozzle.

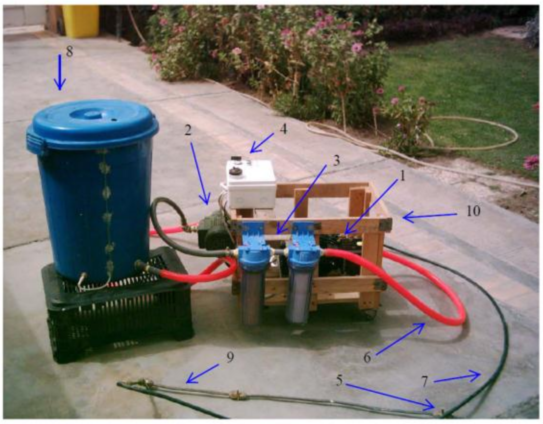

1	High pressure pump	6	Low pressure elastic pipe
2	Low pressure pump	7	High pressure hose
3	5 microns water filter	8	Water tank
4	Operating electrical board	9	Copper Mist network
5	Mist nozzle	10	Wood frame

Figure 3. The test apparatus.

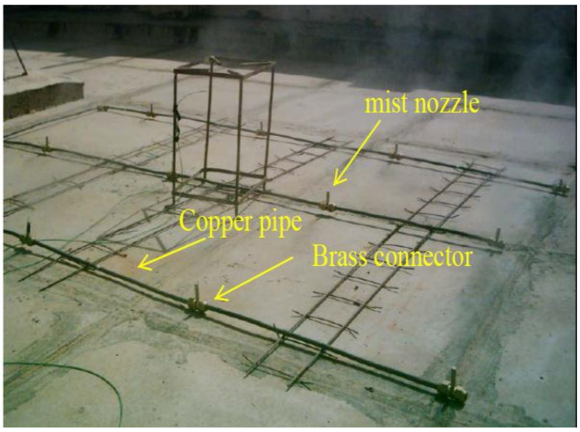

Figure 4. Piping network.

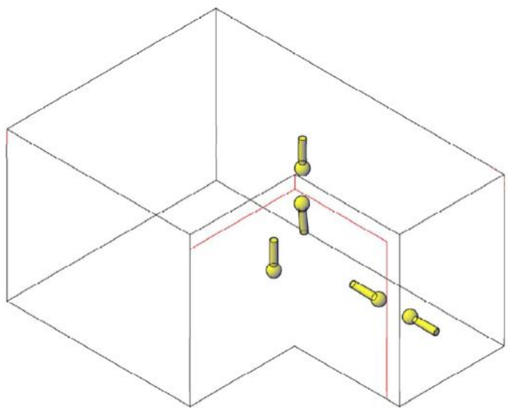

Figure 5.Main thermocouples places.

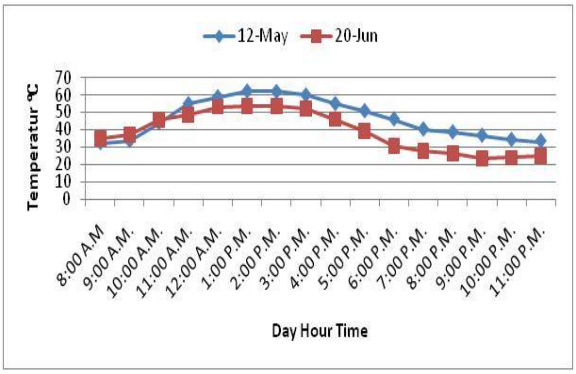

Figure 6. The outside roof surface temperature for the days 12-May (dry),20-June (wet).

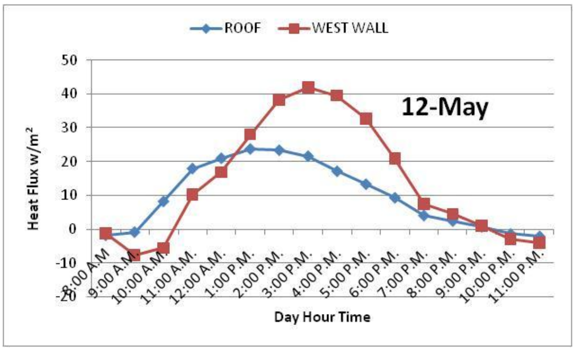

Figure 7. Heat flux throughout the roof and the west wall of the test room for the day 12-May (dry test).

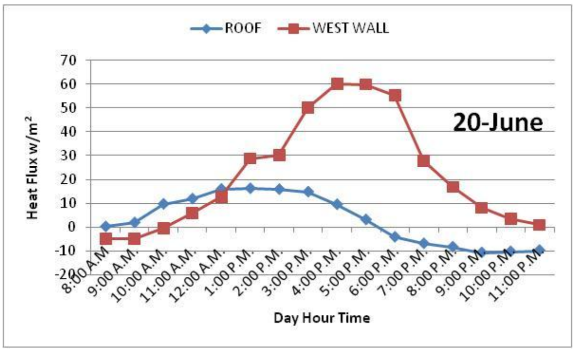

Figure 8. Heat flux throughout the roof and the west wall of the test room for the day 20-June (wet test).

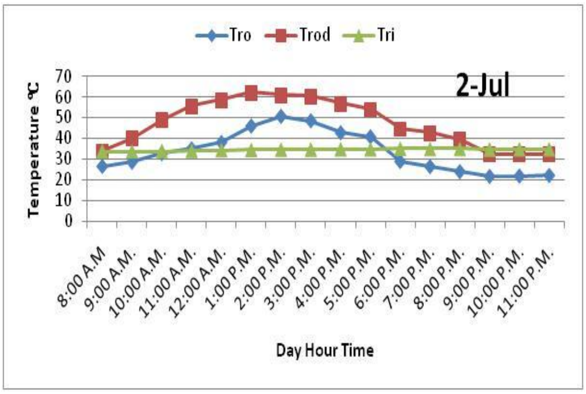

Figure9. The inside roof surface temperatures (tri), outside roof surface temperatures at misted part (tro) and the roof outside surface temperature at the dry part (trod) curves for the day 2-July.

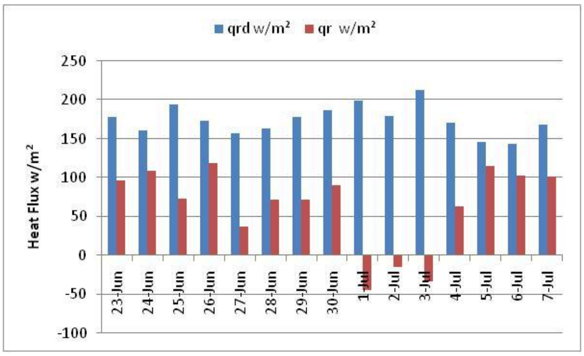

Figure 10. Daily total heat flux throughout the roof at the misted part (qr), the dry part (qrd) at June and July tests.

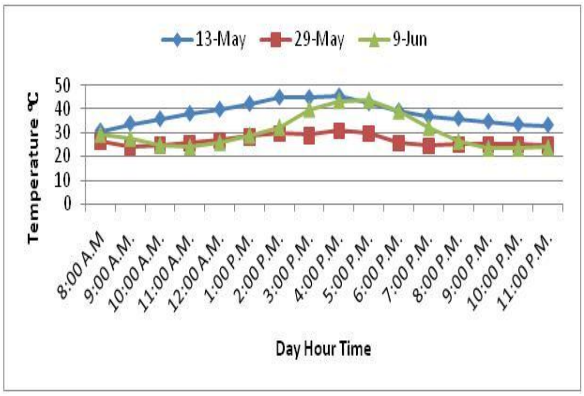

Figure 11. Wall outside surface temperatures of the day's 13- May (dry), 29-May (wet), 9- June (wet).

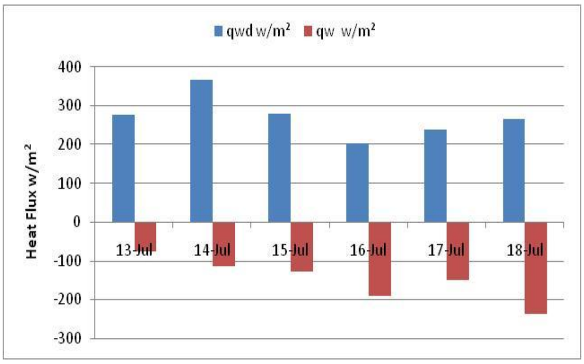

Figure 12. The heat flux throughout wet west wall part (qw), dry west wall part (qwd) of July tests.

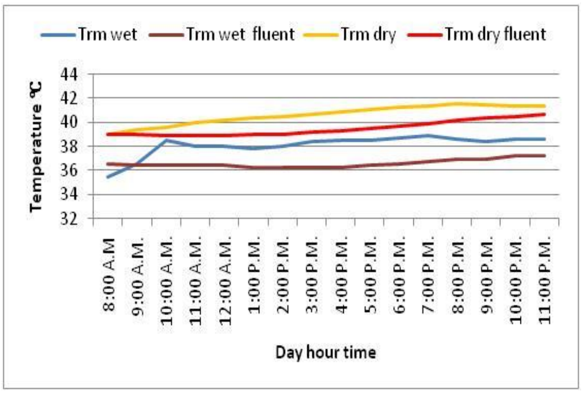

Figure 13. Comparison curves of the daily room temperatures measured experimentally and generated by ansys-fluent.14 software for dry (20/7/2012) and wet (15/7/2012) cases of wall tests.

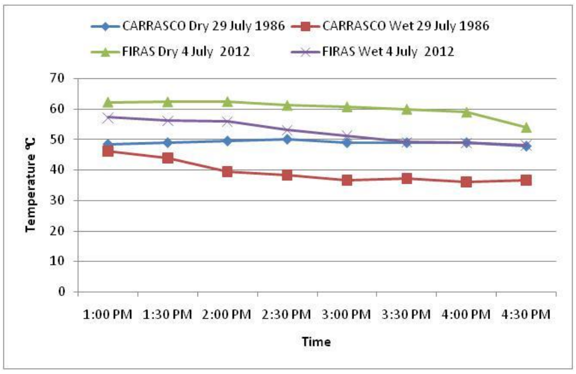

Figure 14. The temperature curves of 29 July 1986 by Carrasco and 4 July 2012 by Firas.

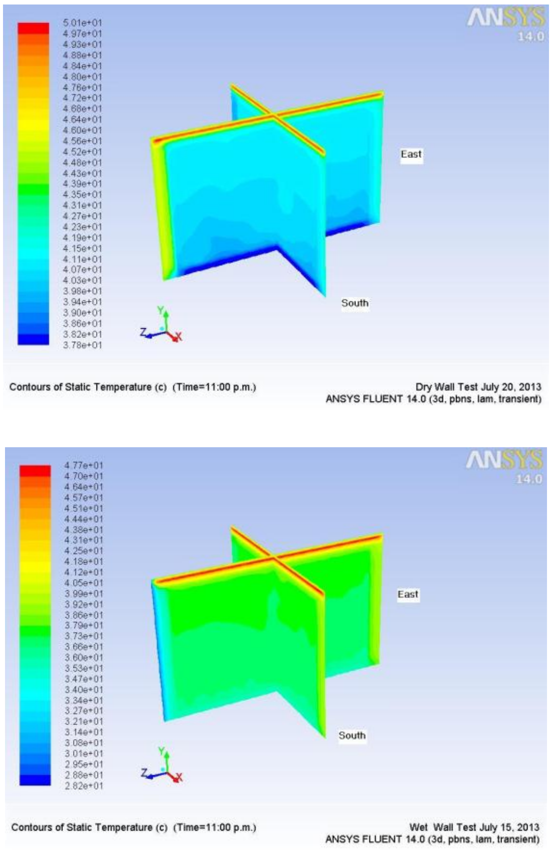

Figure 15. Temperature contours for the dry (20/7/2012) and wet (15/7/2012) wall cases at 11:00 pm.

Effect of Ferric Oxide on Electricity Generation and Waste Water Treatment Using Microbial Fuel Cell Technology

Qusay Jaffer
Assistant Lecturer
Chemical Engineering Department
University of Technology
Email: engineerqusay@yahoo.com

K.GHANAPRIYA
Lecturer
Centre for Advanced Studies in Botany
University of Madras, India.
Email: gpriyak@gmail.com

ABSTRACT

The aim of research is to show the effect of Ferric Oxide (Fe_2O_3) on the electricity production and wastewater treatment, since 2.5% of Ferric Oxide (Fe_2O_3) (heated and non heated) nanoparticles has been used. Characterization of nanoparticles was done using X-ray Diffraction (XRD) and Scan Electron Microscopy (SEM). The influence of acidity was also studied on both wastewater treatment on the Chemical Oxygen demand (COD) and Biological Oxygen Demand (BOD) and voltage output was studied. From the results, it was infused that the dosage of 0.025 g/l and an initial pH 7 were founded to be optimum for the effective degradation of effluents. The results concluded that the treatment of anaerobic sludge wastewater using Ferric Oxide (Fe_2O_3) in combination with microbial fuel cell technology is an efficient method for the treatment of anaerobic sludge wastewater.

Key words: Microbial fuel cell, nanoparticles, wastewater treatment.

تأثير أوكسيد الحديديك (Fe_2O_3) في توليد الكهرباء ومعالجة المياه باستخدام تكنولوجيا خلايا الوقود الميكروبية.

قصي جعفر رشيد
مدرس مساعد
قسم الهندسة الكيمياوية
الجامعة التكنلوجية, العراق

كانا بريا
مدرس
مركز الدراسات المتقدمة في علم النبات
جامعة مدراس, الهند

الخلاصة

الهدف من البحث هو إظهار تأثير أكسيد الحديديك (Fe_2O_3) على إنتاج الكهرباء ومعالجة مياه الصرف الصحي، 2.5٪ من أكسيد الحديديك (Fe2O3) وقد استخدم (مسخن وغير مسخن) النانوية. وقد تم تحديد خصائص المركبات النانوية باستخدام حيود الأشعة السينية (XRD) والمسح الضوئي المجهر الإلكتروني (SEM).تمت دراسة تأثير الحامضية أيضا على حد سواء معالجة مياه الصرف الصحي على نسبة الطلب على الاوكسجين الكيمياوي (COD) ونسبة الطلب على الأوكسجين البيولوجي (BOD) وانتاج التيار الكهربائي تم دراستها. من النتائج، تبين أن جرعة من (0.025) غرام / لتر ودرجة الحامضية (7) لتكون الأمثل فعالة في معالجة مياه الصرف.خلصت النتائج إلى أن معاملة مياه الصرف الصحي الرواسب اللاهوائية باستخدام أكسيد الحديديك (Fe_2O_3) بالاشتراك مع تكنولوجيا خلايا الوقود الميكروبية هو وسيلة فعالة لعلاج مياه الصرف الصحي الرواسب اللاهوائية.

الكلمات الرئيسية : خلايا الوقود الميكروبية, المواد النانوية, معالجة المياه.

1. INTRODUCTION

Efficiently making use of biological processes to recover useful energy from organic wastes is always a goal for the wastewater treatment industry. In the study, microbial fuel cells (MFCs) are considered to be a very popular and promising bio-electrochemical power source for directly recovering electrical energy from carbohydrates as well as organics in wastewater. The application of MFCs in a wastewater treatment process has several advantages over existing processes. In addition to energy recovery as electricity in a wastewater treatment process, MFCs generate less excess sludge in a more stable condition than the aerobic treatment process **Greenman et al., 2009.**

The goal of waste water treatment facility is to reduce organic and inorganic materials in wastewater to a level that no longer supports microbial growth and to eliminate other potentially toxic materials. The efficiency of treatment is expressed in terms of reduction in BOD the relative amount of dissolved oxygen consumed by microorganisms to completely oxidize all organic and inorganic matter in the water sample. The higher the levels of oxidizible organic and inorganic material in the wastewater it will result in high BOD **Kargi et.al 200**.

Nanoparticles are materials having a size in the range of 1–100 nm. Iron oxide, titanium dioxide, fullerenes and carbon nanotubes have been made into nanoparticles **Boxall A.B. et. al 2007**, and **Christian.P. et. al 2008**. Fe_2O_3 is an effective reducing agent and catalyst for various applications in environmental remediation.

The heterogeneous reaction using Fe2O3 involves five steps: (i) mass transfer of the reactant to the Fe_2O_3 surface from the bulk solution; (ii) adsorption of the reactant on the Fe_2O_3 surface; (iii) chemical reaction at the Fe_2O_3 surface; (iv) desorption of the reaction product from the Fe_2O_3 surface; and (v) mass transfer of the product into the bulk solution **Lin. A. et. al 2008**.

The disposal of wastewater containing toxic organic compounds by the industrial community has been increased significantly in the recent past. So the treatment of such wastes generated from the industries is considered necessary as well as important in every aspect. Untreated wastewater if allowed to accumulate, leads to the decomposition of organic material and production of toxic gases. In industrial wastewater treatment, the objective is to remove or reduce the concentration of organic and inorganic compounds **Concetta and Cristina et. al 2005**.

In this study the use of (0.025gm) of Fe_2O_3 nanoparticles in enhancing the power output and wastewater treatment using microbial fuel cell technology was investigated. It proves to be a eco-friendly method along with the renewable source for generating electricity. The nanoparticles are characterized using X-ray Diffraction (XRD) and Scan Electron Microscopy (SEM), while the voltage and current was measured using Multimeter.

2.METHODS AND MATERIALS

2.1. Wastewater Characteristics

Wastewater (Anaerobic sludge) was obtained from Koyembedu sewage treatment plant, Chennai, Tamilnadu, India. Sample was stored in deep freezing unit at -20°C during the investigation. Initial values of the characteristics of wastewater are presented in **Table1.**

2.2. Preparation of Fe_2O_3 Nanoparticles

The Fe_2O_3 nanoparticles were synthesized by the well known liquid phase reduction method. 32.31 g of $Fe(NO_3)_3.9H_2O$ was completely dissolved in 400 ml of deionized water to form a 0.2 M solution and 28.77 g of NaOH was completely dissolved in 1200 ml of deionized water to form a 0.6 M solution. This solution was added drop wise into the above solution. After addition, this reaction continued with constant stirring. The solution was washed with deionized water and then dried in vacuum. The reaction is as follows:

$$Fe\ (NO_3)3.9H_2O + 3NaOH + H_2O \rightarrow FeOOH + 3NaNO_3 + 10\ H_2O \qquad (1)$$

2.3. Construction of Microbial Fuel Cell (MFC)

A sequential anode-cathode two chambered microbial fuel cell (MFC), in which the Fe_2O_3 (heated and non heated) of anode chamber was used as continuous feed for an aerated cathode chamber, was constructed in this experiment to investigate the performance of brewery wastewater treatment in conjugation with electricity generation. using autoclavable bottles each with diameter 30 mm and 100 mL capacity were taken. Two holes of diameter 5.5 mm and 1.5 mm were made on each of the lids for the insertion of the salt-bridge and electrodes. In the anode container, 100 mL of the Anodic Inoculation was used and in the cathode container 100 mL Potassium permanganate (0.1M) solution was used. The container lids were closed and sealed with tape. Salt-bridge was made with potassium chloride and agar in a 5 mm diameter level tube. Graphite sheets of 0.2 mm (thick) X 50 mm (length) X 12.5 mm (breadth) were used as electrodes. The electrodes were first soaked in 100% ethanol for 30 min. After that the electrodes were washed in 1 M Hydrochloric acid followed by 1 M Sodium hydroxide, each for 1 hr. They were then stored in distilled water before use. The electrodes were suspended using copper wires which were used to connect the conducting electrode and the multimeter. The cell was connected with a 10 ohm resistor to complete the circuit. The voltage and current where measured using UNITYDT-830D mutlimeter.

All operations were carried out at room temperature of 28°C. The variation in pH where (3, 5, 7 and 10) of the wastewater sample and was carried out by using 1N (HCl) and 1 N (NaOH).

2.4. Analytical Methods

Voltage (U) yielded from MFC for long time operation was recorded automatically by a computer and converted to power density **Wang et. al 2008**, according to:

$$P\ (W\ m^2) = U * j \qquad (2)$$

Where j is current density (A\ m^2), which is calculated by:

$$j = U/(R*A) \qquad (3)$$

Based on external resistance R (Ω) and projected surface area of cathode,

Total Surface area = $2\ (L*B + L*T + B*T))\ A\ (m^2)$ (4)

2.5. Analysis of Chemical Oxygen Demand (COD) and Biological Oxygen Demand (BOD)

The BOD analysis was done using Young, J.C. procedure with 5 days incubation. COD analysis was done using open reflux method.

The % COD remaining was calculated by the following equation.

$$\%COD\,remaining = 100 - \left(\frac{initial\ COD - final\ COD}{initial\ COD} X\,100 \right) \qquad (5)$$

3.RESULTS AND DISCUSSION

3.1. Characterization of Fe_2O_3

Fig.1 (a) shows the X-ray diffraction pattern of the as-prepared Fe2O3 sample and **Fig.3** (b) shows the X-ray diffraction pattern of Fe2O3 annealed at 300°C. It can be indexed as the orthorhombic system by comparison with data from JCPDS NO: 81-0463 (α-FeOOH). The diffraction peaks at 2θ ≈ 21.2, 33.3, 34.7, 36.6, 52.9, 58.9, 61.3 correspond to (110), (130), (021), (111), (221), (151), and (250) planes of sample respectively (JCPDS no: 84-0713). The information on the particle size was obtained from the full width at half maximum (FWHM) of the diffracted beam using Debye–Sherrer formula. **Qusay J. Raaheed et. Al, 2011**:

$$Dp = \frac{0.89\,\lambda}{\beta \cos \theta} \quad (6)$$

The sample displayed an average crystalline size of 5.65 nm. The application of scherrer's formula to the (313) reflection peak at 2θ = 35.6 indicated the formation of maghemite nanoparticles with approximately ≈ 24nm in mean diameter for the sample annealed at 300°C for 3h and annealed in an air atmosphere at 300 °C for 3 h, to get dark brown coloured nanocrystalline γ-Fe2O3 powders.

The scanning electron microscopy (SEM) image of synthesized Fe_2o_3 particles is shown in **Fig 2.** Results indicate that the synthesized Fe_2O_3 particles are almost spherical. **Fig.2 (a)** shows evenly distributed spherical particles approximately 30 µm in size, and **Fig.2 (b)**, under higher magnification, confirms the spherical shape and the size range of each particle. On the spherical particles there were threads-like or tube-like structures clearly visible in **Fig.2 (b).** These structures increased the available surface area of reaction.

3.2. Voltage and Current measurements:

Aerobic sludge is used to construct a MFC (Cell 1). The cells are connected with a constant load of 10 Ω and periodically monitored for the voltage and current outputs and tabulated. The power density and current density area were calculated respectively.

Similarly there are two other cells constructed as above using aerobic sludge with heated and non heated and designated cell 2 and cell 3 respectively.

The following are the results obtained. In a normal double-chamber MFC, the highest current was observed at neutral pH (between 6.5 and 8) **Jadhav and Ghangrekar et.al, 2009**. In this study using Fe_2O_3 (heated and non heated) the current was higher at pH 5 and pH 10 respectively. This difference is due to the influence of the chemical substance added to the wastewater. The current density and power density too show the same pH and give best results as that of the current and voltage.

4.DISCUSSION

Large part of energy carried by the organic contaminants in wastewater is converted into electricity; MFC might produce less excess sludge, when used as a wastewater process, than the conventional aerobic process. For this reason MFC is a novel wastewater treatment process. **Kim et.al, 2004**. During operation, both the fuel cells anode chamber were continuously monitored for substrate (as COD) removal to enumerate the potential of fuel cell to act as wastewater treatment unit. Both the systems showed their potential for substrate removal indicating the function of selectively enriched mixed microflora in metabolizing the carbon source as electron donors. Relatively higher substrate removal efficiency and substrate degradation rate (SDR) was documented with ferricyanide cathode. During the stable phase of operation, COD removal efficiency of 74.20% and 74.15% a ccounting for SDR of 0.559 kg COD/m3 day and 0.464 kg COD/m3 day was observed for FC and AC respectively. Time taken for carbon exhaustion was relatively more in aerated cathode.

The voltage and current were measured at regular intervals and plotted for each pH **Figs. 3.a and 3.b.** Power density was then calculated and plotted against current density **Figs. 4.a and 4.b.** As show in (fig 5.a and 5.b) a reduction of more than 50% was observed in both the cases.

The MFCs might produce a far less excess sludge when used in the wastewater treatment process, than the conventional aerobic process. In view of this advantage, the MFC was proposed as a novel wastewater treatment process. **Kim et al., 2004.**

5. CONCLUSION

In the present investigation, electricity could be successfully generated from wastewater treatment as it provides a new technology in making the wastewater treatment more affordable for both the developing and the countries. Thus, this combination of wastewater treatment along with electricity generation offers a technology that is affordable and is ecofriendly which might fulfill the needs of the developing nations in the present scenario. The Fe_2O_3 particles prepared through a liquid-phase reduction method the calculated cell parameters are. According to the scherrer's equation the average crystallite size of the product was calculated to be about 35.6 nm as prepare and 24nm for the sample annealed at 300°C for 3hr. The precipitation method led to the formation of α-FeOOH. At temperature around 300°C α-FeOOH decomposes and diffraction peaks corresponding to Maghemite appeared. crystallinity increases. SEM analysis shows that the particles are spherical shape. Further the wastewater with nanoparticle was adjusted at various pH levels revealed that the optimum initial pH for better degradation was found to be pH 5 showed best results for power output and pH 7 showed best reduction in BOD and COD proving high wastewater treatment efficiency percentage. A high current density and power density was obtained at pH 5 and pH 10 for the non heated and heated Fe2O3 respectively. But the reduction in BOD and COD was obtained at pH 7 in case of non-heated Fe2O3 and COD reduction was obtained at pH 3 and BOD at pH 7 for heated Fe2O3. A large part of the energy stored by the organic contaminants in the wastewater is converted into electricity.

REFERENCE

- Boxall, A.B., Tiede, K., Chaudhry, Q., 2007, *Engineered Nanomaterials in Soils and Water: How Do they Behave and Could they Pose a Risk to Human Health. Nanomedical. 2:919-927.*

- Christian, P., Von der Kammer, F., Baalousha, M., Hofmann, T., 2008, *Characterization of Physicochemical Properties of Ivy Nanoparticles for Cosmetic Application. Environ. Toxicol. Chem. 17:326-343.*

- Concetta. M. Tomei., Cristina M. Annesini., 2005, *4 Nitro Phenol Biodegradation in a Sequencing Batch Reactor Operating Aerobic- Anoxic Cycles, J.Environ.Sci.Technol. 39 :5059-5065.*

- Greenman J, Glvez A, Giusti L, Ieropoulos I.,2009 *Lectricity From Landfill Leachate Using Microbial Fuel Cells: Comparison With A Biological Aerated Filter. Enzyme Microb Technol. 44(2):112–119.*

- Jadhav, G.S., Ghangrekar, M.M., 2009, *Performance of Microbial Fuel Cell Subjected to Variation in Ph, Temperature, External Load and Substrate Concentration. Bioresour. Technol. 100 (2) :717–723.*

- Kargi F, Eker S., 2007 Electricity Generation with *Simultaneous Wastewater Treatment by a Microbial Fuel Cell (MFC) With Cu And Cu-Au Electrodes. J Chem Technol Biotechnol. 82(7):658–662. doi: 10.1002/jctb.1723.*

- Kim, B.H., Park, H.S., Kim, H.J., Kim, G.T., Chang, I.S., Lee, J., Phung, N.T., 2004, *Enrichment of Microbial Community Generating Electricity Using a Fuel-Cell-Type Electrochemical Cell. Appl Microbiol Biotechnol. 63:672-681.*

- Lin.A., Weng . C.H.,Chen. F.Y., 2008, *Separation Purification Technol. 43:422–459.*

- Qusay J. Rasheed , Kannaiyan Pandian , Karuppan Muthukumar., 2011. *Treatment of Petroleum Refinery Wastewater by Ultrasound-Dispersed Nanoscale Zero-Valent Iron Particles. Ultrasonics Sonochemistry Doi:10.1016/j.ultsonch.2011.03.015.*

- Wang X, Feng YJ, Lee H., 2008. *Electricity production from beer brewery wastewater using single chamber microbial fuel cell.Water Sci Technol.; 57(7):1117-21.*

NOMENCLATURE

COD	-	chemical Oxygen Demand.
BOD	-	Biological Oxygen Demand.
XRD	-	x-ray Diffraction.
SEM	-	scanning electron microscopy.
D_p	-	average crystallite size.
B	-	Line broadening in radians (FWHM of diffraction peak).
θ	-	diffraction angle.
λ	-	x-ray wavelength.
j	-	current density.
R	-	resistance.
U	-	voltage.
p	-	power density.
W	-	watt.
B	-	breath.
L	-	length.
T	-	width.
A	-	Amper.

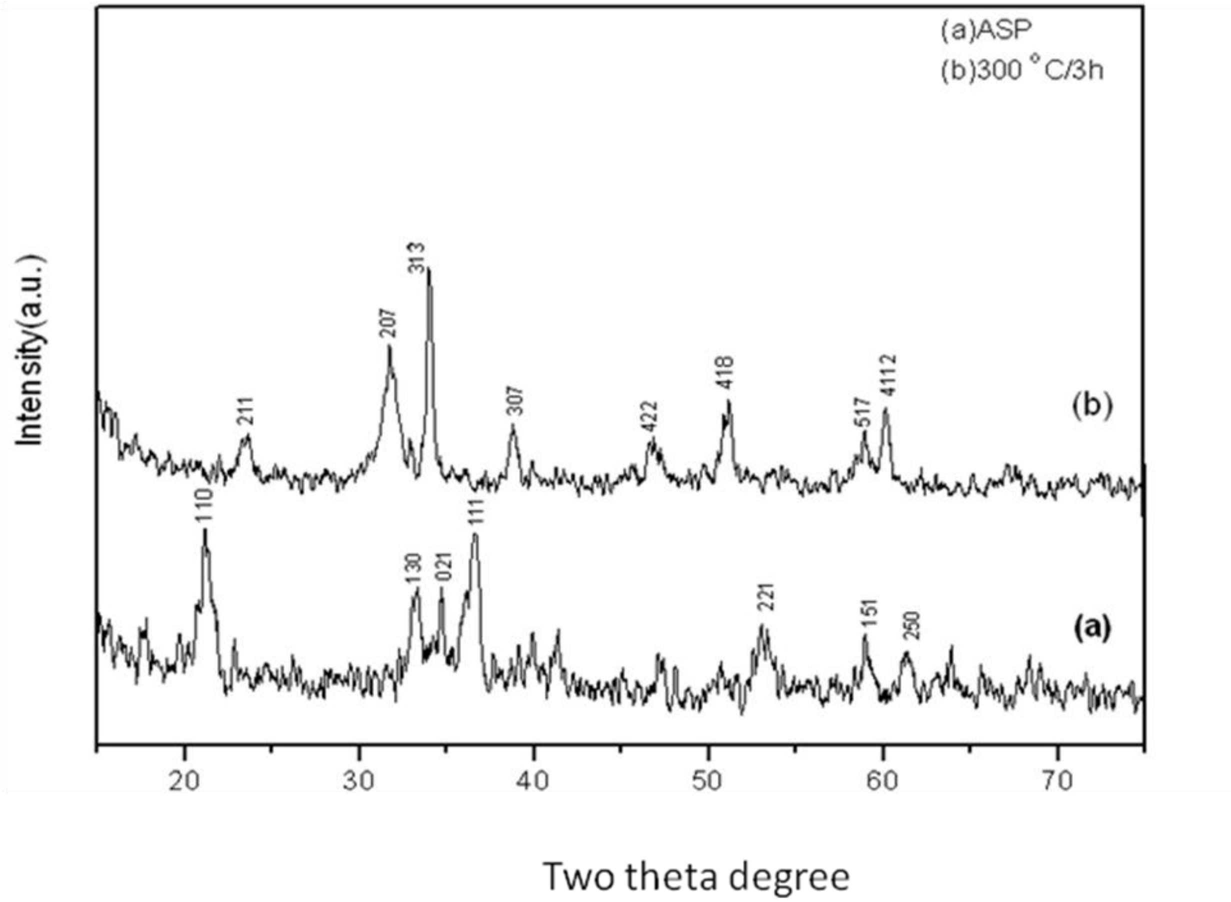

Figure 1. X-ray diffraction pattern of the as-prepared Fe2O3 sample.

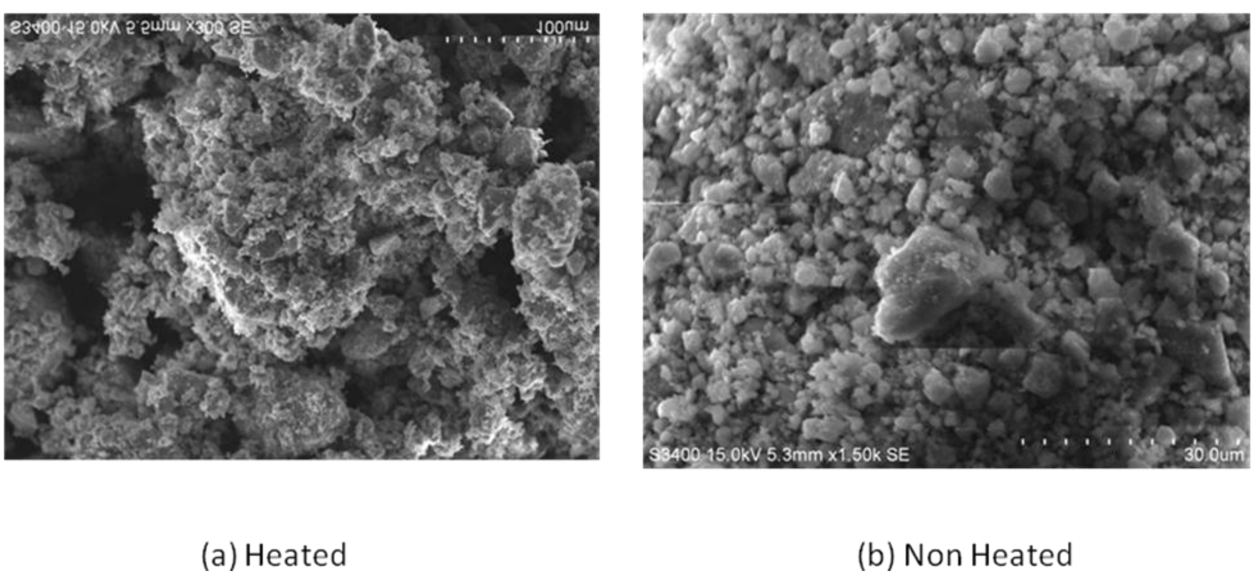

Figure 2. SEM Image of heated Fe2O3and non heated Fe2O3.

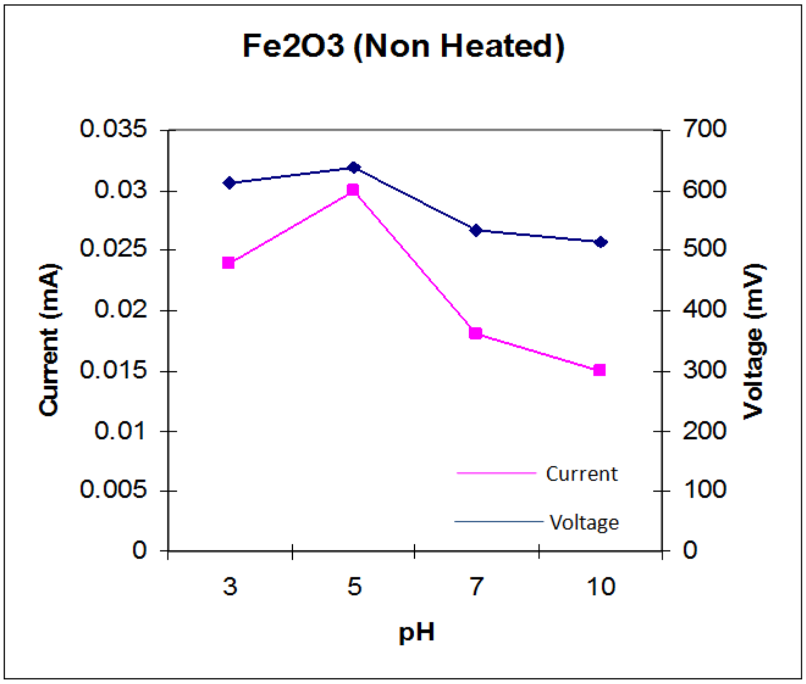

Figure 3.a. Maximum current and voltage produced at different pH using 2.5% (0.025 gm) of the nanoparticle.

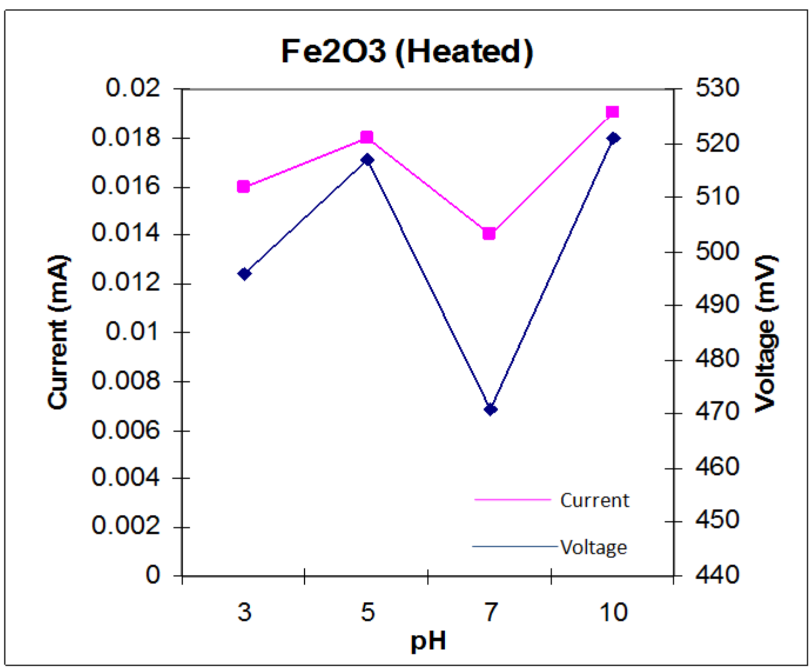

Figure 3.b. Maximum current and voltage produced at different pH using 2.5% (0.025 gm) of the nanoparticle.

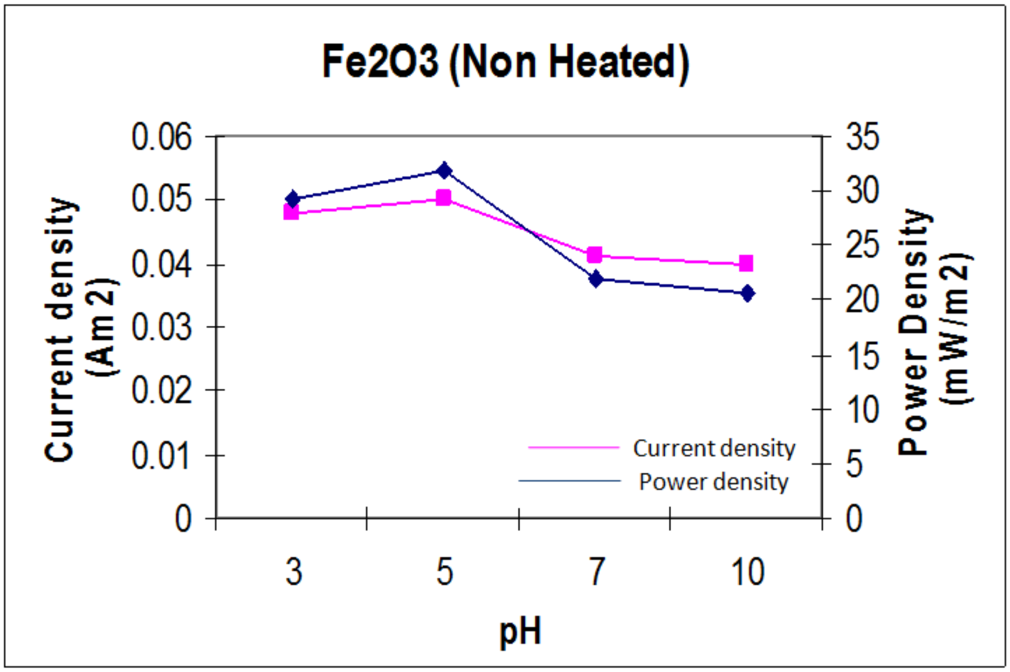

Figure 4.a. Maximum current density and power density produced at different pH using 2.5% (0.025 gm) of the nanoparticle.

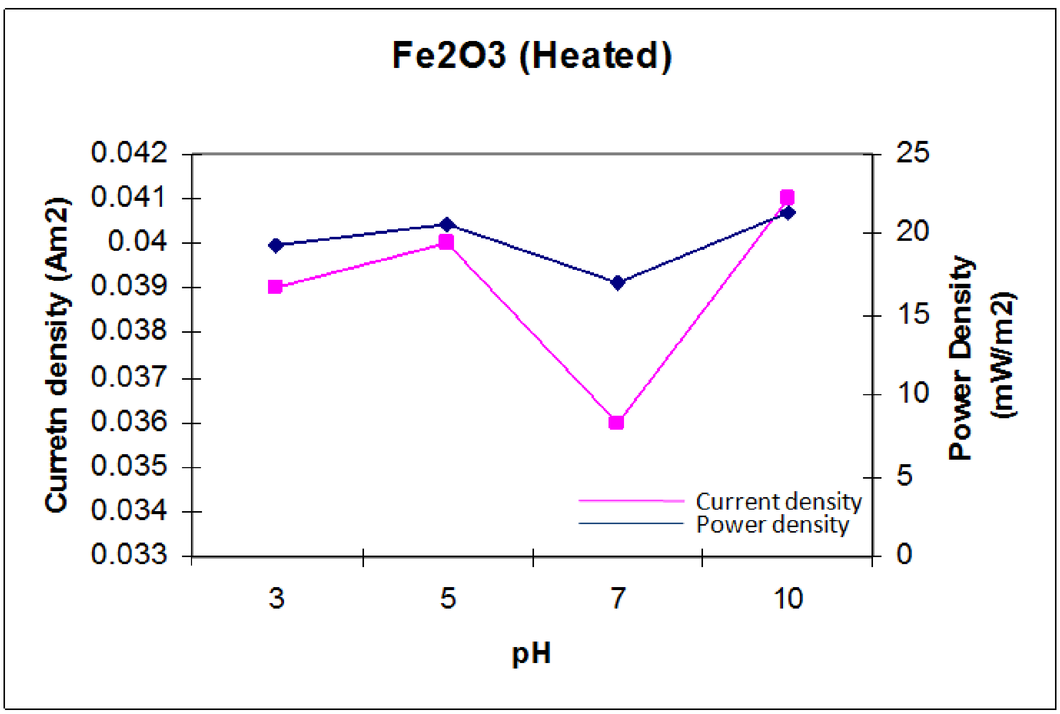

Figure 4.b. Maximum current density and power density produced at different pH using 2.5% (0.025 gm) of the nanoparticle.

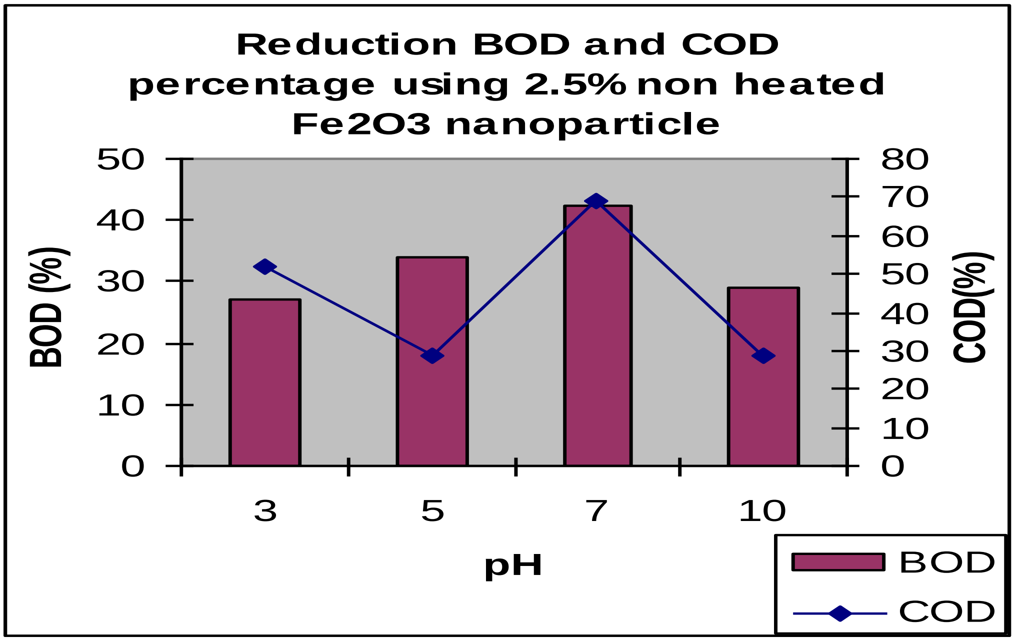

Figure 5.a. BOD and COD reduction at different pH using 2.5% (0.025 gm) of the nanoparticle.

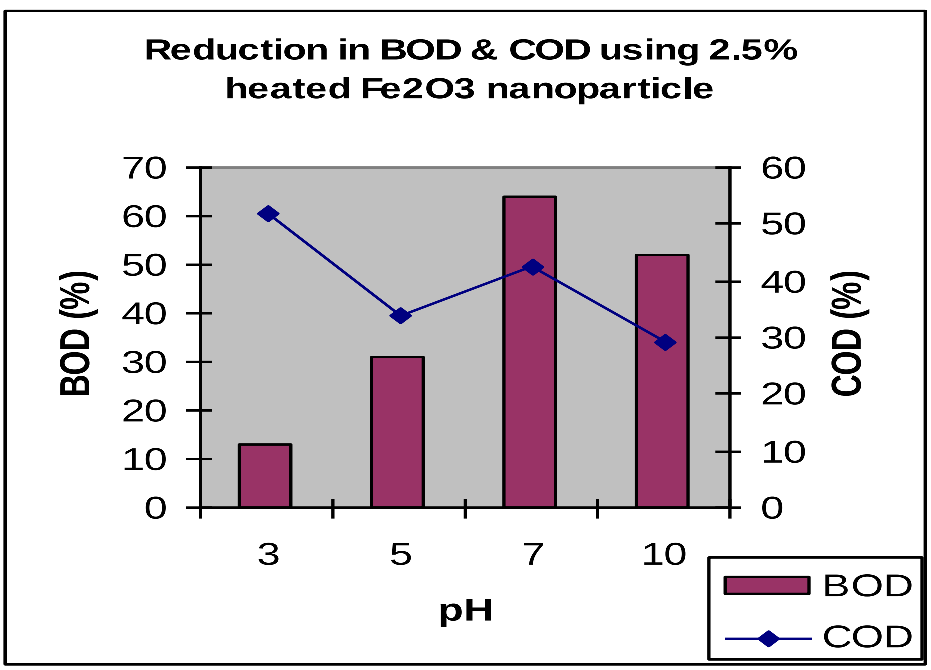

Figure (5.b) . BOD and COD reduction at different pH using 2.5% (0.025 gm). of the nanoparticle.

Table1. Characteristics of wastewater.

Parameters	Value
COD (mg/L)	15,000
Initial pH	7.0
Initial DO(mg/L)	2.2
Total Solids (mg/L)	1700
Dissolved Solids(mg/L)	750
Suspended Solids(mg/L)	1100

قائمة المحتويات

القسم العربي:

تأثير الفلدسبار المحلي على خواص الخرسانة ذاتية الرص

د. ندى مهدي الجيلاوي
استاذ
الهندسة المدنية
كلية الهندسة / جامعة بغداد

هديل ابراهيم احمد
باحث
قسم الهندسة المدنية
كلية الهندسة / جامعة بغداد

الخلاصة

تم في هذا البحث استعمال الفلدسبار في إنتاج خرسانة ذاتية الرص بمقدار (5 , 10 , 15) % كنسبة استبدال جزئي من وزن السمنت . تم دراسة الخواص الطرية للخرسانة الذاتية الرص الحاوية على الفلدسبار (انسياب الهطول باستخدام اختبار القمع على شكل حرف V و قدرة الملئ باستخدام صندوق الاختبار على شكل حرف U) للخلطات الخرسانية و ايضا تم دراسة الخواص المتصلبة للخرسانة الذاتية الرص الحاوية على الفلدسبار(مقاومة الانضغاط و مقاومة الانثناء) . و اظهرت نتائج البحث ان للفلدسبار تأثير سلبي على الخواص الطرية للخرسانة ذاتية الرص و لكن له تأثير ايجابي على خواص الخرسانة ذاتية الرص المتصلبة .

الكلمات الرئيسية : الخرسانة ذاتية الرص , الفلدسبار , الخواص الطرية للخرسانة ذاتية الرص, خواص الخرسانة ذاتية الرص المتصلبة

Effect of Local Feldspar on the Properties of Self Compacting Concrete

Prof.Nada Mahdi Algalawi
Department of Civil Engineering
College of Engineering
Baghdad University
Email : naljalawi @yahoo.com

Hadel Ibraheem Ahmad
Department of Civil Engineering
College of Engineering
Baghdad University
Email : hadeel_ebraheem @yahoo.com

ABSTRACT

This research of using Feldspar in the production self compacting concrete (SCC) (5,10,15)% as partial replacement by weight of cement .In this research some of fresh properties of SCC (slump flow used V-funnel test and filling ability used (U-box test) for concrete mixes and also some of the harden properties of SCC (compressive and flexural tests). The research results showed that negative effect of Feldspar on the fresh properties of self compacting concrete but the positive effect of Feldspar on the harden properties of self compacting concrete .

Keywords : Self compacting concrete , Feldspar , The fresh properties of self compacting concrete , The harden properties of self compacting concrete .

1- المقدمة

الخرسانة ذاتية الرص (Self Compacting Concrete) و يرمز لها (SCC) هي واحدة من أحدث الابتكارات في تكنولوجيا الخرسانة , إذ أَخذت بالانتشار في جميع أنحاء العالم لِما لها من خصائص و مميزات في حالتها الطرية و كذلك بعد التصلب, وهي ذات قابلية تشغيل عالية حيث تنساب خلال التسليح الكثيف او العناصر الإنشائية المعقدة هندسياً تحت تأثير وزنها الذاتي فقط على نحو كافي لتملأ الفراغات بدون أي انعزال او نضوح متجاوز الحد دون الحاجة الى تسليط الاهتزازات عليها (Ravindrarajah,2003) , (Tviksta,2000) , (Vachon,2002). وان للخرسانة ذاتية الرص (SCC) لزوجة تشبه العسل (Honey) وتمتلك هذه الخرسانة سطحاً مستوياً بعد الصب (Placing) , حيث تأخذ شكل معين وهذا بسبب انسيابها السريع, وهي ذات سطح صقيل بحيث يكون لها شكل نهائي أفضل من الخرسانة التقليدية , وإنها تمتلك صفة عدم الانعزال وعدم ميلها إلى الإعاقة (Ravindrarajah,2003), (Dehn,2000).

2- استخدام الخرسانة ذاتية الرص

الخرسانة ذاتية الرص تطورت أول مرة في اليابان كوسيلة لخلق نوعية منتظمة من الخرسانة بواسطة التحكم في أي مشكلة ناتجة عن الرص غير الكافي مــن قبــل القــوى العامـلة كنتيجة لقلة الأيدي العاملة الماهرة و زيادة التصاميم المعقدة و تفاصيل التسليح في الأعضاء الإنشائية الحديثة ويمكن تحقيق مميزات الخرسانة ذاتية الرص(SCC) من خلال خواصها الفريدة في حالتها الطرية, فان انسيابها يكون تحت تأثير وزنها الذاتي فقط وبذلك تحافظ على التجانس , في حين تملأ بشكل كلي الفراغات جميعها ومن خلال حول التسليح الكثيف . اما في حالتها المتصلبة, فإنها تفوق الخرسانة التقليدية فيما يتعلق الأمر من حيث المقاومة والديمومة(Ravindrarajah,2003). اغلب أنواع الخرسانة تعتمد على الرص حتى تضمن القوة والمتانة , وان الرص غير الكافي يؤدي الى حدوث فجوات ومن ثم نقصان في مقاومة الانضغاط و تؤثر أيضاً تأثيراً قوياً في حماية حديد التسليح التي توفرها الخرسانة . ومن النتائج السلبية أيضاً للخرسانة التقليدية أنها تَستخدم الهزاز لرص الخرسانة و هذا ينتج عنه مستوىً عال من الضوضاء فيعد هذا احد مصادر التلوث البيئي (Wallevik,1998) .

3-خصائص المواد الأولية و الإعمال المختبرية

3-1 السمنت

السمنت المستخدم في هذا البحث هو سمنت بورتلاندي اعتيادي (Type I) المصنع من قبل شركة السمنت المتحدة المعروف تجاريا باسم (طاسلوجة-بازيان) . و خواصه الفيزيائية و الكيمائية مطابقة للمواصفة العراقية (م.ق.ع /5 / 1984) .

3-2 الركام الناعم

تم استخدام الركام الناعم (الرمل) وهو مطابق للمواصفة العراقية القياسية (م.ق.ع /45 / 1984) .

3-3 الركام الخشن :-

تم استخدام حصى مكسر مقاسه الأقصى (10 ملم) وهو مطابق للمواصفة العراقية القياسية (م.ق.ع /45 / 1984) .

3-4 الملدن المتفوق

استخدم في هذا البحث مضاف مقلل للماء بدرجة متفوقة والمعروف تجاريا (Glenuim 51) و يوضح الجدول4 الخصائص التقنية للملدن المتفوق المستخدم في هذه الدراسة .

2-5 الفلدسبار

الفلدسبار من المعادن الرئيسية المكونة للصخور النارية كالبازلت . والصيغة الكيميائية للفلدسبار هي (Al_2O_3 . y SiO_2 . n MO) إذ ان : M : قد تكون (Ca , Na , K) . ويمكن ان يتحول هذا المعدن عبر العصور الجيولوجية و بفعل عوامل فيزيائية-كيمائية الى معدن الكاؤلين. و يتكون كيمائيا من السيليكا و الالومينات و يبين الجدول 2 و 3 التحليل الكيمائي و الفيزيائي للفلدسبار المحلي المستعمل . الفلدسبار المستخدم في هذا البحث هو فلدسبار عراقي أخذ من منطقة بحر النجف في محافظة النجف الاشرف وكان بداية عبارة عن حبيبات صغيرة يتراوح أقطارها بين(2- 4 ملم) تم طحنه الى نعومة عالية (12000 سم^2/غم Blaine) وعلى مرحلتين حيث طحن في البداية باستخدام ماكنة لوس انجلوس (Los Angeles machine) باستخدام (15) كرة حديدية ولمدة (8 ساعات) أي ما يعادل (18000 دوره) تقريبا .ومن ثم طحن بواسطة طاحونة الكرات السيراميكية أذ يوضع كيلو غرام واحد في وعاء الطاحونة ويطحن لمدة (18) ساعة وذلك للوصول الى أعلى نعومة ممكنة(حسين,2005) وللحصول على فعالية بوزولانية جيدة تم حرق الفلدسبار بدرجة حرارة مقدارها 650 درجة سيليزية في فرن كهربائي مختبري لأجل تنشيطه لمدة ساعتين و نصف الساعة (الجيلاوي ,2006) .

2-6 الخلطات الخرسانية

لأجل تحقيق الهدف من الدراسة تم تقسيم التجارب المختبرية الى تسع خلطات ما عدا الخلطات المرجعية فهي عبارة عن ثلاث خلطات فقط و تم استخدام طريقة المنظمة الأوروبية للخرسانة جاهزة الخلط (The EMRCO,2005) في تصميم هذه الخلطات كما في الجدول 4 .

2-7 طرق اختبار الخواص الطرية للخرسانة ذاتية الرص :-

2-7-1اختبار القمع على شكل حرف V

ان هذا الفحص يقيم الخواص الطرية للخرسانة ذاتية الرص بأسلوب يختلف عن فحص انسياب الهطول . والشكل 1 يبين الجهاز المستخدم في اختبار القمع على شكل (V) . وتم خلال هذا الفحص قياس الزمن اللازم من لحظة فتح بوابة القمع الى لحظة خروج كل الخرسانة من القمع وهي لحظة رؤية الضوء من خلال فتحة البوابة ويعبر عنه ب (T5min) . وتعتبر الخرسانة ذات خواص رص ذاتي إذا كان هذا الزمن ضمن حدود 6-12 ثانية

2-7 صندوق الاختبار على شكل حرف U

يختص هذا الفحص بالتحقق من قدرة الملئ وإمكانية انسياب الخرسانة ذاتية الرص المحتوية على مختلف أنواع الركام من خلال قضبان حديد التسليح بدون حدوث انفصال حبيبي أو انسداد . يتم حساب قيمة الفرق في ارتفاع سطح الخرسانة بين الحجرتين(H1 – H2) ويجب إن يكون اقل من أو يساوي 30 ملم ، وكلما كان الفرق اقرب للصفر كلما كانت الخرسانة ذات درجة انسياب عالية ولها مقدرة عالية على الانسياب بين قضبان التسليح .

2-8 طرق اختبار خواص الخرسانة المتصلبة

2-8-1 مقاومة الانضغاط

اجري فحص مقاومة الانضغاط بموجب المواصفة البريطانية(BS1881-part116/1983) وتم استخدام نماذج مكعبة الشكل بإبعاد (100× 100× 100) ملم للخلطات الخرسانية تم تسليط الحمل على النموذج مع تسجيل الحمل المسبب للفشل , و تستخرج مقاومة الانضغاط من حاصل قسمة الحمل على مساحة الوجه المعرض للحمل, و تم الفحص بأعمار(28 , 60 , 90) يوم واخذ معدل ثلاث مكعبات.

2-8-2 مقاومة الانثناء

تم فحص مقاومة الانثناء لاعتاب بأبعاد (400× 100 × 100) ملم للخلطات الخرسانية بموجب المواصفة الأميركية (ASTM C 293-07) علما بان النموذج وضع داخل الجهاز بحيث تكون السطوح الجانبية و المواجهة لجوانب القالب إثناء الفحص ملامسة للمساند عمودي على اتجاه الصب .يؤخذ معدل مقاومة الانثناء لثلاثة نماذج لكل خلطة و تم الفحص بأعمار(28 , 60 , 90) يوم و يعبر عنه بميكا باسكال(نيوتن / ملم^2) و يتم حسابه وفقا للمعادلة الآتية :

$$R = 3PL/2\,bd^2 \qquad \ldots\ldots\ldots\ldots (1)$$

إذ ان

R = مقاومة الانثناء (ميكا باسكال) .

P = أعلى حمل مسبب للفشل (نيوتن) .

L = المسافة بين نقطتي الارتكاز (300) ملم .

b = العرض (100) ملم .

d = الارتفاع (100) ملم .

3- النتائج و مناقشة البيانات

3-1 الخواص الطرية للخرسانة ذاتية الرص :-

تمت دراسة تأثير اضافة نسب مختلفة من الفلدسبار(5 , 10 , 15) % كاستبدال جزئي من وزن السمنت مع ثلاث محتويات مختلفة من الماء و هي (170 , 180, 190) كغم / م^3 كما موضحة بالاشكال (3 , 4 ,5) التي تمثل زمن الانسياب (Tv) و قيم (Tv 5min) لخلطات الخرسانة ذاتية الرص للمجموعة الاولى و الثانية و الثالثة على التوالي . اما الاشكال (6 , 7 , 8) التي تمثل نتائج ارتفاع الملئ لصندوق الاختبار على شكل حرف U لخلطات الخرسانة ذاتية الرص للمجموعة الاولى و الثانية و الثالثة على التوالي .

فان اضافة الفلدسبار أدت الى زيادة في زمن الانسياب (Tv , Tv5min) و زيادة فرق ارتفاع الملئ بشكل كبير مقارنة بالخلطات المرجعية (R1,R2,R3) الحاوية على السمنت بدون اضافة المادة البوزولانية .حيث كلما تزداد نسب الاستبدال للمجموعة الاولى ذات محتوى الماء 170 كغم / م^3 للخلطات الحاوية على الفلدسبار كلما يزداد زمن الانسياب لـ (Tv , Tv5min) و يزداد فرق ارتفاع الملئ يعود السبب الى لزوجة الخلطات الخرسانية التي تزداد في الخلطات الحاوية الفلدسبار والسمنت نتيجة لزيادة المواد الناعمة و الى قابلية الانسياب للخرسانة من مقطع الى أخر و الذي يكون أبطء و اصلب . و هذا الكلام ينطبق على المجموعة الثانية ذات محتوى الماء 180 كغم / م^3 والثالثة ذات محتوى الماء 190 كغم / م^3

اما زيادة محتوى الماء من (170–190) كغم / م³ للخلطات الحاوية على الفلدسبار يقلل من زمن الانسياب لكل من (Tv , Tv5min) و ذلك يعود الى سرعة الانسياب نتيجة لتقليل لزوجة الخلطة و يؤدي الى زيادة سرعة الانسيابية لهذه الخلطات الذي يؤدي الى تقليل من الاحتكاك الداخلي بين حبيبات الركام او بين الخرسانة و السطح الملامس لها.

اما لزيادة محتوى الماء من (170–190) كغم / م³ للخلطات الحاوية على الفلدسبار فيؤدي الى زيادة فرق ارتفاع الملئ وذلك بسبب نقصان قابلية التشغيل للخلطات و نقصان سرعة الانسياب للمقطع الآخر من دون حصول أي انعزال او نضوح للخلطات الخرسانية.

3-2 مقاومة الانضغاط و مقاومة الانثناء

يلاحظ زيادة مقاومة الانضغاط و مقاومة الانثناء للخلطات الحاوية على الفلدسبار مع زيادة نسب الاستبدال الجزئي له و بمقدار (5 , 10 , 15) % من وزن السمنت للمجموعة الاولى ذات محتوى الماء 170 كغم/م³ . و هذا السلوك يعود الى الفعالية البوزولانية الفلدسبار حيث تتفاعل هذه المواد البوزولانية مع هيدروكسيد الكالسيوم الناتج من اماهة السمنت و هذا التفاعل يقود الى زيادة التكثيف في المنطقة البينية و من ثم يزيد من مقاومة الربط الداخلي وتقليل الشقوق المجهرية وهذا ينطبق على المجموعة الثانية ذات محتوى الماء 180 كغم/م³ و الثالثة ذات محتوى الماء 190 كغم/م³ و هذا يشابه ما توصل إليه الباحثون (,Khaleel, 2007 : Ali Hussian, 2008), (حسين,2005) و هذا مبين بالشكل (12 , 16) . وكذلك زيادة مقاومة الانضغاط و مقاومة الانثناء للخلطات الحاوية على الفلدسبار مع تقدم زمن الإنضاج للمجموعة الاولى ذات محتوى الماء 170 كغم/م³ تعود الى زيادة نسبة السليكا مما يؤدي الى زيادة تفاعلها مع مركب هيدروكسيد الكالسيوم و الذي ينتج من عملية اماهة السمنت و من ثم تتكون كمية اكبر من المركب (C-S-H) وكذلك زيادة مقاومة الانضغاط و مقاومة الانثناء للخلطات الحاوية على الفلدسبار مع تقدم زمن الإنضاج للمجموعة الاولى ذات محتوى الماء 170 كغم/م³ تعود الى زيادة نسبة السليكا مما يؤدي الى زيادة تفاعلها مع مركب هيدروكسيد الكالسيوم و الذي ينتج من عملية اماهة السمنت و من ثـم تتكون كمية اكبر من المركب (C-S-H) وهو مركب مستقر و كمية اقل من مركب هيدروكسيد الكالسيوم وهذا المركب يكون عادة بشكل بلورات صفائحية كبيرة تحيط بجزيئات الركام (السطح البيني) ويكون الارتباط ضعيفا بالركام مما يؤدي الى احتمالية الفشل في المنطقة البينية بين الركام وعجينة السمنت بسبب ضعف المنطقة لذلك فان هذا التفاعل يؤدي الى زيادة كثافة المنطقة البينية و هذا ينطبق على المجموعة الثانية ذات محتوى الماء 180 كغم/م³ و الثالثة ذات محتوى الماء 190 كغم/م³ و هذه النتائج متوافقة لما توصل إليه الباحثان (حسين,2005), (الجميلي,2008).

يلاحظ من نتائج مقاومة الانضغاط و مقاومة الانثناء المبينة في الاشكال (9 , 10 , 11) التي توضح العلاقة بين مقاومة الانضغاط و زمن الانضاج للفلدسبار للمجموعة الاولى و الثانية و الثالثة على التوالي اما الاشكال (13 , 14 , 15) توضح العلاقة بين مقاومة الانضغاط و زمن الانضاج للفلدسبار للمجموعة الاولى و الثانية و الثالثة على التوالي بان مقاومة الانضغاط و مقاومة الانثناء للخرسانة الحاوية على الفلدسبار تتناقص مع زيادة محتوى الماء من (170–190) كغم/م³ و هذا يعود الى ان زيادة كمية ماء الخلطة تعمل على تحسين قابلية التشغيل لكنها تعمل على أضعاف بنية عجينة السمنت و هذا يؤدي الى انخفاض في مقاومة الانضغاط و زيادة نفاذية الخلطة و هذا يشابه ما توصل إليه الباحث (البدري,2001).

4- الاستنتاجات

أ- ان اضـافة الفلدسـبار بنسـب اسـتبدال جزئـي (5 , 10 , 15) % مـن وزن السـمنت أدى الـى زيـادة زمـن الانسياب (Tv) و (Tv5min) زيادة في فرق ارتفاع الملئ مع زيادة نسب الاستبدال الجزئي . و لكن بزيادة محتوى الماء يقل زمن الانسياب (Tv) و(Tv5min) ويزداد فرق ارتفاع الملئ.

ب- زيادة مقاومة الانضغاط مع زيادة نسب الاستبدال الجزئي الفلدسبار يتراوح بين (27 ,35, 60) % للنسب (5 , 10 , 15) % من وزن السمنت و بزمن إنضاج 90 يوم و ذات محتوى الماء 170 كغم/م³ و تقل قليلا بزيادة محتوى الماء.

ج- زيادة مقاومة الانثناء مع زيادة نسب الاستبدال الجزئي الفلدسبار يتراوح بين (7 ,16, 17) % للنسب (5 , 10 , 15) % من وزن السمنت و بزمن إنضاج 90 يوم و ذات محتوى الماء 170 كغم/م³ و تقل قليلا بزيادة محتوى الماء.

REFERENCE

ASTM C293-07, “Standard Test Method for Flexural Strength of Concrete (Using Simple Beam With Center-Point Loading)” ASTM International .

Ali Hussian, Z. M. , " The effect of Grading of Aggregate on Properties of Self-Compacting Concrete " MSC. Thesis , College of Engineering , Department of civil engineering, AL-Mustansirya University,, January-2008 .

BS 1881, part 116, "Method for determination of compressive strength of concrete cubes" British standards institution, 1989.

Dehn, F., K. Holschemacher, and D. Weisse, “Self-Compacting Concrete - Time Development of the Material Properties and the Bond Behavior”, LACER No. 5, (2000), pp.115-123.

Ravindrarajah, R., Farrokhzadi, and Lahoud, A.," Properties of Flowing Concrete and Self-Compacting Concrete with High Performance Superplasticizer", RILEM Publications, Vol. 1, August 2003, pp.1048-1058 .

Ravindrajah R.S., Siladyi D. and Adamopoulos B., " Development of High Strength Self-compacting Concrete With Reduced Segregation Potential ",Proceeding of the 3rd International RILEM Symbosium, Vol.1, pp.1048, Reykjavik, Iceland, (August 2003).

Tviksta L.G., "Guideline for SCC", Brite EuRam, Task 9 End Product, (2000) pp.3-11.

The Europen Guidelines for Self-compacting Concrete”, European Ready-Mix Concrete Organisation (ERMCO), May 2005, 68 pp.

Vachon, M., " ASTM Puts Self-Consolidating Concrete to the Test" , Ohio, 2002, 1 pp.

Wallevik O., Nielsson I., " Self- compacting Concrete-A rheological Approach ",Proceedings of International Workshop on Self - compacting Concrete ", Kochi University, Japan, (August 1998).

المصادر العربية

– البدري ،فراس فاضل "تقييم الخرسانة عالية الأداء بطرق غير إتلافية" اطروحة ماجستير، جامعة بغداد 2001.

– الجيلاوي ، ندى مهدي فوزي " خواص ألواح الفيروسمنت خفيفة الوزن وذات الرص العالي " رسالة دكتوراه ، قسم الهندسة المدنية ، جامعة بغداد ،آب 2006 .

– الجميلي , لمى احمد عداي .," الخواص الفيزيائية للخرسانة الحاوية على الميتاكاؤولين المحلي " , رسالة ماجستير , قسم الهندسة المدنية , جامعة بغداد , اذار,2009 .

– حسين ,جعفر سلمان مكطوف " خواص الخرسانة عالية الاداء المسلحة بالالياف الفولاذية وباستخدام دقيق الفلدسبار المحلي " ،رسالة ماجستير ،قسم الهندسة المدنية ،جامعة بغداد حزيران 2005.

الجدول1. الخصائص التقنية للملدن المتفوق المستخدم في البحث.

الشكل	**سائل لزج**
اللون	**بني فاتح**
الكثافة النسبية	**1.1 @ 20 C°**
قيمة الحامضية (pH)	**6.6**
اللزوجة	**128 ± 30 CPS @ 20 C°**
المحتوى الطبيعي	**0.5-0.8 liters per100 kg of cement**

الجدول 2 .التحليل الفيزيائي للفلدسبار

الخواص الفيزيائية	**الفلدسبار**
المظهر الفيزيائي	**مسحوق**
اللون	**برتقالي فاتح**
الوزن النوعي	**2.46**
المساحة السطحية (طريقة Blaine) سم^2 / غم	**12000**
دليل فعالية المقاومة (S.A.I)	**97**

الجدول 3. التحليل الكيميائي للفلدسبار

المواصفة ASTM C. 618 /03	المحتوى %	المركبات
الحد الأدنى 70%	89.35	SiO_2
	3.24	Al_2O_3
	0.5	CaO
	0.11	MgO
الحد الأعلى 4%	0.1	SO_3
	0.94	Na_2O
	1.14	K_2O
الحد الأعلى 10%	0.64	L.O.I.

الجدول4 . تفاصيل الخلطات المستخدمة .

w/Cm	الملدن المتفوق لتر/ م³	محتوى الملدن المستخدم لتر لكل 100 كغم من السمنت	الماء لتر/ م³	الحصى كغم/ م³	الرمل كغم/ م³	الفلدسبار كغم/ م³	السمنت كغم/ م³	رمز الخلطة
0.34	4.5	0.9	170	850	825	-	500	R1
0.36	4.5	0.9	180	850	825	-	500	R2
0.38	4.5	0.9	190	850	825	-	500	R3
0.34	4.5	0.9	170	850	825	25	475	Fel 1
0.34	4.5	0.9	170	850	825	50	450	Fel 2
0.34	4.5	0.9	170	850	825	75	425	Fel 3
0.36	4.5	0.9	180	850	825	25	475	Fel 4
0.36	4.5	0.9	180	850	825	50	450	Fel 5
0.36	4.5	0.9	180	850	825	75	425	Fel 6
0.38	4.5	0.9	190	850	825	25	475	Fel 7
0.38	4.5	0.9	190	850	825	50	450	Fel 8
0.38	4.5	0.9	190	850	825	75	425	Fel 9

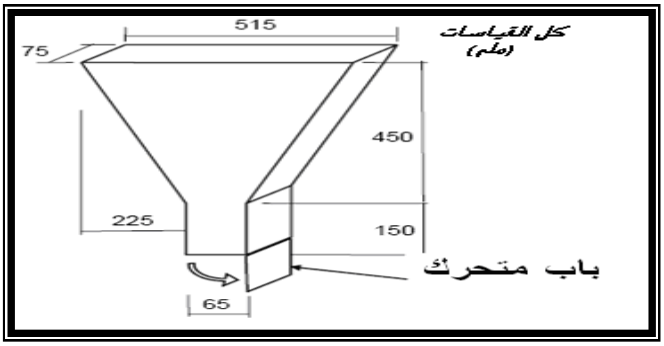

الشكل 1. اختبار القمع على شكل حرف V .

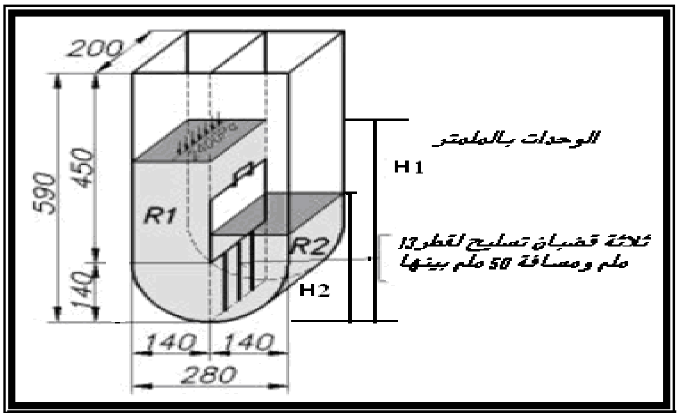

الشكل 2 . صندوق الاختبار على شكل حرف U

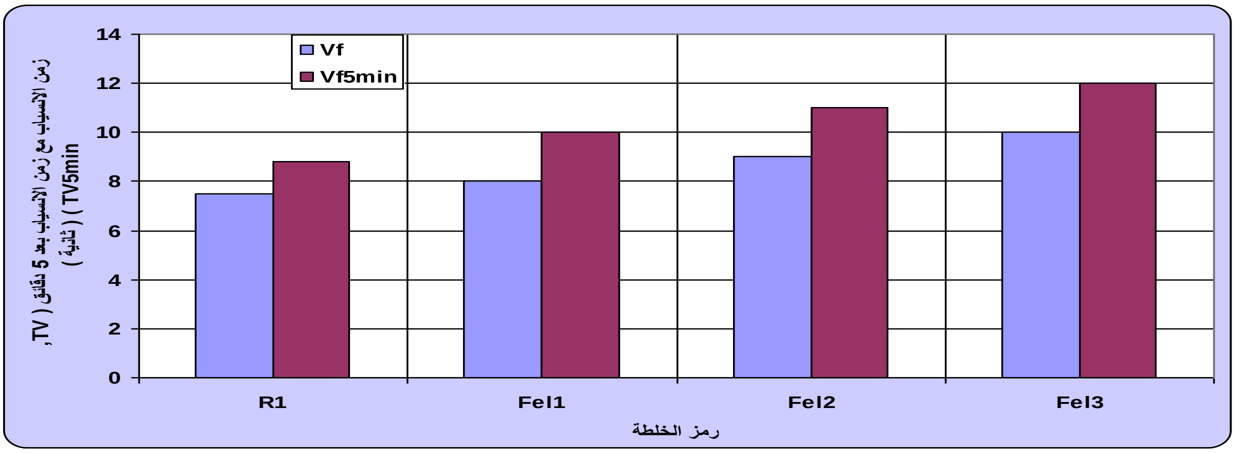

الشكل 3. زمن الانسياب (Tv) و قيم (Tv5min) لخلطات الخرسانة ذاتية الرص للمجموعة الاولى .

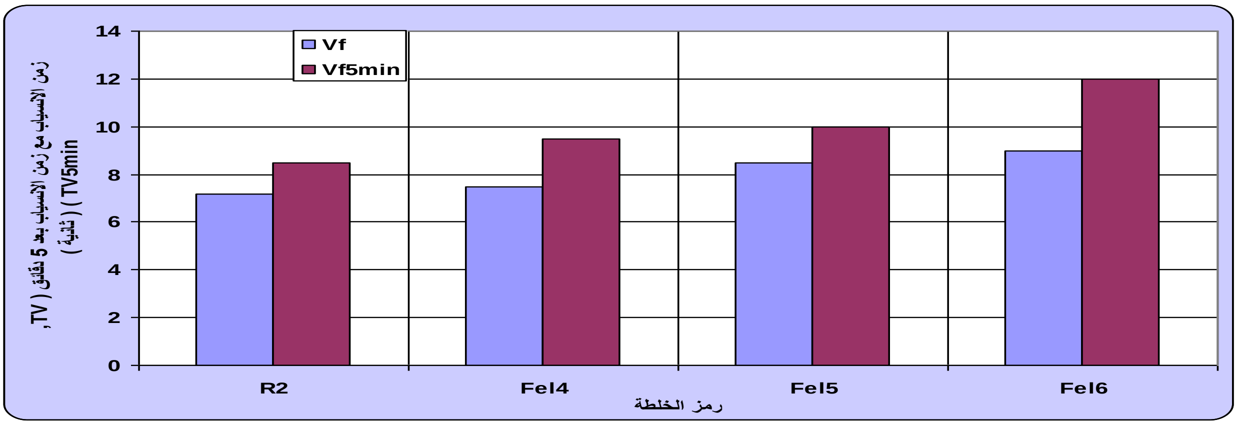

الشكل 4 . زمن الانسياب (Tv) و قيم (Tv5min) لخلطات الخرسانة ذاتية الرص للمجموعة الثانية .

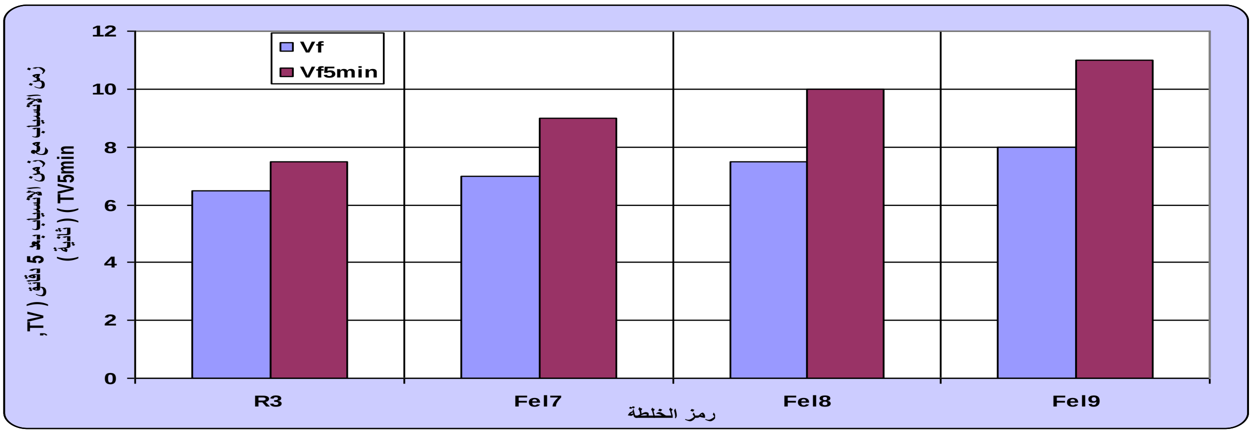

الشكل 5 . زمن الانسياب (Tv) و قيم (Tv5min) لخلطات الخرسانة ذاتية الرص للمجموعة الثالثة .

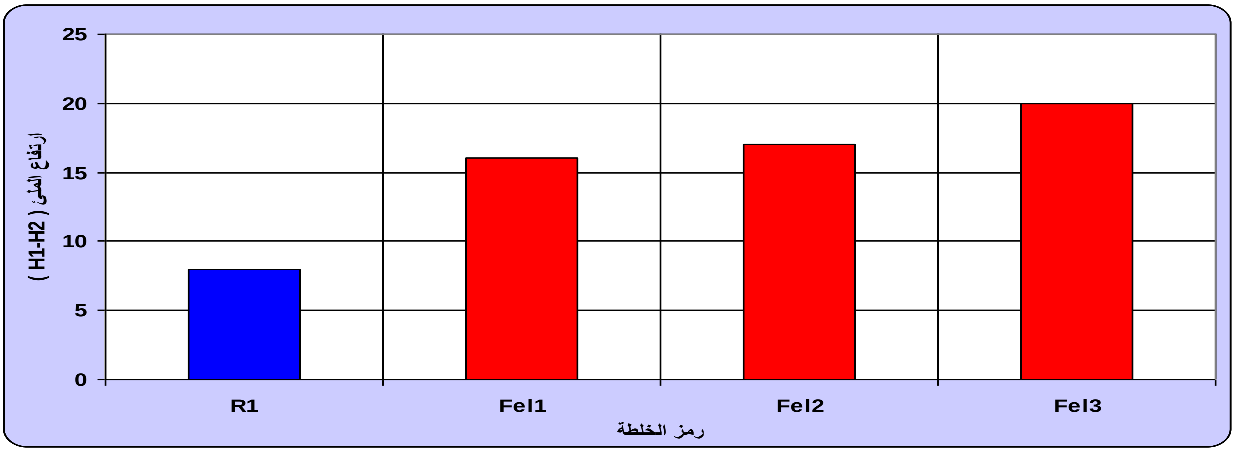

الشكل 6 . نتائج ارتفاع الملئ لصندوق الاختبار على شكل حرف U لخلطات الخرسانة ذاتية الرص للمجموعة الاولى .

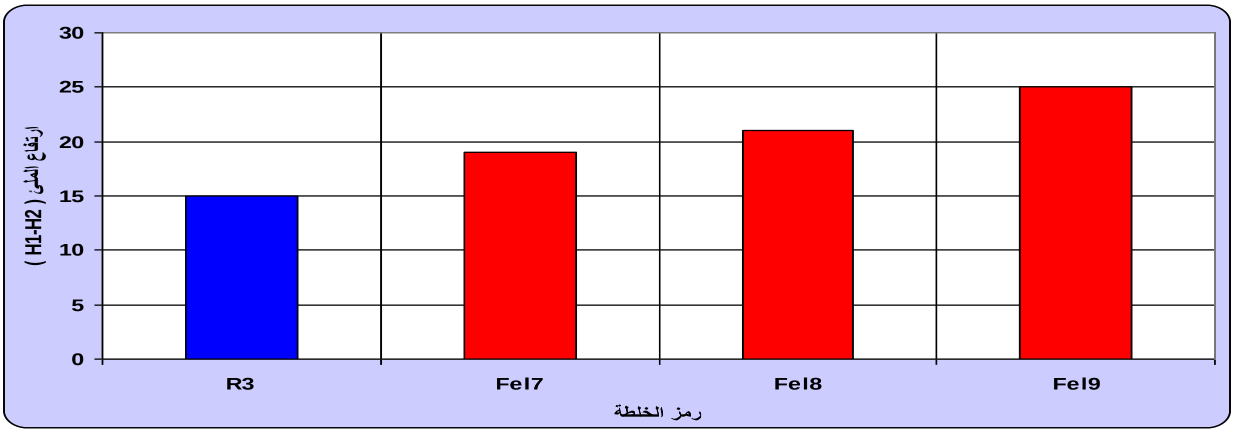

الشكل 7 . نتائج ارتفاع الملئ لصندوق الاختبار على شكل حرف U لخلطات الخرسانة ذاتية الرص للمجموعة الثانية .

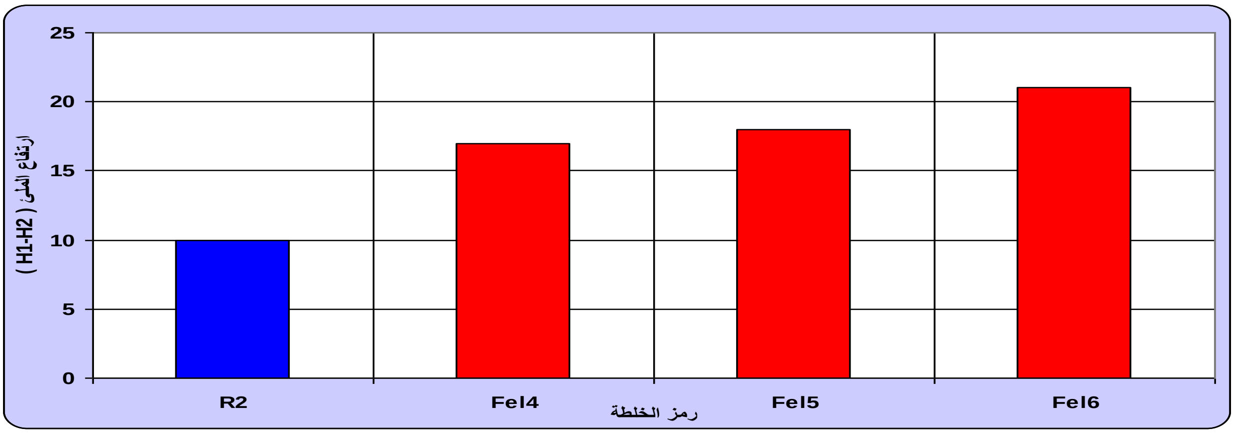

الشكل 8 . نتائج ارتفاع الملئ لصندوق الاختبار على شكل حرف U لخلطات الخرسانة ذاتية الرص للمجموعة الثالثة .

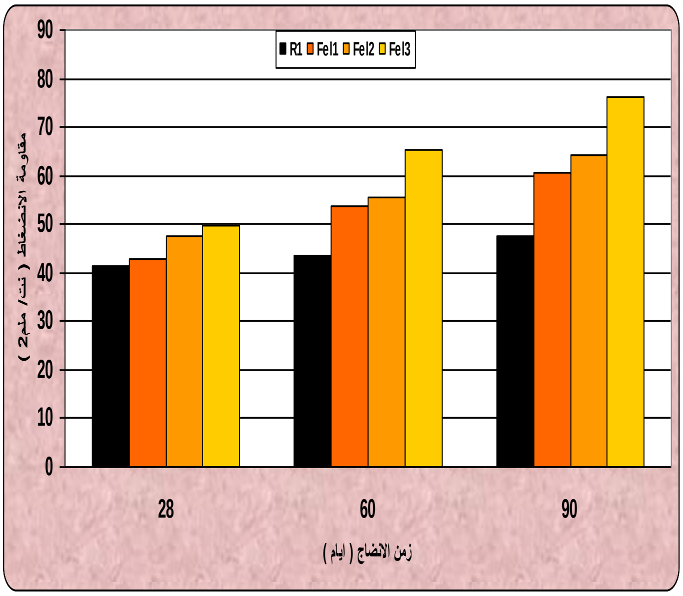

الشكل 9 . العلاقة بين مقاومة الانضغاط و زمن الانضاج للفلدسبار الانضاج للمجموعة الاولى

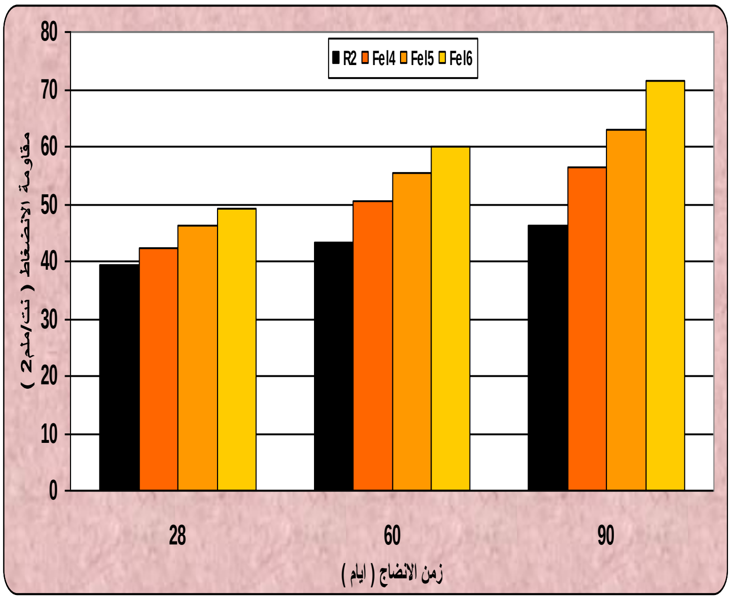

الشكل 10. العلاقة بين مقاومة الانضغاط و زمن للفلدسبار للمجموعة الاولى

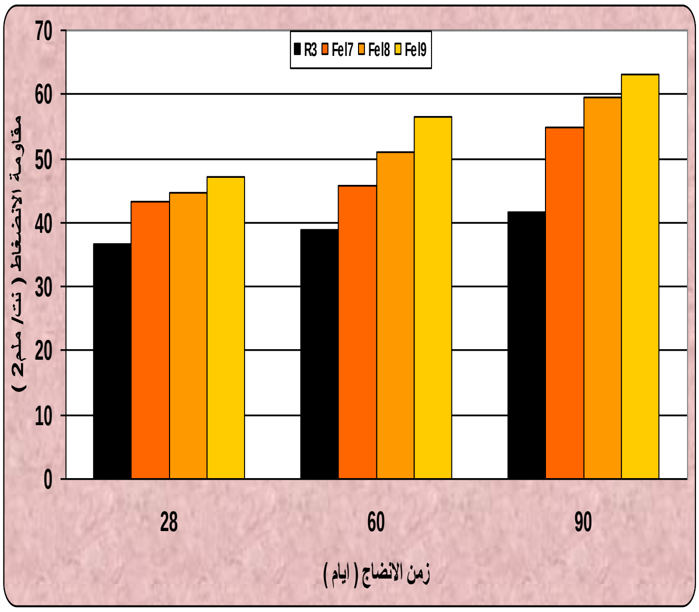

الشكل 11 . العلاقة بين مقاومة الانضغاط و زمن الانضاج للفلدسبار مع للمجموعة الثالثة

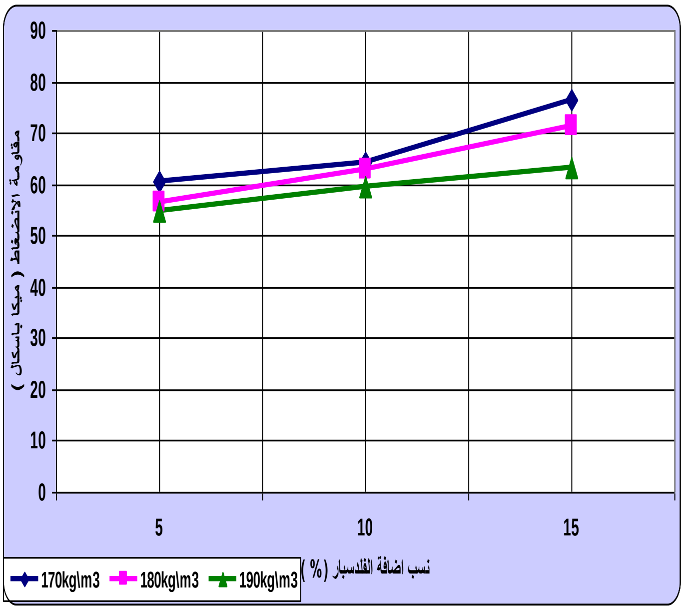

الشكل 12 . العلاقة بين نسب الاستبدال للفلدسبار و مقاومة الانضغاط

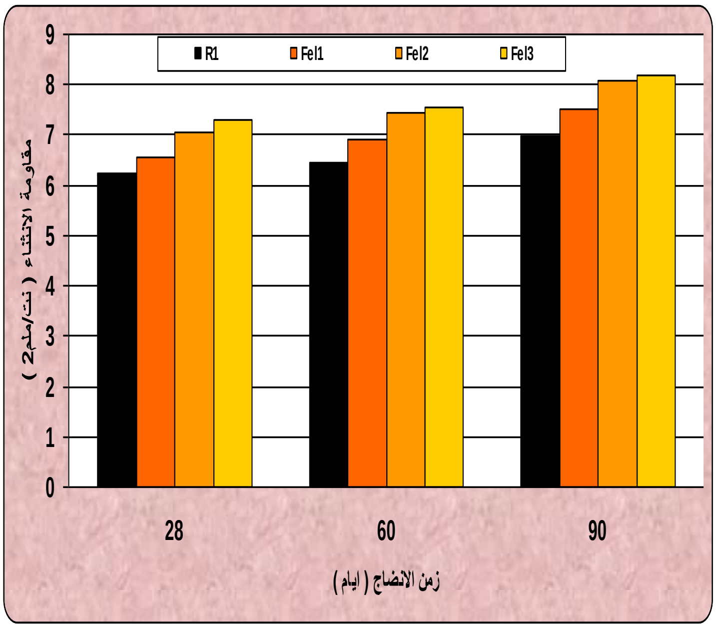

الشكل 13 .العلاقة بين مقاومة الانثناء و زمن الانضاج للفلدسبار للمجموعة الاولى

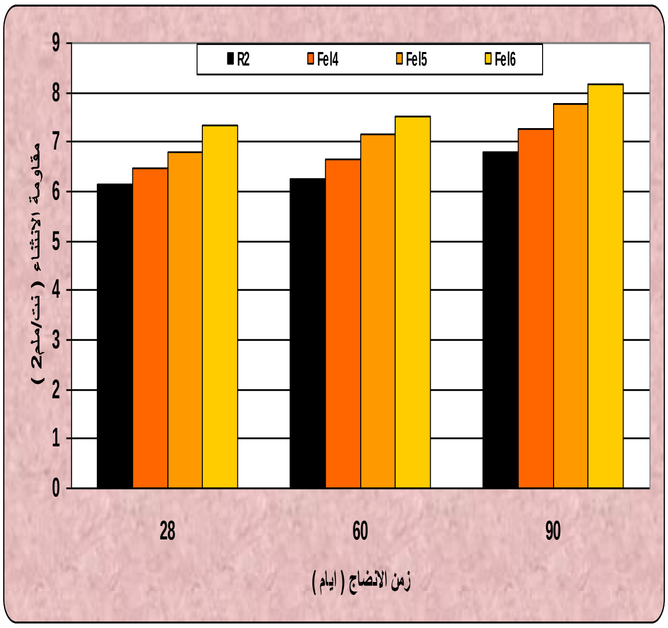

الشكل 14 . العلاقة بين مقاومة الانثناء و زمن الإنضاج للفلدسبار للمجموعة الثانية

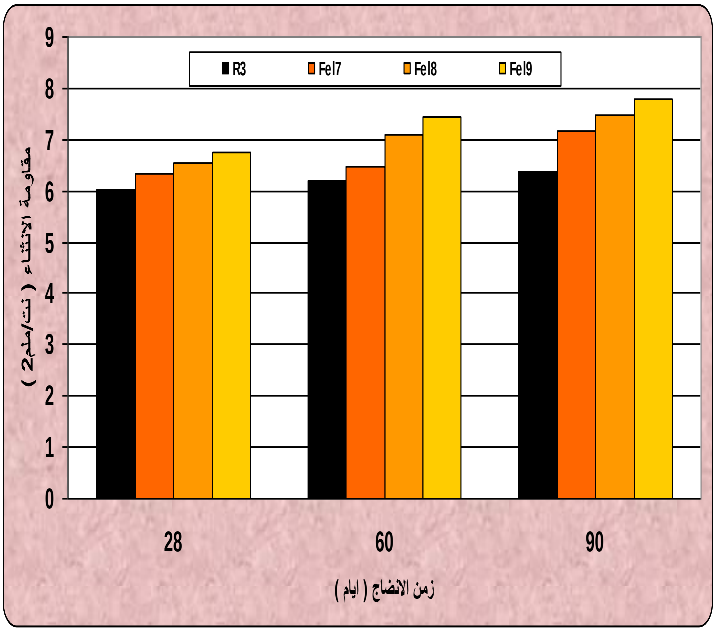

الشكل 15 . العلاقة بين مقاومة الانضغاط و زمن الانضاج للفلدسبار مع للمجموعة الثالثة

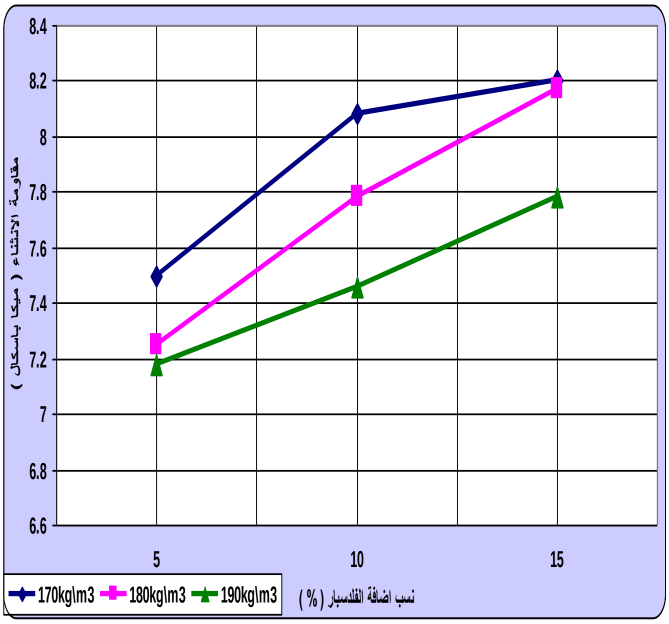

الشكل 16 . العلاقة بين نسب الاستبدال للفلدسبار و مقاومة الانثناء